PhD SCHOOL in
NANOSTRUCTURES & NANOTECHNOLOGIES
University of Milano - Bicocca
Department of Materials Science

PhD Thesis

NANOSTRUCTURED MESOPOROUS MATERIALS OBTAINED BY TEMPLATE SYNTHESIS AND CONTROLLED SHAPE REPLICA

Mario BERETTA
Matr. 040766 (XXII Cycle)

Supervisor: Prof. Piero SOZZANI
Coordinator: Prof. Leo MIGLIO

Defense December 17th 2009

Porous materials are like music:
the gaps are as important
as the filled-in bits

(G.Q. Lu and X.S. Zhao)

Contents

INTRODUCTION

Nanostructured hybrid porous materials

(A lesson from nature)

Silica (Silicon oxide) is perhaps the material the most diffused in the world. It is the material composing crystals such as quartz or opal, larger part of minerals and rocks and it is used by plants and animals to generate shells and support structures.[1] Silica is also largely used in industrial applications, overall in the amorphous form, to produce glasses, as thermal or electrical insulator in ceramic materials or in electronic devices such as transistors. Main properties of this material are great hardness, thermal and chemical stability. An important characteristic of the amorphous silica is the possibility to be arranged in complex structures such as monoliths, thin films and nanometric particles. A particular class of silica systems, very interesting for their large number of application fields, is that of porous silicas.[2]

Porous silica is easy to obtain by condensation methods and can be synthesized in regular nanometric structures that are very similar to most biological structures. In fact, a large number of small, few-cells creatures, such as diatoms, possess very useful and advanced silica-made structures used as defensive apparatus, molecular filtering membranes, light harvesting cells and other different applications.[3] These bio-devices are constituted by a very regular array of pores in silica plates jointed by organic girdle bands and they base their function on periodic alternation of voids and matter. Key points of these structures are the great regularity, with a control at the nanometric level, the large variety of properties and shapes that could be produced using the same basilar structure, the use of arrays of pores for different application and the intimate correlation between inorganic plates and biological structures.

The possibility to use a simple structure, easy and cheap to realize, for a widespread fields of applications is very attractive for scientific world and industrial production. Nanostructured porous materials are a class of materials with large and interesting field of investigation and diatom shell are just an example.[4]

By definition, a nanostructured porous material is a system with a regular pattern of pores of diameter between 1 and 100 nm.[5] These materials show many kinds of pore geometries, structures and chemical compositions and are well known as adsorbent systems, as filtering membranes, as supports for catalytic dispersion or as nano-reactors structures for controlled chemical reactions in confined space.

In last years there has been a growing interest on silica-based nanoporous materials, and in particular on periodic mesoporous silica, for their use as matrices to obtain ordered porous carbon structures by reverse replica effect, to graft functional organic dyes to realize nanomachines and to store bioactive molecules for biocompatible drug delivery applications.[6,7,8]

At the same time, a new class of hybrid nanostructured porous materials, periodic mesoporous organosilicas (PMOs) was discovered.[9] These materials are composed by organic cores of different nature directly integrated in pore walls by covalent bonds with silicon atoms. They show a very regular structure, often at molecular level, a large surface area and they join the mechanical stability of porous silica systems with the reactivity of organic molecules.[10]

Both these systems have been studied for their interactions with gases or liquid phases of different nature and for the possibility of post-synthetic reactions with the target of realizing high performing functional devices of nanometric dimension, based on the same concepts of simple structure and high performance of those generated by biological creatures.[11]

In this work we have focused our attention on the synthesis and characterization of mesoporous structures with different pore wall nature. Aims of this study are to find methods to obtain regular structures with controlled properties and geometries, using template synthesis and shape replica process, and synthesize new porous materials with hybrid or graphitic-like carbon walls.

To better understand what are nanoporous materials, general properties and synthesis strategies, in the 1st chapter a short overview of pore and structure classification has been done, followed by a description of synthetic top-down and bottom-up approaches

and general nanoporous material applications. A last paragraph will be dedicated to mesoporous materials and the concept of mesochemistry.[12]

2nd chapter is centred on surfactant molecules and templating supramolecular aggregates as a key point to control material properties such as surface area and pore diameter. A mathematical model of minimal energy surfaces is used to explain supramolecular surfactant structures formation and shapes.[13] At the end of this chapter we will focus the attention on interaction between surfactant molecules and silica precursors, as a key point for the condensation of regular silica and organosilica porous materials.[14]

A particular class of mesoporous materials, mesoporous carbons, will be described in 3rd chapter. These structures are related to mesoporous silica since they are obtained by a reverse replica process from these silica matrices and studied for their high surface area and adsorption properties. To obtain carbon material, different organic precursors have been reported in literature, such as sucrose and block copolymers.[6,15]
After these three general chapters, four experimental chapters follow.

4th chapter presents our work about mesoporous silica of MCM-41 family with different morphologies.[16] In fact, micrometric particles of silica could assume different well-defined geometrical forms. We have synthesized, following the synthesis reported in literature, five silica samples with different micrometric shapes, such as tubes or spheres. The samples have been characterized with X-ray diffraction and adsorption techniques, comparing their surface areas and their pore diameters with the aim to understand how the micrometric shape could influence the material properties. SEM imaging, finally, has been used to check directly particle shape homogeneity and to perform statistics of particle dimension.

We have also studied an hybrid periodic mesoporous organosilica, as described in 5th chapter, synthesizing both the 1,4 bis(triethoxysilyl)benzene precursor and the periodic porous structure.[17] This phenylen organosilica has a periodic alternation of silica layers and aromatic rings along the pore wall and this order is visible in X-ray diffraction pattern, that shows a characteristic peak associated to a molecular distance of 7,6Å,

typical of phenylensilica block dimension. This material has been characterized by adsorption of nitrogen and other chemical species, showing great affinity with vapors of aromatic organic molecules. The sample was also analyzed with advanced solid state NMR techniques to investigate the pore wall chemical structure.

Morphologic mesoporous silica was also used to perform confined polymerizations with different kinds of monomers such as styrene and methylmethacrylate, as described in 6th chapter.[18] Obtained nanocomposites were investigated with adsorption measurements, differential scanning calorimetry, thermogravimetric analysis and solid state NMR. From these analysis, we have found that polymer fills pore systems for about 70-90% and that the two phases are strictly interactive, as demonstrated by advanced 2D solid state NMR spectra. Aim of this polymerization is to obtain polymeric micro-objects of defined morphology and regular porous structure by shape replica process.[19]

In 7th chapter we focus our attention on silica-polyacrylonitrile nanocomposites and, in particular, on their evolution in temperature. In fact, polyacrylonitrile shows interesting thermal reactions that change its chemical structure until the formation of a graphitic-like structure.[20] Nanocomposites have been so heated until complete carbonization and analyzed with Raman and ATR techniques. Results have been compared with those obtained from bulk polyacrilonitrile thermal treated in the same way. With the same method we have also carbonized and characterized phenylensilica matrix to understand the evolution of the organic linkers at high temperatures in non-oxidative atmosphere. Final target of this work is silica dissolution in an aqueous solution of hydrofluoric acid to obtain graphitic-like porous carbon micro-objects with defined morphology.

At the end of this work, experimental appendices are reported, concerning adsorption theory, Raman analysis, solid state NMR experiments and other characterization techniques described in previous chapters.

References:

1) S. Weiner, L. Addadi, H.D.Wagner; *Materials Science and Engineering C* **2000**, *11*, 1-8

2) a) R.K. Iler, *The chemistry of Silica*, Wiley, New York, **1979**; b) W.M. Meier, *Atlas of Zeolite Structure Types 2nd edition*, Butterworths, London, **1988**; c) H.S. Nalwa, *Handbook of Organic-Inorganic Hybryd Materials and Nanocomposites, Vol. 1*, American Scientific Publishers, North Lewis Way, **2003**; d)K.K Unger, *Journal of Chromatography library, vol 16: Porous silicas and use as supports for liquid column chromatography*, Elseiver, Amsterdam, Nederland, **1979**

3) a) F. Round, R. Craford, D. Mann, *The Diatoms*, Cambridge University Press, Cambridge, UK, **1999**; b) R. Wetherbee, S. Crawford, P. Mulvaney, in *Biomineralization*, (Ed: E. Baeuerlein), Wiley-VCH, Weinheim, Germany, **2004**

4) G.Q. Lu, X. S. Zhao, *Nanoporous Materials, science and engineering*, Series of chemical engeneering, Vol.4, Imperial college Press, London, UK, **2004**

5) K.S.W. Sing, D.H. Everett, R.H.W. Haul, L. Moscou, R.A. Pierrotti, J. Rouquerlot, T. Siemieniewska; *Pure Appl. Chem.* **1985**, *57*, 603

6) a) H. Yang, D. Zhao; *J. Mater. Chem.* **2005**, *15*, 1217-1231 b) M. Tiemann; *Chem. Mater.* **2008**, *20*, 961-971

7) S. Angelos, E. Johansson, J.F. Stoddart, J.I. Zink; *Adv. Funct. Mater.* **2007**, *17*, 2261-2271

8) S. Giri, B.G. Trewyn, V.S.Y. Lin; *Nanomedicine* **2007**, *2*, 99-111

9) a) M.P. Kapoor, S. Inagaky; *Bull. Chem. Soc. Jpn.* **2006**, *79*, 1463-1475; b) S. Fujita, S. Inagaki; *Chem. Mater.* **2008**, *20*, 891-908

10) F. Hoffmann, M. Cornelius, J. Morell, M. Froeba; *Angew. Chem. Int. Ed.* **2006**, *45*, 3216-3251

11) D. Losic, J.G. Mitchell, N.H. Voelcker; *Adv. Mater.* **2009**, *21*, 2947-2958

12) M. Antonietti, G.A. Ozin; *Chem. Eur. J.* **2004**, *10*, 28-41

13) S.T. Hyde, I.S. Barnes, B.W. Ninham; *Langmuir* **1990**, *6*, 1055-1062

14) a) Q, Huo, D.I. Margolese, U. Ciesla, P. Feng, T.E. Gier, P.Sieger, R. Leon, P.M. Petroff, F. Schüth, G.D. Stuky; *Nature* **1994**, *365*, 317-321; b) Q, Huo, D.I. Margolese, U. Ciesla, D.G. Demuth, P. Feng, T.E. Gier, P.Sieger, A. Firouzi, B.F. Chmelka, F. Schüth, G.D. Stuky; *Chem. Mater* **1994**, *6*, 1176-1191

15) a) S.H. Joo, S. Jun, R. Ryoo; *Microporous and Mesoporous Materials* **2001**, *44-45*, 153-158; b) R. Ryoo, S.H. Joo, M. Kruk, M. Jaroniec; *Adv. Mater.* **2001**, *13*, 677-681

16) a) J.S. Beck, J.C. Vartuli, W.J. Roth, M.E. Leonowicz, C.T. Kresge, K.D. Schmitt, C.T.W. Chu, D.H. Olson, E.W. Sheppard, S.B. McCullen, J.B. Higgins, J.L. Shlenker; *J. Am. Chem. Soc.* **1992***, 14*, 10834-10843; b) C.T. Kresge, M.E. Leonowicz, W.J. Roth, J.C. Vartuli, J.S. Beck; *Nature* **1992***, 359*, 710-712; c) H. Yang, N. Coombs, O. Dag, I. Sokolov, G.A. Ozin; *J. Mater. Chem.* **1997**, *7*, 1755-1761

17) a) S. Inagaki, S. Guan, T. Oshuna, O. Terasaki; *Nature* **2002**, *416*, 304-307; b) K.J. Shea, D.A. Loy, O. Webster; *J. Am. Chem. Soc.* **1992**, *114*, 6700-6710

18) a) S.M. Ng, S. Ogino, T. Aida; *Macromol. Rapid Comm.* **1997**, *18*, 991-996; b) C.G. Wu, T. Bein; *Science* **1994**, *266*, 1013-1015

19) P. Sozzani, S. Bracco, A. Comotti, P. Valsesia, R. Simonutti, O. Terasaki, Y. Sakamoto; *Nature Materials* **2006**, *5*, 545-551

20) a) Z. Wangxi, L. Jie, W. Gang; *Carbon* **2003**, *41*, 2805-2812; b) C. Weidenthaler, A.H. Lu, W. Schmidt, F. Schüth; *Microporous and Mesoporous Materials* **2006**, *88*, 238-243

CHAPTER 1

Nanoporous materials

"With clay, we make a jar. But it is the empty space inside that we need."
This ancient Chinese proverb resumes in few words the target of science about porous systems: create materials with empty spaces inside to use their cavities. Porous materials are well known since a long time and used for different applications, such as filtration, liquid adsorption and so other. During research and evolution of new porous systems a better control of pore size, a decrease of pore diameter and a well-organized structure are necessary to increase base properties. If pore diameter have nanometric dimensions, we can speak of *nano*porous materials. Nanoporous materials have unique surface, structural and bulk properties that enhance their application in various fields such as ion exchange, separation, catalysis, sensor, biological, molecular isolation and purification.[1]
In this chapter we will speak about classification, synthesis and the study of this type of systems; what are the general applications in common devices and what are the research perspectives about these materials.

1.1 Definition of pores and porosity

There are two main kinds of pores: closed pores and open pores. Closed pores are empty spaces completely immersed in bulk material, without communication with the external ambient. Materials with closed pores are useful in sonic and thermal insulation, or as lightweight materials for structural applications. Open pores, instead, are connected with material surface and are used for separation, catalysis and sensing applications.[1] In the case of open pores, nevertheless, we must do a necessary distinction between pores and surface roughness. By definition, an open pore is more deep than large, while surface roughness are larger and more diffused on the surface than deep. Concerning properties of porous materials, contribution of roughness is normally not considered.

To make a first and quick distinction between different porous systems, it is useful to considerer porosity parameters: such as the ratio between the pores volume and the total material volume. Generally, porous materials have porosity between 0.2 and 0.95.[2]
In this thesis we will discuss about systems with open pores, since the main work is focused on interaction between the porous system and other molecules diffusing from outside.

1.2 Classification of nanoporous materials

There is a large variety of nanoporous materials, with many different properties, structures and applications. To classify these systems in general groups we can make a distinction about pore diameter dimension, the type and the structure of pores, the nature of material that form pore walls or their macrometric aspect. Each classification focuses the attention on a specific characteristic and, usually, they are independent by the others.
In the next paragraphs we will discuss separately different kinds of classification, and in particular those concerning pore size and structure.

1.2.1 Classification by pore dimensions

The useful way to classify a nanoporous material is by the diameter size of their pores, because most of properties, interesting for applications of adsorption and diffusion, are dependent by this parameter. The prefix *nano-* means a typical dimension between 1 and 100 nm. In this range material properties change drastically, overall for interaction and diffusion when materials interact with other molecules. In fact, pore diameter establishes what is the bigger molecule that could diffuse inside the material and the comparison between pore size and guest molecule dimension gives an idea about diffusion and interaction properties. If the two dimensions are similar we can expect that molecule-wall interactions will be prevalent respect to molecule-molecule interaction. By the other way, if guest molecules are smaller than pore size, there will be both molecule-wall than molecule-molecule interactions during the diffusion process.

Accord to IUPAC definition[3], nanoporous materials are classified in three main groups depending on their pore dimension (d):

- **Microporous materials (d<2 nm):** These materials have very narrow pores. They can host only small molecules, such as gases or linear molecules, and generally show slow diffusion kinetics and high interaction properties. They are generally used as gas purification systems, filtering membranes or gas-storage materials.
- **Mesoporous materials (2<d<50 nm):** These materials have pores with diameter enough large to host some big molecules, for example aromatic systems or large polymeric monomers. Diffusion kinetic of adsorbed molecules is often due to capillarity, with a initial interaction with pore walls followed by pore filling. These systems can be used as nano-reactors for polymerization or adsorbing systems for liquids or vapours.
- **Macroporous systems (d>50 nm):** Pores of these materials could host very large molecules, such as polyaromatic systems or small biological molecules, and interactions with pore walls are often secondary respect to interactions with other molecules, overall in case of very small guest molecules. These material are principally used as matrices to store functional molecules, as scaffolds to graft functional groups, such as catalytic centres, and as sensing materials thanks to the quick diffusion of chemical species in the pore system.

By this definition, it seems that porous material have all pores of the same dimension. In real systems, however, pores have not all the same pore diameter, it could change along pore shape, for example in complexes pore structures, or the material could have two groups of nanopores with different dimensions. In the first case, the general procedure is to use a medium parameter, otherwise the bimodal distribution must be specified. Pore diameter could be calculated in different ways. A direct method is to use a mercury porosimeter, that use infiltration of liquid mercury, under a controlled pressure, inside pore system to estimate total pore volume, mean pore diameter and, in case of powders, mean particle size. This method, however, is not applicable to samples with low mechanical resistance because of the great applied pressures. Indirect methods are mathematical models applied on nitrogen adsorption isotherms. These models, such as

Barrett-Joyner-Halenda (BJH) or Dubinin-Radushkevich equation, calculate pore diameter considering pores with defined geometric shape and analyzing adsorption curve.[4] For a more detailed discussion about these methods we remand on the Appendix part.

1.2.2 Classification by dimensionality

In nanoporous materials pores have not necessary *spherical* shape. Empty spaces could be structured in isolated cages, in parallel channels, in complex three-dimensional structures and so other, as illustrated in figure 1.1:

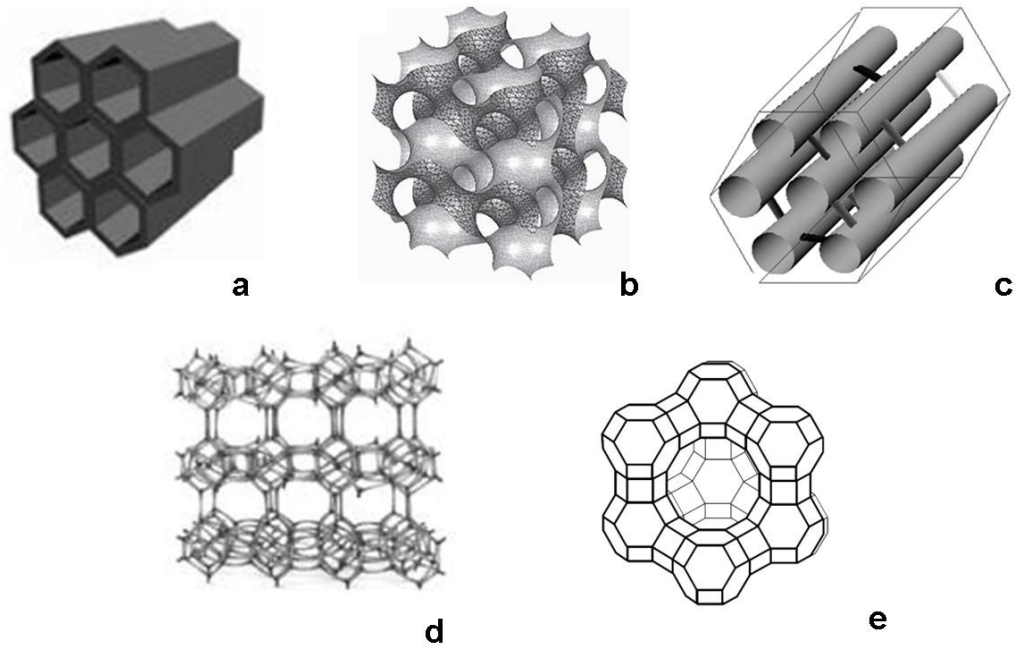

Figure 1.1

Examples of porous structures: linear, parallel channels (a), three dimensional interconnected pores (b), channels with secondary interconnections (c), three dimensional cage (e) and single cage systems (e) [5,6]

It means that not all pore dimension must be nanometric. For example, considering materials with cylindrical channels, the length of a single channel could be of few microns, bigger than nanometric range.

Considering the three dimensions, we can classify each system by the number of dimensions that are not in the nanometric range:

- **0-dimensional systems:** in these materials pores have all three dimensions in nanometric range and, often, have spherical shapes and are directly connected with the external ambient. They are generally used to store single molecules, stabilized inside cavities by three-dimensional interactions with the walls. An example of this type of materials are zeolites.
- **1-dimensional systems:** these materials are formed by parallel channels of micrometric length, often organized in regular patterns (such as hexagonal). Channels could be straight or curved, isolated or communicating, but generally they retain the same pattern along all the material. Materials with nanochannels could be used as nanoreactors, as diffusion systems in purifying membranes or for gas storage. An example of this type of systems are porous organic self-assembled materials such as dipeptides or silica structures such as MCM-41.
- **2-dimensional systems:** with two dimensions over the nanometric range, these materials are constituted by large lamellae of nanometric thickness, often separated by pillars to avoid collapsing of the structure. Main applications of these materials are intercalation with other materials, like ions in electrical devices, or cracking of molecules. Typical materials belonging to this group are nanostructured clays.
- **3-dimensional systems:** the materials of this group are constituted by complex structures of channels and/or cages interconnected to create a three-dimensional structure. They are mainly used as storage systems or as scaffolds to obtain porous materials in metal or carbon by negative replica-shape effect. Examples of this group are numerous three-dimensional structures in silicon or metal oxide.

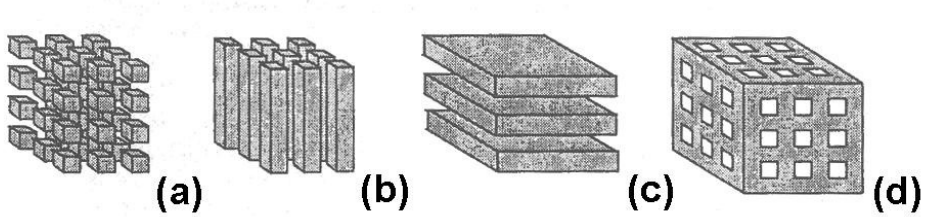

Figure 1.2

Scheme of low-dimensional systems:

0-dimensional (a), 1-dimensional (b), 2-dimensional (c), 3-dimensional (d) [7]

The number of nanometric dimensions influences materials properties due to geometry of the system. In fact, materials with only one or two nanometric dimensions are anisotropic and mechanical, transport and reactivity properties are different in the three spatial directions. Low dimensional systems could be used for their anisotropy.[5] For example, monodimensional systems could be used as tubes or cables for molecular transport, when bidimensional structures are more common systems for ion or molecular intercalation.

These methods to classify nanoporous systems reported in literature are valid for each type of material. Other distinction are based on the nature of pore walls or the macrometric shape of samples.

1.2.3 Classification by chemical composition

Nanoporous materials could posses very different chemical nature. In literature are reported examples of nanoporous metals, organics, polymers, carbons and so other.

A classification of these systems by chemical nature of pore walls is difficult, due to the large variety of constituent materials, but could give a first idea of chemical and mechanical properties of the sample. Nanoporous materials could be generally classified in organic, inorganic and hybrid porous systems.[6]

Organic systems are often aggregates of molecules stabilized by hydrogen bonds or Van der Waals interactions to form a regular structure with specific empty spaces inside. They are employed overall for their specific interactions with other organic molecules and their mechanical and thermal resistance is generally small.

Inorganic nanoporous structures are characterized by a large number of covalent bonds and are chemically and thermally very stable. They do not show specific interactions with a particular kind of molecules and are generally utilized for their great mechanical properties that make them good support structures.

Hybrid materials, finally, are both chemically and thermally stable as inorganic systems, but with possibility to use a large variety of functional organic groups as reaction centres or adsorbing devices.

1.2.4 Classification by macrometric aspect

Nanoporous systems could be obtained in an incredible variety of macrometric forms, such as powders, thin films, monoliths or small particles.[6]

Properties of nanoporous systems are influenced by this aspect as well as the nanostructure they possess. Monoliths, as example, show very high mechanical properties, but adsorption is limited by the number of pores open to the surface respect to the total pore volume. By the other way, powders present a large number of openings and adsorption is faster, but their mechanical properties are influenced by the small size of the grain.

Macrometric aspect is very important for integration of porous systems into functional devices. Thin films, for example, are suitable for sensors and actuators while small particles could be well packed in chromatographic columns.

1.3 Synthesis of nanoporous materials

To obtain a material with pores it is possible to follow two main ways:

1) Create empty spaces in a bulk material (top-down approach)
2) Synthesize the material with empty spaces already inside (bottom-up approach)

1.3.1 Top-down approaches

With this approach we start from a bulk material, poreless, and we create empty spaces by physical or chemical etching.

Because this technique is similar to ancient lithographic procedures, but reduced until nanometric level, it is often called “nanolithographic” method.[8] Physical etchings are realized by ablation with focused lasers, electron or ion beams.[9] By this way we can estimate the deepness of pores with an high degree of precision, because it is possible to calculate ablation rate for each material with few experiments; however the obtained pores are often larger near the surface and there could be limits of precision to perform successive ablations at short distances on the same sample, due to mechanical sensibility of the instruments.

Chemical etchings, instead, are obtained by corrosion of the material with an opportune substance (acid, base or other solvents). To avoid an uniform ablation of the surface, the

material must be covered with a mask, resistant to chemical etching, with nanometric pores to let etching be effective where necessary.[10] With this procedure we can obtain different patterns of pores, simply changing the pattern of resistive mask, but we don't have complete control of penetration rate, depending on external factors such as solvent concentration or temperature, and, if the material is not perfectly homogeneous, the obtained pores could have irregular shapes.

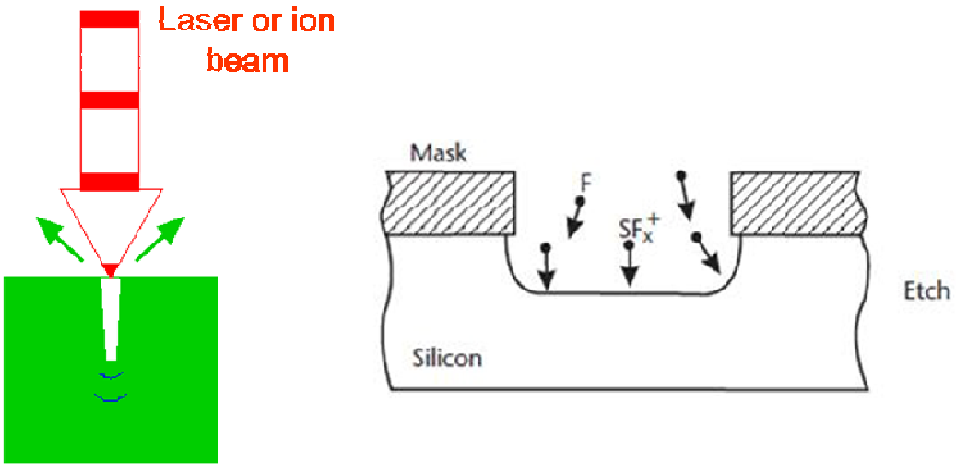

Figure 1.3

Schematic representation of physical (left) and chemical (right) etching process [9,10]

A great limitation of top-down methods is that pores are obtained starting from the surface, so they could assume only spherical or cylindrical shapes, without possibility of controlled secondary interconnections. These approaches have the great disadvantage to be generally expensive, because high-technological instruments or especial realized masks, there is not complete control of pore shape and deepness and overall it is not completely effective on certain materials, such as polymers or some metal oxides.

Nevertheless, by these processes it is possible to realize a pore pattern directly on a device ready to be assembled in an apparatus, avoiding purification or post synthesis treatments typical of bottom-up synthetic methods.

Top-down processes are ideal for pure bulk materials, such as metals or semimetals, that are difficult to obtain in highly purity with chemical methods. An example of material obtained with this method is porous silicon.[11] Silicon surface, covered with a polymeric mask, is exposed to an oxidative solution of Nitric and Hydrofluoric acids. This solution

etches bulk silicon creating a series of parallel linear pores perpendicular to the surface. After an established time, generally few minutes, etching solution is removed, the sample washed with water, dried and the polymeric mask removed with organic solvents. The obtained material shows interesting fluorescent properties and could be used for post-synthesis treatments to obtain functional devices such as gas sensors.

1.3.2 Bottom-up approaches

Bottom-un approaches are principally based on chemical methods, in which material precursors arrange or react to form the porous nanostructure. Empty space could be generated in two main ways: precursors self-assemble themselves in a regular and porous supramolecular structure, or they condense around specific molecules, named templatings, that, once removed, leave the pore space.

In the first case structure stability is due to weak intramolecular interactions, such as hydrogen bonding, Van der Waals forces or dipole-dipole interactions.[12] Empty spaces are generated because precursors dispose themselves in particular conformations, to maximize interactions with other molecules, and the resulting structure shows a well-defined porosity. These systems are relatively easy to obtain, just because they are auto-assembling, and properties like pore size or surface area are low sensitive to little fluctuations in synthesis conditions. To obtain supramolecular aggregates, the simplest way is the precipitation from oversaturated solution by slow cooling. The porous structure is obtained by filtration and solvent evaporation. With this method it is also possible to regenerate a damaged structure. Because there are not covalent bonding between precursor molecules, until the structure of precursor is not changed it is possible to re-dissolve the material and obtain a new system ready to use. Furthermore, some of these molecules could auto-assemble themselves in structures with different symmetry, depending on environmental conditions such as temperature or presence of determinate chemicals. Examples of these materials are organic compounds like urea and TPP, some families of dipeptides, and other biological molecules.[13]

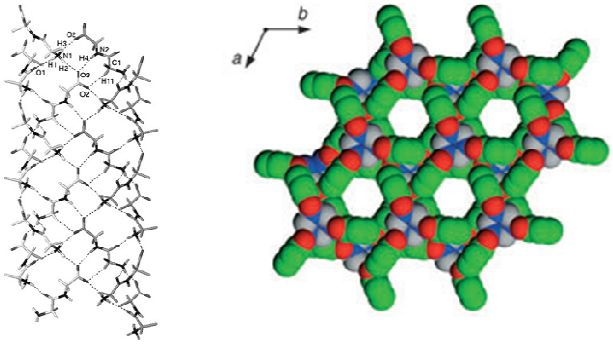

Figure 1.4

Examples of organic porous materials obtained by self-assembling: dipepitdes (left) and TPP (right) [13]

In template synthesis, instead, empty spaces are generated using a medium as scaffold.[14] This medium is named templating or structuring direct agent (SDA). A templating structure could be constituted by a large number of different materials, such as organic molecules, supramolecular aggregates, polymers or solid structures of silica or other oxides. During the synthesis, material precursors condense around the templating to create the final structure. Once terminated the condensation, templating is removed to leave the empty spaces, as indicated in figure 1.5:

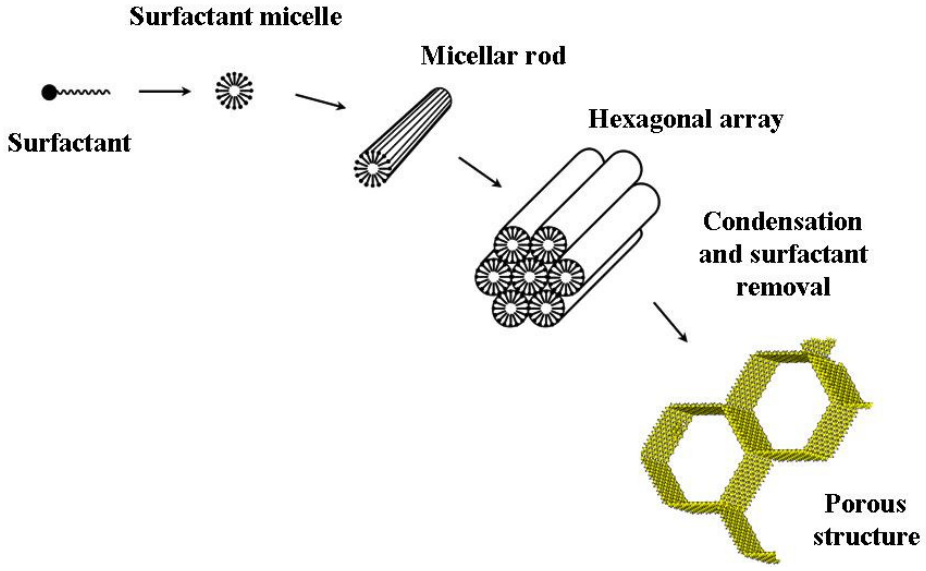

Figure 1.5

General scheme of template synthesis

Template synthesis presents the great advantage that interaction between SDA and final material is not specific and, by this, the same templating could be used in a large number of synthesis with different materials.[15] By the other way, templatings are sensitive to synthesis conditions and, sometimes, could assume a regular nanostructure only in determinate conditions of concentration, temperature and acidity.

1.4 Nanoporous materials properties and applications

Nanoporous materials have the following general characteristics:[1]

- High adsorption capacity: the very regular structure, high surface area and pore volume properties consent to nanoporous materials to be excellent adsorptive media for gases, vapors or, in some cases, small molecules.
- High selectivity: the narrow pore size distribution and specific interaction with pore walls make these systems ideal devices for mixture separation or ideal nanoreactors for confined chemical reactions.
- Favourable adsorption kinetics: large number of pore openings at the surface and regular pore structure consent a quick diffusion of guest species, that completely fill the material in relatively short time.
- Good mechanical properties: once formed, nanoporous materials are resistant to hurts and mechanical stresses, so they could be handled without fear to break porous structure.
- Stability and durability in use: nanoporous materials are stable in ambient condition and adsorption and desorption process are completely reversible. These materials can be used and re-used for long time without lost their properties.

A first, visible application is as gas or vapor adsorption systems. This is not limited only to storage systems, but also for environmental separation and for sensor applications.
In fact, nanoporous systems show great affinity to a large number of pollutant chemicals, such as nitrogen or sulphur oxides, and so they could be useful systems for sequestration of these substances from atmosphere.[16] Moreover, great surface area consents a quick interaction with gas phases, so those nanoporous systems with

conductive properties that change in presence of specific chemicals, for example by oxidation or reduction, they could be exploited as excellent chemical sensors.[17]

Narrow pore distribution, instead, makes nanoporous systems ideal filtering membranes or static media for chromatographic column separation.[18]

A regular structure with large surface area can be also used to disperse active catalytic centres or to interact with specific wavelengths for catalytic and photocatalytic applications.[19] A likewise application is the grafting of specific functional systems on pore walls or at pore opening to create a series of nanomachines, for example light activated open/closed system described in figure.[20]

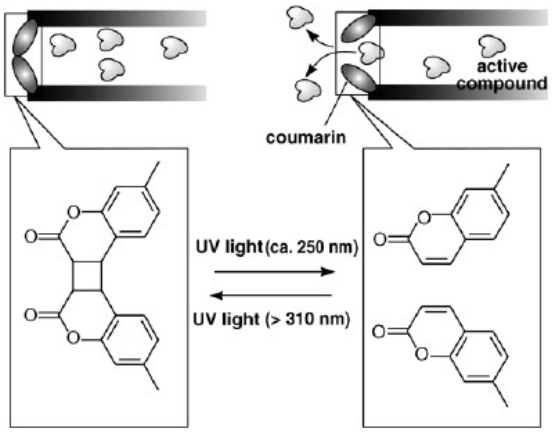

Figure 1.6

Light-activated open-close switch grafted on silica pores [20]

Pore space could be used also for confined and controlled chemical reactions.[21] In fact, restricted space can influence chemical reactions limiting the number of possible reactants or avoiding formation of specific configurations due to steric impedance. Pores could be used as nanoreactors to obtain polymers with high order degree and defined molecular weight or to perform enantiomeric reactions with the production of only one species.

Moreover, porous systems are also used as scaffolds to obtain porous materials with different nature by reverse replica effect.[22]

Last, but not least, we must consider that lot of porous systems, and in particular silica and organosilicas, are non-toxic systems and biodegradable media, so they could be used as drug delivery systems in biological applications.[23]

This is only a quick overview of application for porous systems because it is a very large field. Some of these have industrial application from long time, while other are still in project and experimentation.

1.5 Analysis techniques

There are different techniques to characterize nanostructured porous systems.

The following is only a short overview, for a better discussion we will remand to the appendices part.

For porous materials, most interesting results come from adsorption measurements. By adsorption of nitrogen at liquid nitrogen temperature it is possible, using mathematical methods such as BET and BJH, to estimate surface area and pore size distribution.[4] Adsorption of other gases or vapors at different temperatures, instead, give informations about material affinity with other chemical species and it is possible to estimate how much substance could be stored in a gram of sample.

To study regular pore structures two useful techniques are small-angle X-ray diffraction and transmission electron microscopy (TEM). The first technique is based on multiple reflections of X-rays due to periodic structures. Looking at the obtained diffractogram it is possible establish the structure geometry, typical distances and, by comparison of the results with adsorption data, we can estimate pore walls thickness. Electron microscopy consent to see directly the pore structure in an image. It is a useful technique, for example, to study possible defects in material or curvatures in the case of parallel nanochannels.

Thermal analysis and exposure to chemical reactants are used to study thermal and chemical stability, while electrical experiments show if the systems have conductive properties.

1.6 Mesoporous materials

The prefix *meso-* means "in-between". Of course, it means in-between of nanometric range, but in this case also in-between molecular and solid-state physic, in-between molecular and continuum approach, in-between covalent chemistry and micromechanical techniques.[24] Mesopores, in fact, are enough large to host more than one molecule in their cross-section, but not large enough to let bulk properties become major than surface interactions. By the other way, mesostructures are at half way between single molecules and extended structures, so their properties, mechanical, electrical and magnetic, are different from each of two extremes.

To obtain mesoporous objects we can speak of mesochemistry. Mesochemistry can be defined at first as the controlled generation of objects with characteristic features on the mesoscale by chemical reactions and principles specific for this level of molecular assembly.

Controlled generation can means:

- Control of size, shape, surface area and curvature of mesoobjects.
- Control of surface, interfacial chemistry and texture of pore walls.
- Control of morphology, arrangement and order of pores.
- Control of topological defects.

Two examples of mesomaterials are mesoporous silicas and periodic mesoporous organosilicas, that have pores of diameter size in the mesoscopic range.[20,25] These materials are obtained by template synthesis using a template process. The templating system is a supramolecular aggregate of amphiphilic molecules able to auto-organize themselves in regular structures once dissolved in water. These are a good example of minimal surface energy and mesochemistry, because during the reaction single molecular aggregates coalesce in more complex frameworks that, however, are not extended liquid crystal phases, but remain in the order of few nanometers and show interesting shapes that could be reported to minimal surface theory.[26] For a larger discussion of these macromolecular aggregates, we will remand of the next chapter.

Furthermore, during growth from the first seed, templatings show natural tendency to bend themselves in curved shapes that are very similar to biological form (i.e. shells or other bio-silica based apparatus) and this is another important point of mesoscale

properties, because growing objects don't extend in an infinite regular structure (bulk material), but make particles of well defined dimensions.

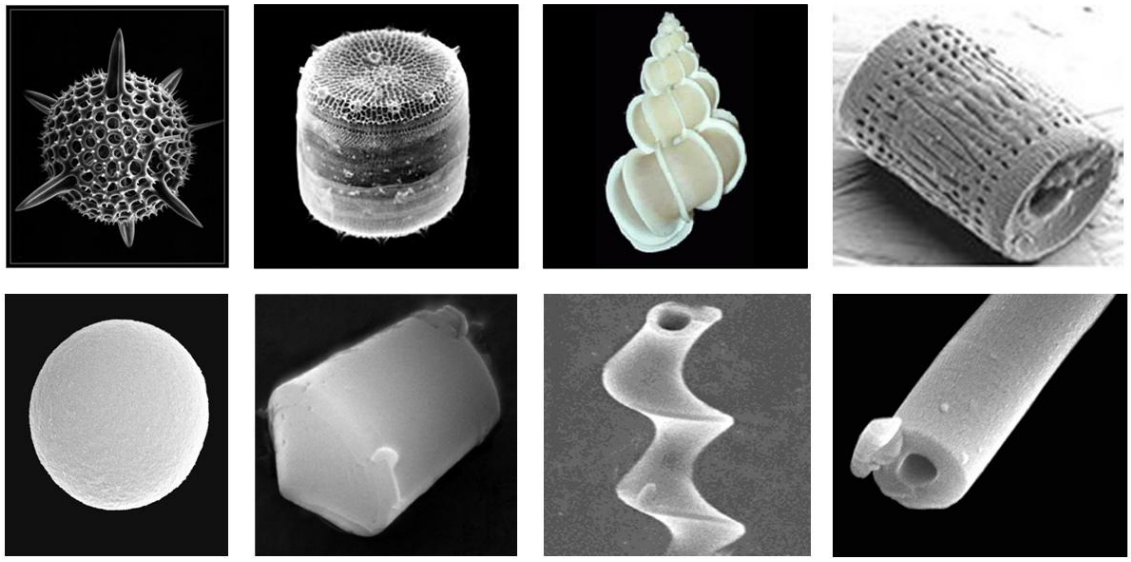

Figure 1.7

Comparison between biological structures (on the top) and silica meso-objects (on the bottom)

Mesoporous object have been used as nanoreactors for confined polymerizations or condensations.[27] In this case, the mesoscale is related to the single pore, because it can host more than one polymeric chain, but not enough to speak of bulk polymer. By this, obtained materials cannot show all polymeric properties, because some of these, such as glass transition, are due to a larger number of chains respect to those confined in a single cavity.

1.7 References:

1) a) G.Q. Lu, X. S. Zhao, *Nanoporous Materials, science and engineering*, Series of chemical engeneering, Vol.4, Imperial college Press, London, **2004**; b) H.S. Nalwa, *Handbook of Organic-Inorganic Hybryd Materials and Nanocomposites, Vol. 1*, American Scientific Publishers, North Lewis Way, **2003**

2) K. Ishizaki, S. Komareni, M. Nanko, *Porous materials-process technology and applications*, Kluwer Academic Publishers, Boston, **1998**

3) K.S.W. Sing, D.H. Everett, R.H.W. Haul, L. Moscou, R.A. Pierrotti, J. Rouquerlot, T. Siemieniewska; *Pure Appl. Chem.* **1985**, *57*, 603-619

4) F. Roquerol, J. Roquerol, K. Sing, *Adsorption by powders and porous solids*, Academic Press, London, **1999**

5) U. Müller, *Inorganic structural chemistry*, Wiley, New York, **1996**

6) G.A. Ozin, A.C. Arsenault, L. Cademartini, *Nanochemistry, A chemical approach to Nanomaterials 2nd ed.*, RCS Publishing, Cambridge, UK, **2009**

7) G. Pacchioni, *Lezioni di Chimica dello stato Solido,* I.S.U., Italy, **1999**

8) J.L. Balladore, M.Pyee, H. Camon, E. Bourdel, J.P. Martinez, N. Sekkaki; *Microelectronic Engineering* **1987**, *6*, 201-206; b) D.L.J. Vossen, J.J. Penninkhof, A. van Blaaderen; *Langmuir*, **2008**, *24*, 5967-5969

9) E. Skantzakis, V. Zorba, D.G. Papazoglou, I. Zergioti, C. Fotakis; *Appl. Surf. Sci.* **2006**, *252*, 4462-4466

10) a) P.C. Simpson, A.T. Wooley, R.A. Mathies; *Biomedical Microdevices* **1998**, *1*, 7-25; b) T. Corman, P. Enoksson, G. Stemme; *J. Micromech. Microeng.* **1998**, *8*, 84-87

11) L.T. Canham; *Appl. Phys. Lett.* **1990**, *57*, 1046-1048

12) J.M. Lehn, *Supramolecular Chemistry*, VCH editions, Germany, **1955**

13) a) C.H. Görbitz; *New J. Chem.* **2003**, *27*, 1789-1793; b) P.Sozzani, S.Bracco, A. Comotti, L. Ferretti, R. Simonutti; *Angew. Chem. Int. Ed.* **2005**, *44*, 1816-1820

14) W. Jones, C.N.R. Rao, *Supramolecular organization and material design*, Cambridge university press, Cambridge, **2002**

15) I. Soten, G.A. Ozin; *Current opinion in Colloid & Interface Science* **1999**, *4*, 325-337

16) R.T. Yang, *Adsorbents, Fundamentals and Applications*, John Wiley & Sons, Brisbane, **2003**

17) M. Urbiztondo, P. Pina, J. Santamaria; *Ordered Porous Solids* **2009**, 387-411

18) K.W. Gallis, J.T. Araujo, K.J. Duff, J.G. Moore, C.C. Landry; *Adv. Mater.* **1999**, *11*, 1452-1455

19) J.A. Cusumano, in *Perspectives in Catalysis*, ed. J.M. Thomas and K. I. Zamraev, Blackwell scientific publication, Boston, **1992**

20) a) F. Hoffmann, M. Cornelius, J. Morell, M. Froeba; *Angew. Chem. Int. Ed.* **2006**, *45*, 3216-3251; b) S. Angelos, E. Johansson, J.F. Stoddart, J.I. Zink; *Adv. Funct. Mater.* **2007**, *17*, 2261-2271

21) K. Moller, T. Bein; *Chem. Mater.* **1998**, *10*, 2950-2963

22) a) H. Yang, D. Zhao; *J. Mater. Chem.* **2005**, *15*, 1217-1231 b) M. Tiemann; *Chem. Mater.* **2008**, *20*, 961-971

23) a) S. Giri, B.G. Trewyn, V.S.Y. Lin; *Nanomedicine* **2007**, *2*, 99-111; b) W. Zhou, P. Gao, L. Shao, D. Caruntu, M. Yu, J. Chen, C.J. O'Connor; *Nanomedicine* **2005**, *1*, 233-237

24) M. Antonietti, G.A. Ozin; *Chem. Eur. J.* **2004**, *10*, 28-41

25) U. Ciesla, F. Schüth; *Microporous Mesoporous Mater.* **1999**, *27*, 131-149

26) Q. Huo, D.I. Margolese, G.D. Stucky; *Chem. Mater.* **1996**, *8*, 1147-1160

27) C.G. Wu, T. Bein; *Science* **1994**, *264*, 1757-1759

CHAPTER 2

Template synthesis

As explained in the previous chapter, a method to obtain nanostructured porous materials is to use a medium as removable scaffold to leave empty spaces in the material once removed at the end of the synthesis. This medium is called templating or structuring direct agent (SDA) and the process is commonly named template synthesis. In this process, the precursor of final material condenses around the SDA until formation of a stable structure. After this, templating is removed generating voids.

Due to the large variety and nature of templating systems it is possible to imagine a great number of possible porous geometries. Nevertheless, to obtain a nanostructured porous system it is necessary to observe these conditions:

- Interaction between precursor and templating must be enough stable to give precursor time to react and condense, but not too much stable to avoid template removal.
- Once removed the templating, resulting structure must be stable.
- During condensation, templating and precursor must create a regular structure.

Interactions between templating and precursor are very important, because a risk is to obtain two separated, non-interactive phases and, so, no pore formation.

In this chapter we will discuss about template synthesis process, focusing attention on types of interaction between templating and precursor, on different types of templatings and on what are the conditions that influence final structure. Amphiphilic molecules and crystal liquid phases are a particular class of surfactants used to synthesize large porous systems and, in particular, mesoporous silica. These templating agents are very sensitive to environmental conditions and we will discuss deeply on relationships between synthesis conditions and forms assumed by these systems, that are a key point to understand different structures formation.

2.1 Interactions between templating and precursor

As previously explained, there are different templatings and different precursors, but generally the types of interaction could be resumed in four principal categories:[1]

- **Electrostatic:** Both templating and precursor posses electrical charges. This interaction could be direct, if the two charges are of different sign, or mediated by a ion if the two charges have the same sign.
- **Hydrogen bonding:** Templating and precursor are neutral. Interaction is supported by hydrogen bonding or dipole-dipole interaction.
- **Hydrogen bonding/electrostatic:** In this case a neutral templating interact with a charged precursor with the help of an acid hydrogen or a basic hydroxyl group.
- **Covalent:** Templating and precursor are linked with a weak covalent bond, that is easy to break after synthesis.

Despite the type of interaction, however, this is localized on templating surface.

2.2 Templating systems

Templating systems are of different nature. They could be single molecules, supramolecular aggregates, ordered systems of nanoparticles or porous nanostructures.[2] Normally, there is a main distinction in hard templatings and soft templatings.

Hard templatings are constituted by oxides, polymers or metals and possess a defined shape that is independent from environmental conditions. Generally, they are in form of solid particles or regular porous structures. The precursor of the new material diffuses between particles or inside pores and, once condensed, hard templating was removed by chemical etching or thermal degradation. These structures are already nanostructured, in the case of porous systems, or could create regular patterns in certain conditions (slow decantation, electrical or magnetic alignment). Typical examples of hard templatings are polymeric nanospheres to obtain opals or mesoporous silicas to synthesize porous carbon structures.[3,4] A key step in porous materials production using hard templatings is the precursor diffusion in templating pores or in empty spaces between particles. Material precursor must be homogeneously distributed in all the structure to avoid formation of bubbles or empty spaces that will be traduced in undesired voids in the final material. Hard templatings present the great advantage to have defined structure,

independent from synthesis conditions. This means that they could be used in a large number of synthesis with conditions of strong acidity or basicity, higher temperatures or for reactions without solvent. Moreover, because the final material is generated in regular empty spaces, it is possible to predict the final material structure.

Soft templatings, instead, are generally constituted by organic molecules or block copolymers.[1,5] The principal characteristic of these molecules, also named surfactants, is the ability to assume a defined conformation in solution until creation of a very regular structure. Final structure is influenced by solution parameters such as concentration, temperature or pH.[6]

Concerning the synthesis of porous structures, until now it is not fully understood if these regular structures in solution are obtained by a strict cooperation between surfactant and precursor or if the precursor limits itself to condense around a pre-existent liquid crystalline phase of surfactant. Once obtained the final material, surfactant could be removed by washing or thermal degradation. Common types of soft templatings are ammonium salts, amphiphilic molecules with polar heads and long hydrophobic chains, and block copolymers. Soft templatings present the great advantage to conduct the synthesis by an auto-assembling process, so diffusion problems are avoided. They are easy to use and the final structure could be finely tuned controlling solution conditions. However, each surfactant assumes specific configurations and they are not always predictable. A particular class of surfactants, amphiphilic molecules, has been object of numerous works intended to understand relation between synthesis conditions and final structures.

2.3 Surfactant structures

The word surfactant is an abbreviation to indicate “surface active molecules”.

This type of molecules are, generally, amphiphilic molecules with hydrophilic and hydrophobic parts in their chemical structure. Typical examples are quaternary ammonium salts with long alchilic chains and block copolymers with hydrophilic and hydrophobic groups. In solution, these molecules show natural tendency to auto-arrange in complex supramolecular structures with the target of minimize the total energy.[7]

Figure 2.1

Examples of surfactant structures. From left to right: disordered micellar rods, hexagonal-packed micellar rods, three-dimensional structures and lamellar structures [7]

System total energy could be considered formed by two distinct interactions: one is between surfactant and solvent, the other is between the surfactant molecules themselves. Each molecule, interacting with the solvent, is subjected to two energy contributions: one that stabilizes the systems and another that brings to system destabilization. Since stabilizing contribution is given by the molecule part that is affine to the solvent nature (hydrophilic for aqueous solutions and hydrophobic for organic solvents), surfactant shows a natural tendency to expose to the solvent the affine part, avoiding contacts with the other one. Interaction of surfactant with itself follows similar concepts: by interaction of parts with the same polarity energy system is stabilized, while interaction of different parts produces destabilization. Because of this, surfactant molecules tend to form a separated phase system, with hydrophilic and hydrophobic zones.

Generally, these systems are used prevalently in aqueous solutions. In the following discussion we will considerer the specific case of polar solution, with hydrophilic heads put in contact with solvent and apolar groups segregated in limited spaces.

Considering both the two contributions, polar surfactant solutions show complex structures such as micelles, vesicles and liquid crystal phases.[6]

An important characteristic of these structures are the minimal energy surfaces.

In literature, there is a large number of works about mathematical models to understand and rationalize these surfaces starting from surfactant geometry, interaction forces and ambient conditions.[8] These calculations are very complexes and they are not the aim of this work, so are here reported only general conclusions useful to understand micellar shape formation.

In fact, surfaces could be expressed with curves and planes in a simply model. We can imagine three-dimensional space as divided in small cubic portions. Each of these could be filled with aqueous solution or organic substance, with surfactant as a barrier between the two phases. Considering groups of eight cubes with faces in contact, there are three principal cases of interest:

- Four connected cubes are organic and four aqueous: in this case surfactant surface is a plane (h).
- Two consecutives cubes are organic and six aqueous (b). Surfactant surface forms an edge and could be expressed by a mean curvature H:

$$\langle H \rangle = \frac{\sum(+d) - \sum(-d)}{4d\sum(0)}$$

  where Σ(±d) denotes the areas of parallel surfaces ad a distance d on the either side of the interface and Σ(0) the area of interface.
- Only one cube is organic and other seven are aqueous (a). Surfactant surface is in this case a corner and its curvature could be approximated with a Gaussian curve K:

$$\langle K \rangle = \frac{\pi/2}{3\varepsilon^2/4} = \frac{2\pi}{3\varepsilon^2}$$

  where ε is the cube edge length.

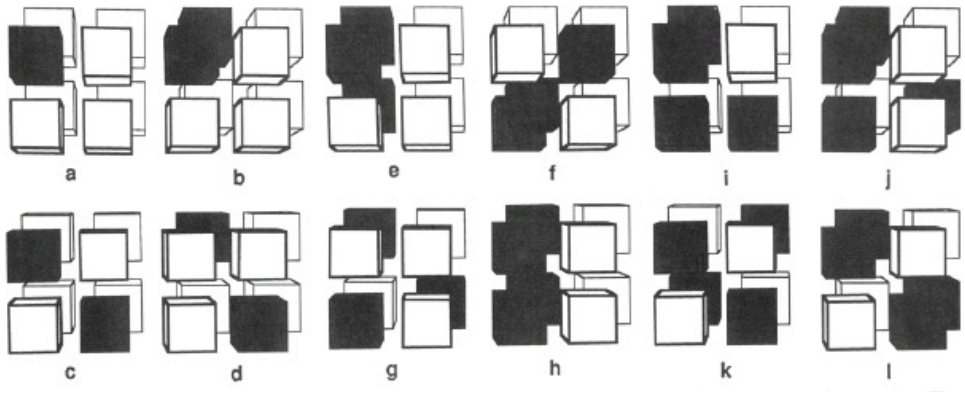

Figure 2.2

Schematic representation of possible configurations of eight cubes for contact.
In the figure white cubes are aqueous media, while black ones are organic phase [9]

As illustrated in figure 2.2, there are also other possible combinations of aqueous and organic cubes. Nevertheless, they could be retraced to the three described cases or have more organic than aqueous parts, and this is far from our real case of diluted surfactant solutions. For these reasons other geometries will not be considered in this discussion

Once fragmented total surface in planes, mean and Gaussian curvatures, we can approximate organic phase as small and express final curvature basing on geometrical characteristics of surfactant molecule.[9] At this point, it is useful to condense all the geometrical characteristics in one single number, named "surfactant parameter".

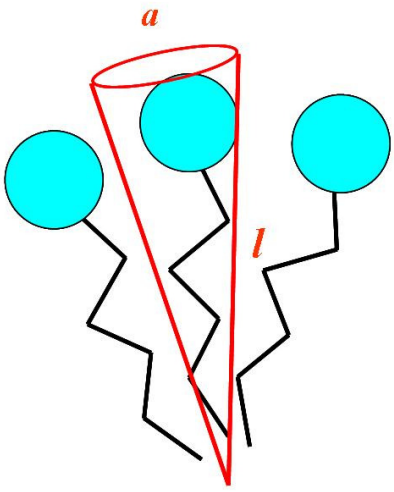

Figure 2.3

Scheme of surfactant molecules

This parameter relate the total molecular volume (v) with the alchilic chain length (l) and polar head area (a) in the following ratio:

$$S = \frac{v}{al}$$

Once determined the surfactant parameter for a specific molecule, we can use the final relation:

$$S = 1 \pm Hl + \frac{Kl^3}{3}$$

to express surface curvature of surfactant structure in terms of simply mathematic curves.[10]

This could be an approximate model, but it is useful to predict structural changes during environment modifications. In fact, supramolecular structures are sensitive to external conditions such as concentration, temperature and pH. Effects of single conditions could be integrated in surfactant parameter.[11] Effects of concentration and temperature could be seen in molecular volume and chain length. Increasing concentration, molecules are more strictly packed, so volume and length tend to decrease, while increasing temperature produces a faster molecular motion, so the same parameters increase. Instead, the pH affects overall polar head area. Changes in solution polarity, brings to different electrostatic interactions and to changes of effective polar area. Studying all these relationships, it is so possible to trace a phase diagram, that relates surfactant structure with solution parameters, for each surfactant molecule.

An example of surfactant phase diagram is illustrated in figure 2.4:

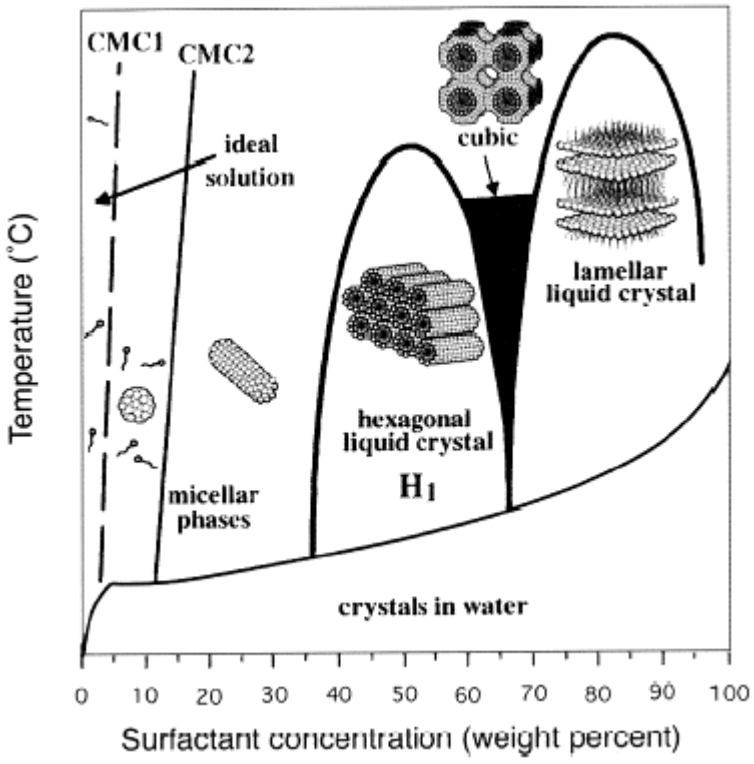

Figure2.4

Phase diagram of hexadecyltrimethylammonium surfactant [12]

This model is valid for most of ammonium salts with long alchilic chains and copolymers with only one polar block linked to a long apolar group, while is not good

for block copolymers with more than one polar group. In case the model cannot be applied to a specific templating, it is possible to study and create a phase diagram performing different experiments on a small scale.

Phase diagrams are useful instruments to predict the liquid crystal structure and help to choose opportune synthesis conditions.[12] Nevertheless, it is necessary to take in consideration also interaction with material precursor.

Polarity of molecules and their dimensions could influence the supramolecular structure changing synthetic parameters.

To bring a practical example: organic precursors are apolar molecules, showing the preference to stay in an hydrophobic phase, so they can interact with surfactant hydrophobic tails changing molecular volume and, by this, change final surfactant structure.

Because there are numerous surfactants and precursors, often the simplest way to solve the problem is perform a series of small experiments to directly check the final structure. Moreover, the interaction between precursor and surfactant can also influence the condensation step, introducing a number of defects that are reflected in pore wall regularity and smoothness.[13]

Interaction of surfactants with silica and organosilica precursors, however, have been deeply studied and discussed in literature, due to the large number of structures and shapes that these materials could assume.

2.4 Interactions between surfactants and siloxanes or organosiloxanes

Mesoporous silicas and organosilicas are generally synthesized with quaternary ammonium salts or block copolymers as Structuring Direct Agents.[14]

Both of these materials are obtained by condensation of silanols (SiOH groups) by acid or basic catalysis. Common silica and organosilica precursor are silicates and organosilicates (SiOR groups, where R is an organic group like methyl or ethyl), because silanol groups are extremely reactive ant tend to auto-condense due to the presence of water in atmosphere, so SiOR groups are hydrolyzed directly during the synthesis in presence of acid or base. These external organic groups make precursors hydrophobic, so at the beginning of the reaction they are dissolved in the apolar phase

created by surfactant alifatic chain. This step is very important, because surfactant helps to solvate material precursor to obtain an homogeneous dispersion. In fact, synthesis performed without the presence of surfactant, projected to obtain poreless structures with the same synthetic conditions, are limited by creation of separated phases, where material precursor cannot react because it is not in contact with the acid or the base.

After hydrolization, precursor polarity changes and, interacting with templating polar heads, start to condense and to form the final structure. Acid or basic conditions are determinant parameters, because they heavy influence regularity of final structure. From what we have said until now, we can separate material synthesis in two separated processes:

1. Hydrolization of silica precursors to form hydroxy silanes (silanols).
2. Condensation of silanol groups by water elimination.

These two processes are quite independent and could proceed at different rates. To obtain regular structures it is necessary to give time to hydrolized precursors to condense with the more stable geometry, so it will be better to have a large number of free silanols that condense slowly. PH of the solution change drastically rates of the two processes, in particular basic conditions favour hydrolization process, when acid environment increase condensation speed. By these simply considerations, we can deduce that structures obtained in basic conditions have more time to condense in a regular arrangement of bonds, when acid synthesis bring to a structure quickly condensed and with a certain number of defects. In some cases, such as in extreme basic conditions, could also happens that condensation process is so inhibited that there will be any formation of solid particles.

As previously explained, furthermore, interaction with polar heads is an important parameter for the final material, because it could influence pore size and crystal-like pore walls. By now, in fact, one could think that pore size depends only by surfactant tail length, the longer the tail, the greater the pore diameter, nevertheless there are other factors that must to be considered, such as synthesis conditions and nature of the surfactant.

Possible interactions in aqueous solutions are different, but they could be resumed in three main classes that are illustrated in figure 2.5.[1]

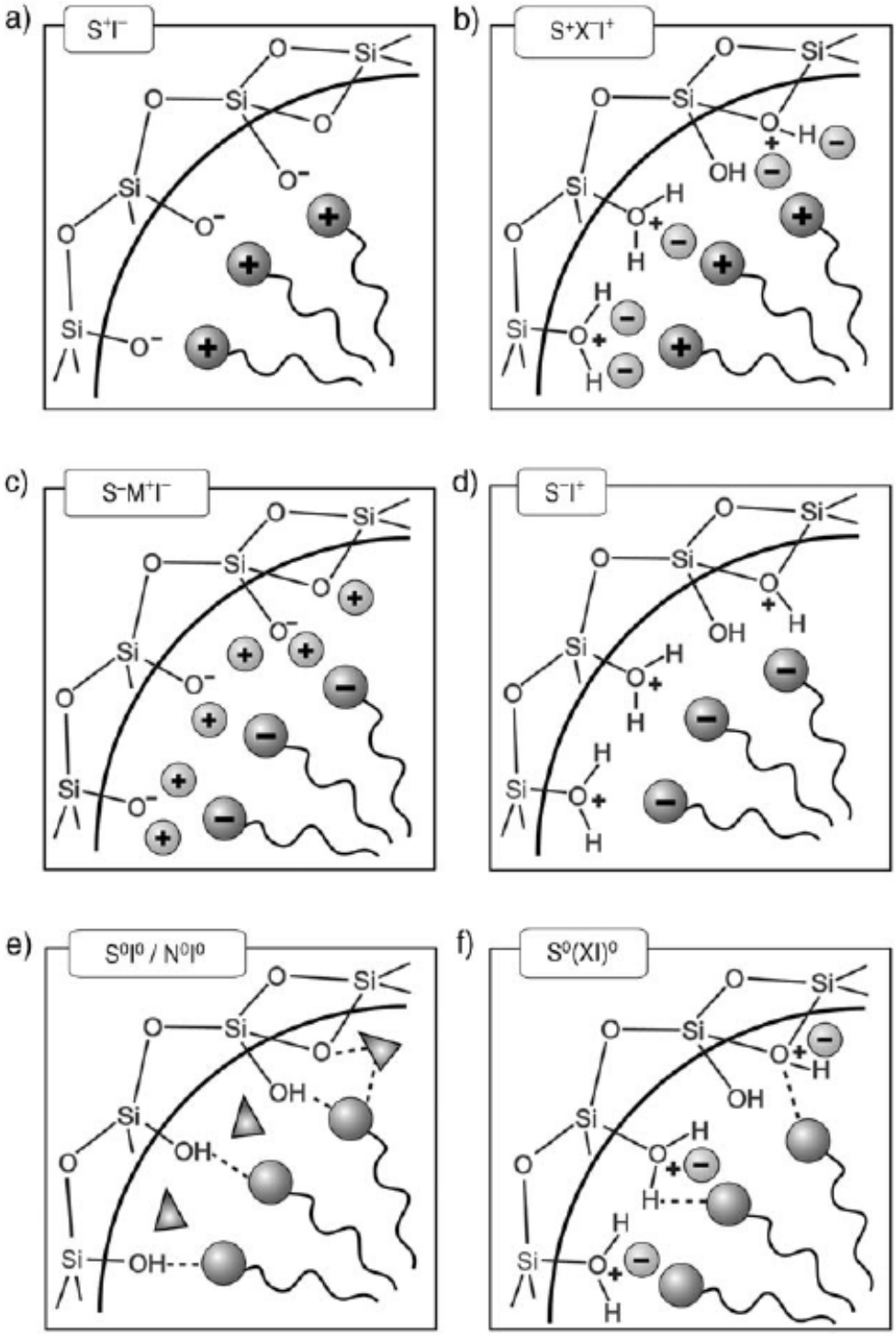

Figure 2.5

Interactions between surfactant polar heads and silica precursors during condensation: direct electrostatic interaction (a,d); mediated electrostatic interaction (b,c); neutral interaction (e) and mixed neutral-electrostatic interaction (f)[1]

- **Direct electrostatic interactions (S^-I^+ or S^+I^-):** Surfactant and silica precursor are charged, with opposite sign, and interact by electrostatic forces. Pore size is determined by alchilic chain length and pore walls are generally smooth and without large defects.
- **Mediated electrostatic interactions ($S^+X^-I^+$ or $S^-M^+I^-$):** Because surfactant and silica precursor are charged with the same sign, electrostatic interaction needs the presence of an ion of opposite charge as intermediate (often it is the counter ion of ammonium salt). In this case pore size depends from surfactant length and ion dimensions and pore walls, cause not perfect distribution of counter ions, sometime are rough and present defects.
- **Neutral interactions (S^0I^0):** Interaction is supported by hydrogen bonding, dipolar or Van der Waals forces, without effective charges. Pore size depends principally by surfactant dimensions, little differences and small defects could be due to interposition of water molecules clusters.

These are main types of interactions between template and precursor. However, other synthesis conditions, such as temperature or acidity, could influence interaction forces and bring to a little changes in pore diameter or structure regularity.

2.5 References:

1) a) Q, Huo, D.I. Margolese, U. Ciesla, P. Feng, T.E. Gier, P.Sieger, R. Leon, P.M. Petroff, F. Schüth, G.D. Stuky; *Nature* **1994**, *365*, 317-321; b) Q, Huo, D.I. Margolese, U. Ciesla, D.G. Demuth, P. Feng, T.E. Gier, P.Sieger, A. Firouzi, B.F. Chmelka, F. Schüth, G.D. Stuky; *Chem. Mater* **1994**, *6*, 1176-1191; c) P.T. Tanev, T.J. Pinnavaia; *Science* **1995**, *267*, 865-867; d) P.T. Tanev, T.J. Pinnavaia; *Chem. Mat.* **1996**, *8*, 2068-2079; e) S.A. Bagshaw, E. Prouzet, T.J. Pinnavaia; *Science* **1995**, *269*, 1242-1244; f) E. Prouzet, F. Cot, G. Nabias, A. Larbot, P. Kooyman, T.J. Pinnavaia; *Chem. Mat.* **1999**, *11*, 1498-1503; g) D. Zhao, L. Feng, Q. Huo, N. Melosh, G.H. Fredrickson, B.F. Chmelka, G.D. Stucky; *Science* **1998**, *279*, 548-552; h) D. Zhao, Q. Huo, L. Feng, B.F. Chmelka, G.D. Stucky; *J. Am. Chem. Soc.* **1998**, *120*, 6024-6036; i) S.A. Bagshaw, T. Kemmit, N.B. Milestone; *Microporous and Mesoporous Materials* **1998**, *22*, 419-433; j) D.M. Antonelli, J.Y. Ying; *Angew. Chem. Int. Edit. Engl.* **1996**, *35*, 426-430; k) D.M Antonelli, A. Nakahira, J.Y. Ying; *Inorg. Chem.* **1996**, *35*, 3126-3136; l) M.S. Wong, J.Y. Ying; *Chem. Mat.* **1998**, *10*, 2067-2077

2) a) W. Jones, C.N.R. Rao, *Supramolecular organizationand material design*, Cambridge university press, Cambridge, **2002**; b) H.S. Nalwa, *Handbook of Organic-Inorganic Hybryd Materials and Nanocomposites, Vol. 1*, American Scientific Publishers, North Lewis Way, **2003**

3) M.C. Orillal, N.M. Abrams, J. Lee, F.J. DiSalvo, U. Wieser; *J Am. Chem. Soc.* **2008**, *130*, 8882-8883

4) R. Ryoo, S.H. Joo, M. Kruk, M. Jaroniec; *Adv. Mater.* **2001**, *13*, 677-681

5) D. Myers, *Surfaces, interfaces and Colloids: Principles and applications* 2nd edition, Wiley-VCH, **1999**

6) a) Q. Huo, D.I. Margolese, G. D. Stucky; *Chem. Mater.* **1996**, *8*, 1147-1160; b) W.M. Gelbart, A. Ben-Shaul, D. Roux, *Micelles, Membranes, Microemulsions and Monolayers*, Springer, New York, **1994**

7) a) G.A. Ozin; *Canadian Journal of Chemistry* **1999**, *77*, 2001-2014; b) M.D. Ward, M.J. Horner; *Cryst. Eng. Comm.* **2004**, *6*, 401-407

8) a) S.T. Hyde; *J. Phys Chem* **1989**, *93*, 1458-1464; b) N. Gov, I. Borukhov, D. Goldfarb; *Langmuir* **2006**, *22*, 605-614

9) S.T. Hyde, I.S. Barnes, B.W. Ninham; *Langmuir* **1990**, *6*, 1055-1062

10) Y. Talmon, S. Prager; *J. Chem. Phys.* **1978**, *69*, 2984-2991

11) W. Ying, D. Zhao; *Chem. Rev.* **2007**, *107*, 2821-2860

12) a) S.T. Hyde; *Langmuir* **1997**, *13*, 842-851; b) A. Khan; *Current Opinion in Colloid & Interface Science* **1996**, *1*, 614-623 c) C.J. Brinker, Y. Lu, A. Secunger, H. Fan; *Adv. Mater.* **1999**, *11*, 579-585

13) S. Che, S. Lim, M. Kaneda, H. Yoshitake, O. Terasaky, T. Tatsumi; *J. Am. Chem. Soc.* **2002**, *124*, 13962-13963

14) a) J.S. Beck, J.C. Vartuli, W.J. Roth, M.E. Leonowicz, C.T. Kresge, K.D. Schmitt, C.T.W. Chu, D.H. Olson, E.W. Sheppard, S.B. McCullen, J.B. Higgins, J.L. Shlenker; *J. Am. Chem. Soc.* **1992***, 14*, 10834-10843; b) S. Fujita, S. Inagaki; *Chem. Mater.* **2008**, *20*, 891-908

CHAPTER 3

Porous carbon

Porous carbon materials are diffused in many actual scientific applications. They are used, for example, as electrode materials for batteries, fuel cells and capacitors; as sorbents for separation processes and gas storage or as supports for different catalytic processes. Their use in such diverse applications is directly linked not only to their great physical and chemical properties, such as electronic and thermal conductivity, chemical stability and low density, but also to their wide availability.[1]

Carbon, in fact, could be easily produced by reduction of many organic compounds by heating at high temperatures in a non-oxidative atmosphere or by electrical-arc discharge.[2] Nevertheless, in last years many research groups on this field have focused their attention on the control of porosity and pore size of these systems, trying to obtain new structures, ever more regular, for industrial applications.

In this chapter we will illustrate some techniques to obtain regular porous carbon structures, from carbon precursors and the applications of these systems. A specific paragraph will be dedicated to graphitic-like carbons and their unique properties due to extended aromatic system.

3.1 Synthesis of porous carbon structures

Conventional porous carbon materials, such as activated carbon and carbons molecular sieves, are synthesized by pyrolysis of organic precursors, such as coal, wood, fruit shells or polymers, at elevated temperatures.[3] This process lets to obtain large amounts of carbon material and, at the same time, could be used to recycle certain types of wastes. Materials obtained by this methods, however, have relatively broad pore-size distribution in both micropore and mesopore ranges. Overall micropore presence should be a problem, since microporous carbons show slow mass transport of molecules, due to space confinements imposed by small pore size, low conductivity, caused by presence

of large surface defects, and collapse of porous structure during high-temperature treatments or graphitization.

To try a control of pore size distribution, different synthetic approaches have been hypothesized. Principal ways have been carbonization of carbon precursors composed of one thermosetting component and one thermally unstable component, carbonization of aerogels or cryogels, hard template synthesis through impregnation, carbonization and templating removal, and self-assembly using soft templatings through co-condensation and carbonization.[4-7] Among these ways, only last two bring to ordered structures with well-controlled mesopores and low microporosity.

Hard template methods use a regular nanostructure with free and accessible empty spaces that can be infiltrated with carbon precursor. After carbonization, this structure was removed to generate pores in the carbon material. About this method, that is a key point for this work and that is also called reverse replica effect, we will better discuss in the next paragraph.

Soft template methods, instead, use amphiphilic molecules aggregates. There are four key requirements to the successful synthesis of a mesoporous carbon material using this way:

- Ability of the precursor components to self-assemble in nanostructures.
- Presence of at least one pore-forming component and at least one carbon-yielding component.
- Stability of the pore-forming component that can sustain the temperature required for curing the carbon yielding component but can be readily decomposed with the least carbon yield during carbonization.
- Ability of the carbon-.yielding component to form a highly cross-linked polymeric material that can retain its nanostructure during the decomposition or the extraction of the pore forming component.

To satisfy all these requirements, generally block copolymer systems are used.[1] Block copolymers, in fact, can assume very regular nanostructures, could be synthesized using specific block for carbonization (i.e. polymers with hydro or amino groups) and, once assumed the specific configuration, it is possible to use different degradation

temperatures and spatial confination to generate mesopores. By this way, it is also possible to obtain mesoporous carbon films, useful for sensoring or capacitor systems.
Finally, in last few years, a new way is going to be deeply studied.
Because carbon could be obtained by every type of organic compound heated at a specific temperature in a non-oxidative atmosphere, hybrid materials are ideal candidates to obtain hybrid carbon-inorganic composites.
Aerogels and xerogels have been already mentioned as a unsatisfactory way to produce porous carbons. Their greatest defect is perhaps the non-ordered structure, that don't consent them to produce a well ordered carbon material.
Periodic mesoporous organosilicas, however, are very similar to these systems, but they have very regular mesostructure and are already porous. A few number of works about carbonization of PMOs are reported in literature.[8] By these works, it seems that after carbonization the mesostructure changes, but it is retained. Until now is not fully understood what happens during the carbonization, but there are experimental evidences that pore size and surface area of these new systems are very regular.

3.2 Hard Template synthesis, the reverse replica effect

As previously illustrated, hard template methods exploit a material able to assume a nanostructured shape with empty spaces inside as a sort of mould to obtain pores in the final carbon system, exactly like the ancient method to make jars with a piece of wood to retain the form.[9] Because the shape of the final carbon material is a sort of negative image of the starting material (see fig. 3.1), this process is also named reverse replica effect.

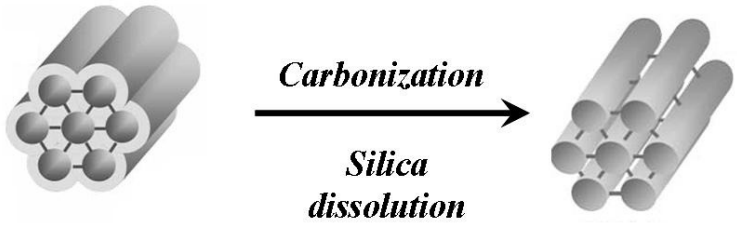

Figure 3.1
General scheme of reverse replica effect

The most used material as hard templating is probably silica. This is due to its great thermal stability, to the possibility to synthesize a large variety of silica nanostructures and to the easy method to dissolve silica with hydrofluoric acid without compromise carbon material. Silica could be used as uniform nanoparticles or as porous material.[10,6] In the first case, particles are let pack very close one with others to create a regular structure, and pore dimension of final material could be choose selecting particles diameter. Nevertheless, even using advanced techniques a limited number of packing defects could be introduced and, moreover, only honeycomb structure or similar can be obtained by this method.

The use of porous silica matrices, instead, consent to reply very different three-dimensional structures and these are generally very regular and with low number of defects. First example of mesoporous carbon obtained by reverse replica effect from a mesoporous silica matrix was reported in 1999 by Ryoo and co-workers.[11] In that work, they let diffuse in a three-dimensional porous silica matrix an aqueous solution of sucrose and sulphuric acid. After a carbonization process by heating over 900 °C in argon atmosphere, they dissolve silica frameworks to collect a carbon material with an XRD pattern similar to that of starting silica and surface area of about 1500 m^2/g.

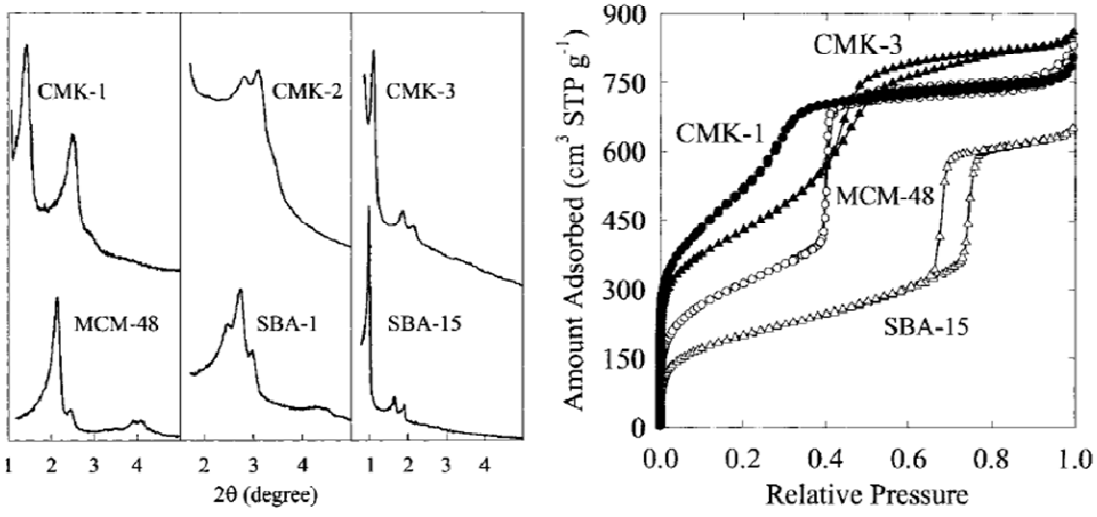

Figure 3.2

Comparison between XRD and Nitrogen adsorption of silica matrices and related porous carbons [11]

Starting from this first work, a large number of other groups try to use this method on a variety of silica matrices starting from different carbon precursors, such as sugars, organic molecules and polymers.[12]

Key point for the reverse-replica effect was the three-dimensional connection of matrix pores. More than one author, in fact, explains as a porous structure without interconnection between single pores, such as MCM-41 silica, cannot be a good templating for reverse-replica effect with carbon, because after silica dissolution, the resulting material collapses in a disordered carbon system. By this, common silica used are MCM-48 and SBA-15.[13] In these systems, in fact, two levels of porosity are present: one principal in the mesoscale and a second one in the microscale, that acts as a connection between the principal pores. During impregnation, both the pores are filled by carbon precursor and, after carbonization and silica removal, smaller carbon structures become pillars that link principal carbon components avoiding porous structure collapsing, as illustrated in figure 3.3:

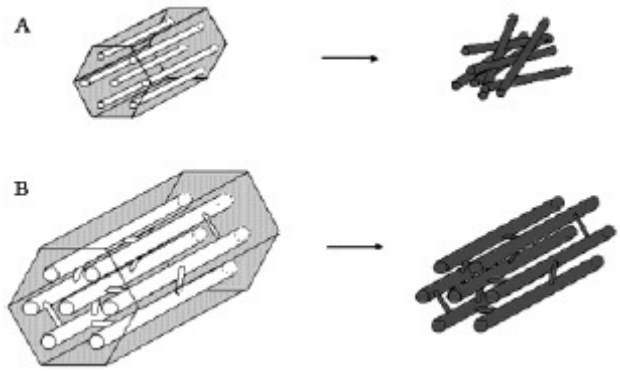

Figure 3.3

Expected collapse of carbon reverse replica of MCM-41 silica (A)
and retain of porous structure in carbon reverse replica of SBA-15 silica (B) [11]

During reverse replica process, another important factor is the impregnation step. As discussed in chapter 2, an incomplete filling of matrix pores leaves voids in the final carbon structure and these voids could, for example, generate a series of fracture points or heavy influence on final material properties. A complete pore filling is not easy, because the small dimension of pores. In fact, if the pore cross section is very small liquid could cover completely the opening, trapping inside gases and stopping the

diffusion process. To favourite precursor diffusion inside the matrix it is necessary to use interaction forces between the two. Generally, these interactions could be distinct in hydrogen bonding with free hydroxyl groups on pore walls, coordination bonds with formation of small aggregates, Coulombic interactions and Van der Waals forces.[14] Carbon precursors interact with pore walls and start to diffuse along those, filling completely pores by capillarity.

To obtain a complete pore filling, general notices are to leave a long time for diffusion and matrices with larger pores to make easier precursor motions in pore system. In certain cases, pore are too large to a complete filling and, by this, three dimensional tubular carbon structures are obtained, as illustrated in figure 3.4:

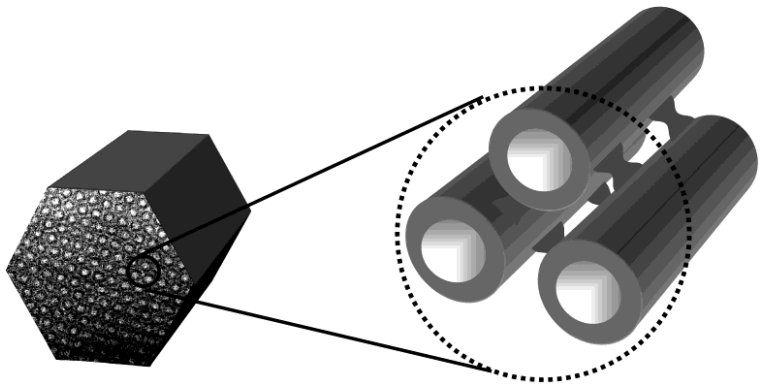

Figure 3.4

Schematic representation of a carbon hollow nanopipes structure [1]

3.3 Carbon precursors

There are different types of carbon precursors.

It is true that, by principle, each organic molecule is a possible carbon precursor, nevertheless not all organic molecules could be converted in carbon material in an easy and cheap way and not all sources could be transferred into mesopores.

In published works, common carbon precursors are sugars, polymers and copolymers, extended aromatic molecules, such as perilene, organic molecules able to react resins and sometimes the same surfactant used to generate the porous silica matrix.[15] Sugars are carried in porous matrix by aqueous solutions, dehydrated with sulphuric acid and then carbonized, while polymers are often directly synthesized in the pore space. In the case of sugars and molecules very important is the solution viscosity, because high

viscous solutions are difficult to let diffuse and request long diffusion times and a mechanical help such as compression at high pressure. Presence of solvent, however, could represent a problem, because could be retained inside pores and bring to the generation of void spaces inside carbon medium during the carbonization process. These voids are one of the causes of microporosity in carbon materials. The same problem is present with organic polyconjugated molecules, that need to be transferred by use of an organic solvent.[16]

Concerning polymers and block copolymers, generally they are not let diffuse with a solvent, but directly synthesized inside porous scaffold through a confined polymerization after diffusion of monomers. The same method is used for organic molecules like phenol or furfuryl alcohol, that are make diffuse inside pores in liquid phase and then put in contact with another molecule, for example formaldeid for phenol, that reacts to form complex networks and resins. This last example is one of the common methods to obtain tubular carbons in large pore matrices.[17]

The choice of carbon precursor is very important to control final material characteristics. In fact, to reduce themselves from hydrocarbons to elemental carbon, precursors must loss hydrogen, oxygen and nitrogen atoms, if present. This loss acted by generation of gaseous species, such as hydrogen, water, ammonia and so other.[1] These gases, however, are generated during carbonization process, so when temperature is high and organic material is going to become hard and fragile, the presence of these species can create a diffuse microporosity. In the case of hydrogen, gaseous molecules are small and can diffuse quickly and without defect creation, but in case of large molecules, such as water, diffusion is slower and microporosity more accentuated. This fact is due not only to molecular size, but also to the affinity with the matrix. In fact, water and ammonia are polar molecules and can be stabilized by silica matrix forming small clusters stable at high temperatures.[18]

By this, carbon material obtained by polymers and similar present a lower grade of microporosity, because during carbonization they generate overall hydrogen or light hydrocarbons molecules, but it is more difficult to obtain an homogeneous filling of porous structure and, often, there is not a complete control over the polymer structure before carbonization process. Instead, with sugars it is easy to fill porous structures and they could carbonize in few possible structures. Nevertheless carbons obtained by

sugars generally show diffused microporosity, due to water release during carbon conversion.

3.4 Graphitic-like carbon materials

Most of carbons produced by hard template method has an amorphous chemical structure, with a disordered network of both sp^2 and sp^3 carbon atom hybridizations. This disorder is generally attributed to uncontrolled elimination of small molecules during reduction and to the absence of molecular order in carbon precursor, where single atom carbons are free to assume different spatial positions. To obtain regular carbon structures, it is necessary to force single atoms to assume specific hybridizations and force them to react in specific configurations.

As happens in nature, pure sp^3 carbon structures (diamonds) could be obtained in high temperature and pressure conditions, jointed to a long time carbonization.[19] These structures are so very difficult and expensive to realize and, until now, they are not still deeply studied. Instead, pure sp^2 carbon structures (graphene or graphite) are easier to synthesize and they do not request high pressure conditions. By definition, a graphene is a single sheet of condensed aromatic carbons in sp^2 form, when graphite is composed by different graphene sheets close packed at a distance of 1.42 Å. In mesoporous carbons, graphitic structures are rare cases, because of the difficulty to organize extended planar structures in a restricted space, when graphene could assume curved shapes and are more diffused. Precursors able to give a graphitic-like structure are extended aromatic molecules and especial polymers such as polyacrylonitrile or polymers with aromatic groups.[20] Moreover, there are other methods to obtain mesoporous carbon systems with graphitic-like structures, for example a synthesis by CVD (Chemical Vapour deposition) at temperatures higher than 900 °C or starting from amorphous carbon materials and inducing graphitization by thermal treatment over 2000 °C.[1]

Ordered mesoporous materials with graphitic-like structure were pursued by several research groups because of their unusual properties.[21] In fact, these systems show great thermal conductivity and mechanical stiffness, stability in air at high temperatures and, overall, high electrical conductivity. In particular, their fracture strength are comparable with that of carbon nanotubes (over 1 GPa), conductivity is often greater than similar

graphitic structures, so these materials are ideal for electronic applications, as described below.

3.5 Carbon materials applications

Mesoporous carbon materials are studied for a large number of possible applications. Some of these are typical of mesoporous materials, when other are strictly related to carbon chemical nature.

As activated carbons, they could be used for water or gas purification, becoming a solid medium to trap and remove chemical wastes, or they could be used as separating medium in chromatographic column for organic separations.[22]

In literature, first application reported in many works is hydrogen storage. Hydrogen is a light and small molecule, difficult to stabilize and to trap at low pressures and ambient temperature.[23] Carbon structure, nevertheless, show a particular affinity with this gas and can be used to store large quantities, up to 0.6 %wt, in environmental conditions. To increase this value, it is necessary to increase mesoporous carbon surface area and create structures more regular to obtain maximum packing in the fewest volume. Moreover, they are lightweight and resistant at high temperatures (over 400 °C), so it is possible to think about their employment in storage systems for car alimentation.

Strictly connected to hydrogen storage is hydrogen production. Hydrogen production processes are expensive and request presence of catalytic steps. Moreover, produced gas must be purified from small quantities of secondary gases such as carbon dioxide or water.[24] Mesoporous carbon materials could be used to solve both these problems, exploiting them as scaffolds to disperse catalyst nanoparticles and as selective adsorption media for purification of produced gas.

Another energetic application for these materials is their use as electrodes in lithium ion batteries and supercapacitors. Respect to classical graphitic systems, mesoporous carbons don't need to be activated by chemical processes and, also if completely discharged removing all lithium ions, they retain the structure and do not show collapse blocking device functionality.[25] Similar structures are reported in literature, realized by coverage of porous materials or metal systems by a thin film of carbon.[26] Important characteristic in this case is the electrical conductivity of these systems. Amorphous

carbons are often non-conductive, when those graphitic-like have a good electron mobility and could be easily integrated in electrical devices.
Finally, thanks to their great chemical, thermal and mechanical stability, porous carbons could be used as lightweight charges for bulk polymers with the final target to increase polymer mechanical properties by formation of a nanocomposite.[27]

3.6 *References:*

1) C. Liang, Z. Li, S. Dai; *Angew. Chem. Int. Ed.* **2008**, *47*, 3696-3717

2) J. Lee, J. Kim, T. Hyeon; *Adv. Mater.* **2006**, *18*, 2073-2094

3) a) R.C. Bansal, J.B. Donnet, F. Stoeckli; *Active Carbon*, Marcel Dekker, New York, US, **1988**; b) R.T. Yang, *Adsorbents: Fundaments and Applications*, Wiley-Interscience, New York, US, **2003**; c) T.R. Gaffney; *Curr. Opin. Solid State Mater. Sci.* **1996**, *1*, 69-75

4) a) J. Ozaki, N. Endo, W. Ohizumi, K. Igarashi, M. Nakahara, A. Oya, S. Yoshida, T. Izuka; *Carbon* **1997**, *35*, 1031-1033; b) T. Kowalewski, N.V. Tsarewsjy, K. Matylaszewsky; *J. Am. Chem. Soc.* **2002**, *124*, 10632-10633

5) a) H. Tamon, H. Ishizaka, T. Yamamoto, T. Suzuki; *Carbon* **1999**, *37*, 2049-2055; b) R.W. Pekala; *J. Mater. Sci.* **1989**, *24*, 3221-3227

6) R. Ryoo, S.H. Joo, M. Kruk, M. Jaroniec; *Adv. Mater.* **2001**, *13*, 677-681

7) a) C.D. Liang, K.L. Hong, G.A. Guiochon, J.W. Mays, S. Dai; *Angew. Chem. Int. Ed.* **2004**, *43*, 5785-5789; b) S. Tanaka; N. Nishiyama, Y. Egashira, K. Ueyama; *Chem. Commun.* **2005**, 2125-2127

8) a) J. Pang, V.T. John, D.A. Loy, Z. Yang, Y. Lu; *Adv. Mater.* **2005**, *17*, 704-707; b) J. Pang, L. Yang, D.A. Loy, H. Peng, H.S. Ashbaugh, J. Mague, C.J. Brinker, Y. Lu; *Chem. Commun.* **2006**, 1545-1547

9) J. Lee, S. Han, T. Hyeon; *J. Mater. Chem.* **2004**, *14*, 478-486

10) A. Zakhidov, R. Baughman, Z. Iqbal, C. Cui, I. Khayrullin, S. Dantas, J. Marti, V. Ralchenko; *Science* **1998**, *282*, 897-901

11) a) R. Ryoo, S.H. Joo, S. Jun; *J. Phys. Chem. B* **1999**, *103*, 7743-7746; b) M. Kruk, M. Jaroniec, R. Ryoo, S.H. Joo; *J. Phys. Chem. B* **2000**, *104*, 7960-7968

12) a) B. Tian, S. Che, Z. Liu, X. Liu, W. Fan, T. Tatsumi, O. Terasaki, D. Zhao; *Chem. Commun.* **2003**, 2726-2727; b) S. Che, A.E. Garcia-Bennet, X. Liu, R.P. Hodkins, P.A. Wright, D. Zhao, O. Terasaki, T. Tatsumi; *Angew. Chem. Int. Ed.* **2003**, *42*, 3930-3934; c) J. Lee, J. Kim, Y. Lee, S. Yoon, S.M. Oh, T. Hyeon; *Chem. Mater.* **2004**, *16*, 3323-3330; d) M. Kruk, B. Dufour, E.B. Celer, T. Kowalewski, M. Jaroniec, K. Matyjaszewski; *J. Phys. Chem. B* **2005**, *109*, 9216-9225; e) S.B. Yoon, J.Y. Kim, J.S. Yu, K.P. Gierszal, M. Jaroniec; *Ind. Eng. Chem. Res.* **2005**, *44*, 4316-4322; f) A.Y. Lo, S.J. Huang, W.H. Chen, Y.R. Peng, C.T. Kuo, S.B. Liu; *Thin Solid Films* **2006**, *498*, 193-197

13) a) S.Jun, S.H. Joo, R. Ryoo, M. Kruk, M. Jaroniec, Z. Liu, T. Oshuna, O. Terasaki; *J. Am. Chem. Soc.* **2000**, *122*, 10712-10713; b) S.H. Joo, S. Jun, R. Ryoo; *Microporous and Mesoporous Materials* **2001**, *44-45*, 153-158; c) M. Kaneda, T. Tsubakiyama, A. Carlsson, Y. Sakamoto, T. Oshuna, O. Terasaki, S.H. Joo, R. Ryoo; *J. Phys. Chem. B* **2002**, *106*, 1256-1266; d) W. Guo, X.S. Zhao in *Studies in surface Science and Catalyisis 156*, (M. Jaroniec and A. Sayari editors), Elseiver B.V. **2005**, 551-556 e) H. Li, Y. Sakamoto, Y. Li, O. Terasaki, M. Thommes, S. Che; *Microporous and Mesoporous Materials* **2006**, *95*, 193-199; f) M. Tiemann; *Chem. Mater.* **2008**, *20*, 961-971

14) a) H. Yang, D. Zhao; *J. Mater. Chem.* **2005**, *15*, 1217-1231; b) Y. Wan, Y. Shi, D. Zhao; *Chem. Mater.* **2008**, *20*, 932-945

15) a) J.S. Lee, S.H. Joo, R. Ryoo; *J. Am. Chem. Soc.* **2002**, *124*, 1156-1157; b) J. Lee, J. Kim, Y. Lee, S. Yoon, S.M. Oh, T. Hyeon; *Chem. Mater.* **2004**, *16*, 3323-3330; c) T.W. Kim, I.S. Park, R. Ryoo; *Angew. Chem. Int. Ed.* **2003**, *42*, 4375-4379; d) J. Lee, S. Yoon, T. Hyeon, S.M. Oh, K.B. Kim; *Chem. Commun* **1999**, 2177-2178 e) S.B. Yoon, J.Y. Kim, J.S. Yu; *Chem. Commun.* **2002**, 1536-1537

16) a) M. Kruk, B. Dufour, E.B. Celer, T. Kowalewski, M. Jaroniec, K. Matyjaszewski; *J. Phys. Chem. B* **2005**, *109*, 9216-9225; b) J. Parmentier, L.A. Solovyov, F. Ehrburgger-Dolle, J. Werckmann, O. Ersen, F. Bley, J. Patarin; *Chem. Mater.* **2006**, *18*, 6316-6323

17) a) M. Kruk, M. Jaroniec, T.W. Kim, R. Ryoo; *Chem. Mater.* **2003**, *15*, 2815-2823; b) A.Y. Lo, S.J. Huang, W.H. Chen, Y.R. Peng, C.T. Kuo, S.B.Liu; *Thin Solid Films* **2006**, *498*, 193-197

18) a) M. Rozwadowski, M. Lezanska, J. Wloch, K. Erdmann, R. Golembiewski, J. Kornatowski; *Langmuir* **2001**, *17*, 2112-2119; b) J.S. Oh, W.G. Shim, J.W. Lee, J.H. Kim, H. Moon, G. Seo; *J. Chem. Eng. Data* **2003**, *48*, 1458-1462; c) B. Grünberg, T. Emmler, E. Gedat, I. Shenderovich, G.H. Findenegg, H.H. Limbach, G. Buntkowsky; *Chem. Eur. J.* **2004**, *10*, 5689-5696.

19) a) V.A. Davydov, A.V. Rahmanina, V. Agafonov, B. Narymbetov, J.P. Boudou, H. Szwarc; *Carbon*, **2004**, *42*, 261-269; b) J. Robertson; *Pure & Appl. Chem.* **1994**, *66*, 1789-1796

20) a) *Chemistry and Physic of Carbon, Vol. 7* (E. Fitzer, K. Mueller, W. Schaefer, P.L. Walker jr. Editors), Marcel Dekker, New York, **1971**; b) *Chemistry and Physic of Carbon, Vol. 15* (H. Marsh, P.L. Walker jr. Editors), Marcel Dekker, New York, **1971**; c) W. Zhang, J. Liu, G. Wu; *Carbon*, **2003**, *41*, 2805-2812

21) a) T.W. Kim, I.S. Park, R. Ryoo; *Angew. Chem. Int. Ed.* **2003**, *42*, 4375-4379; b) C.H. Kim, D.K. Lee, T.J. Pinnavaia; *Langmuir* **2004**, *20*, 5157-5159; c) H.F. Yang, Y. Yan, Y. Liu, F.Q. Zhang, Y. Meng, M. Li, S.H. Xie, B. Tu, D.Y. Zhao; *J. Phys. Chem. B* **2004**, *108*, 17320-17328; d) Y.D. Xia, R. Mokaya; *Adv. Mater.* **2004**, *16*, 1553-1558; e) Y.D. Xia, R. Mokaya; *Chem. Mater.* **2005**, *17*, 1553-1560; e) Y.D. Xia, Z.X. Yang, R. Mokaya; *J. Phys. Chem. B* **2004**, *108*, 19293-19298

22) a) S.H. Joo, S.J. Chol, I. Oh, J. Kwak, Z. Liu, O. Terasaki, R. Ryoo; *Nature*, **2001**, *412*, 169-172; b) J.E. Hampsey, Q. Hu, Z. Wu, L. Rice, J. Pang, Y. Lu; *Carbon* **2005**, *43*, 2977-2982; c) L. Guo, L. Zhang, J. Zhang, J. Zhou, Q. He, S. Zeng, X. Cui, J. Shi; *Chem. Commun.* **2009**, 6071-6073

23) U. Eberle, M. Felderhoff, F. Schüth; *Angew. Chem. Int. Ed.* **2009**, *48*, 6608-6630

24) J.D. Holladay, J. Hu, D.L. King, Y. Wang; *Catalysis Today* **2009**, *139*, 244-260

25) J. Lee, S. Yoon, T. Hyeon, S.M. Oh, K.B. Kim; *Chem. Comm.* **1999**, 2177-2178

26) H. Liu, L.J. Fu, H.P. Zhang, J. Gao, C. Li, Y.P. Wu, H.Q. Wu; *Electrochemical and solid-state Letters* **2006**, *9*, A529-A533

27) K.A. Watson, J.G. Smith, J.W. Connel; *International SAMPE technical conference* **2001**, *33*, 1551-1560

CHAPTER 4

Periodic mesoporous silica

Periodic mesoporous silica was discovered in 1992 by Mobil corporation.[1] This discovery was an important news for scientific community, because, for the first time, it was possible to "escape from microporosity prison". In fact, before this date pore diameter was limited by molecular dimension of templates and it was very difficult to obtain regular structures with pores bigger than 1-2 nm. Using supramolecular aggregates of surfactant molecules, instead, it was possible to generate regular structures still ordered in the nanometric range, but with larger pores. The same synthetic procedure was then applied to a large variety of other materials, such as aluminosilicates or metal oxides, but silica is the most versatile material and with the largest number of possible structures.[2] Periodic mesoporous silica is a very interesting material because, as zeolites, it shows great affinity for water and other vapor species, great stability and large structural versatility. Moreover, they are easy and cheap to obtain, with synthetic procedures that are easily applicable in industrial processes.

In this chapter we will do a general overview about mesoporous silica, its general properties and synthetic strategies, focusing the discussion about an hexagonal mesoporous silica similar to MCM-41. This is a periodic mesoporous silica system able to auto-organize itself and to grow in well defined micrometric shapes. In this PhD work we have performed different synthesis of porous silica with different shapes and we have deeply investigated this materials exploiting it as matrix for confined polymerizations and the replica effect.

4.1 General properties

Periodic mesoporous silica has high surface area, often over 1000 m^2/g, and narrow pore distribution, centred between 2 and 5 nm. It shows great thermal and chemical stability: pore structure is stable at high temperatures, over 1200 K and silica walls are inert to most etching agents, both acid or basic, with exception of hydrofluoric acid and

concentred basic solutions. Structures show great mechanical properties, depending also from pore thickness, and they are very resistant to abrasion and compression.[3] Pore wall thickness is variable and it depends from synthesis conditions, but generally it is in the order of few nanometers. Silica that constitutes walls is amorphous and the material surface is hydrophilic. On internal surface hydroxyl groups are present, that are uncondensed groups. Their number is related to synthesis conditions because, as explained in paragraph 2.4, since they bring to different condensation degrees.[4] Generally, basic synthesis are a little slower, bring to a major condensation and so to a small number of free hydroxyl groups on pore walls, while acid synthesis conditions produce less condensed structures with a large number of free hydroxyl. The presence of these free groups on pore walls influences material adsorption properties, hydrophilic character and the possibility to diffuse a second specie inside pores.

The general properties here reported are common to all mesoporous silicas and not dependent from pore geometry. In next paragraph we will illustrate what silica structures are known in literature.

4.2 Structural classification

There is a large number of silica periodic mesoporous structures. They are obtained by similar procedures but, even though little differences in pore diameter size, wall thickness or condensation, the main difference is the pore organization in three-dimensional space,[5] as shown in figure 4.1.

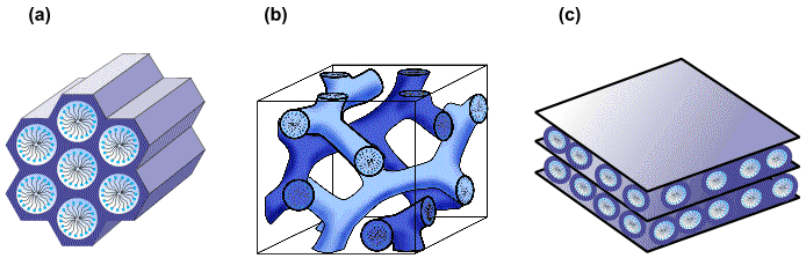

Figure 4.1

Examples of structural geometries of mesoporous silica structures:
MCM-41 (a) , MCM-48 (b) and MCM-50 (c) [5]

Depending on synthesis conditions, it is possible to obtain:

- **Linear, parallel nanochannel structures:** in these structures pores are formed by long cylindrical channels, normally packed one close to the others in an hexagonal pattern. Nanometric channels are parallels and could be completely isolated, communicating by casual holes or connected by a secondary channel system of smaller size. Examples of this group are MCM-41, with parallel, isolated channels, and SBA-15, with channels connected by secondary pores.
- **Cubic three-dimensional structures:** in this case pores are organized in short channels interconnected in a three-dimensional structure with cubic symmetry. Typical of these systems is MCM-48 material.
- **Lamellar structures:** this case is unusual, but the same interesting. These structures are constituted by large planes with an organized pattern of holes, parallels or perpendicular to the lamellae. One example of this structure is MCM-50.

There are more structures than those described here, some more complexes, but are rare cases and, often, they present large structural defects that heavy influence material properties.

4.3 Mesoporous silica applications

Mesoporous silica is used for a large number of applications.

It is a good adsorbent for water, ethanol and other polar molecules, so they can be used in purification methods, drying systems or as separating medium in liquid chromatographic columns. The presence of free silanol groups, moreover, gives the possibility to perform condensation inside pores to graft specific functional groups, such as metal clusters, light-emitter molecules, organometallic molecules and catalytic centres.[6] A typical mesoporous silica has a silanol density of about 4 mmol/g of material. Their distribution is not necessary homogeneous, but could be estimated, applying different techniques, in a range of 2.5-3.0 SiOH per nm^2.[7] One interesting and quite recent research field is the superficial grafting. In this case functional molecules are not let diffuse in bulk material, but they react only near the surface. By this method it is possible, for example, to create functional nanomachines with molecules able to

switch through two conformations and realizing open-close devices to store and transport chemical species without problems of chemical loss or external contamination.[8] Because of silica is a biocompatible material, these devices could be exploited as drug delivery systems in medical applications.[9]

Nevertheless, grafting is not the only method to insert functional molecular devices in a silica structure. Functional organic molecules for optical applications could be dispersed in the initial synthesis mixtures ad be trapped inside silica channels by the surfactant.[10] By this way, it is possible to obtain photonic devices with main functional groups protected by silica walls. After surfactant removal, silica channel system could be also used to store large molecules or as nanoreactors to obtain large structures by confined reactions. Aims of these reactions could be the production of specific molecular conformations, imposed by the space confinement, or the generation of a second material inside pore structure and, then, the formation of a silica nanocomposite. Silica nanocomposites could have structural functions, as charges for bulk polymers to increase mechanical properties or avoid flame propagation, or can be used to obtain new porous structures after silica dissolution by etching with hydrofluoric acid.[11] Typical examples of these confined reactions are *in situ* polymerizations, that bring to polymeric nanocomposites. For a more detailed discussion about these nanocomposites we will remand to the chapter 6.

4.5 MCM-41 and hexagonal packed mesoporous silica systems

MCM-41 is a mesoporous silica composed by isolated parallel channels disposed in an hexagonal packing, as illustrated in figure 4.2 (See below). It is synthesized using hexadecyltrimethylammonium salts as surfactant in basic conditions.[12]

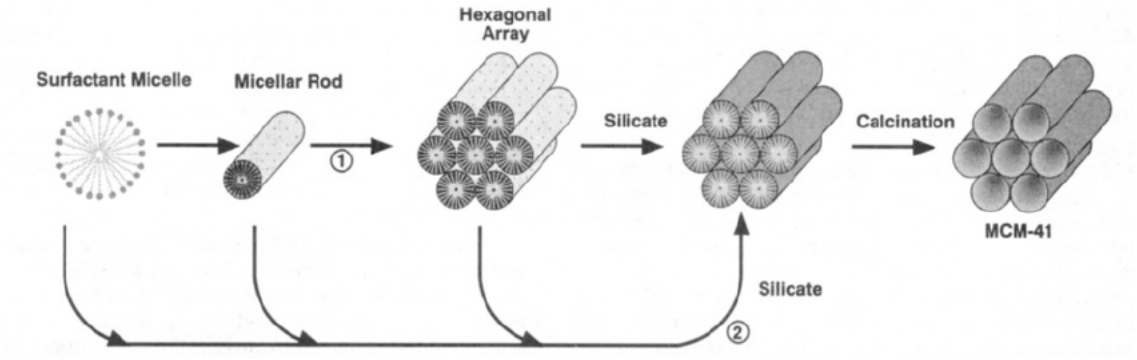

Figure 4.2

Scheme of synthesis reaction of MCM-41 silica. Here are represented both the silica condensation around a liquid crystal surfactant phase (1) and the cooperative self-assembling (2) [12]

It posses a surface area of about 1200 m^2/g, pore diameter around 3nm and could be obtained principally in form of micrometric particles or thin films. Use of acid conditions instead of basic conditions brings to the formation of another mesoporous silica with hexagonal packed channel system and similar surface area and pore diameter, but with many structure defects that generate small openings in pore walls. Unique characteristic of this silica, however, is that particles could assume well defined geometric shapes, such as gyroids, hollow tubes, hexagonal fibres or spheres. This morphology could be controlled by a precise control of synthetic conditions like reactant concentrations, pH of the mixture, temperature and reaction time.[13] Possibility to control material shape and properties starting from synthesis is a key point for future applications, because geometric shapes could be thought for unique applications, related to their specific form, such as tubular containers for macromolecules such as DNA, linear connectors for electrical or optical devices or high packing spherical particles for chromatographic columns.

In this work, we have synthesized hexagonal mesoporous silica with different morphologies and we have studied relationships between synthesis conditions and final micrometric shapes and between these shapes and the material properties such as surface area, pore diameter and particle size.

4.5.1 Control of micrometric shape

As previously explained, hexagonal mesoporous silica has parallel channels with defined micrometric morphology. By this description, one could expect that these are linear morphologies, such as fibers or hexagons. Despite this, silica shapes are generally curved geometries, as illustrated in figure 4.3:

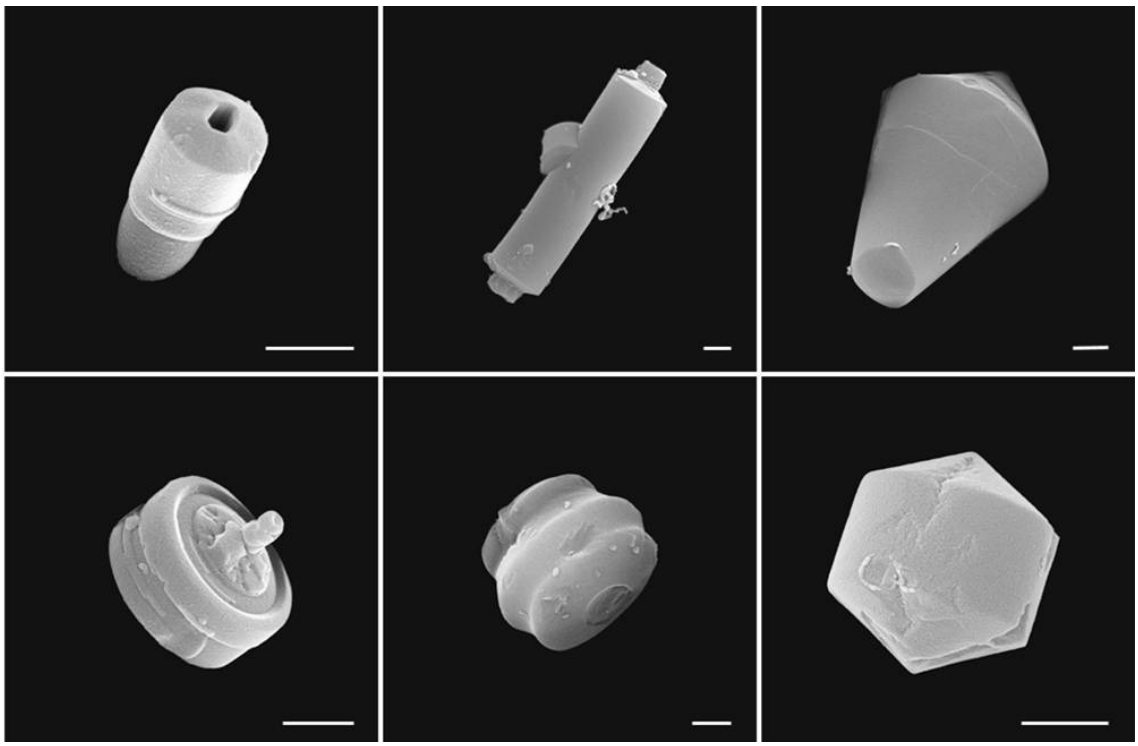

Figure 4.3

SEM images with examples of micrometric silica shapes

About morphology formation, there are different hypothesis, and no one seems to have necessary characteristics to be chosen as the right one or the most probable. This fact is strictly related to the unsolved question if silica and surfactant collaborate to the crystal liquid phase formation or if silica condenses around a pre-existent phase. In literature, however, two main explanation for micrometric morphogenesis process are presented. In the first one, particle seeds are generated in solution and particles grow from these by addition of material at the seed surface. Because of seeds are small objects, of only few nanometers, they tend to assume stable geometries and so curved shapes.[14] This model is a good explanation for gyroids and spheres, but it is not applicable to silica linear

fibres or tubes. The other model considers channels growing parallels and linear. During growth, but before silica condensation, some defects are generated in surfactant supramolecular structure, by entropy or other statistic factors, causing a slow bending of the channel system until formation of circular structures.[15] This model could be applied to most of silica shapes, but can't explain how, changing reaction time, a well defined micrometric morphology can change in another one.

To follow the first steps of silica synthesis is very difficult, because they are fast and involve small objects, so a definitive explanation is quite impossible. Nevertheless, relating synthesis conditions with obtained morphologies, it is possible to extrapolate some considerations:

- **Effects of surfactant concentration:** Surfactant concentration is one of most important parameters. As explained in chapter 2, it is possible to establish a phase diagram for each surfactant and only in specific conditions of concentration we can obtain the desired supramolecular structure. In case of lower concentration, molecules are too much dispersed to aggregate themselves in regular clusters, when at higher concentrations interactions among surfactant molecules become very complexes and they evolve generating high geometrical three-dimensional shapes. In the specific case of MCM-41 and hexadecyltrimethylammonium, it is necessary to remain in the range that let the surfactant auto-organize in micellar rods.
- **Effects of temperature:** high temperatures cause vigorous molecular motions. This could introduce a major number of defects in the liquid crystal structure and, by this, generate more complexes and curved shapes. Temperature influences also condensation rate, so at lower temperatures objects are smaller and more straight than those synthesized at high temperatures.
- **Effects of pH:** acidity or basicity of aqueous solution influence the number of free charges on surfactant surface. A large number of free charges causes a stronger repulsion between polar heads, so cylindrical micelles tend to be straight and linear. Very strong acid or basic synthesis bring to rope-shaped objects, when pH near to neutral value causes formation of cylindrical and round objects.

- **Effects of co-surfactants or other molecules:** in some cases, introduction in the synthesis environment of a co-surfactant or an organic molecule can bring to a twist in the surfactant structure and the formation of helical structures. These molecules could be chiral molecules, that use their chiral centre to auto-organize in a helical structure, or other organic molecules that act on pH solution and organic surfactant phase.
- **Effects of time:** one parameter often forgotten is time reaction. One could think that, once condensed all hydroxyl groups present in reaction environment, nothing else could happen. Nevertheless, for long time reactions condensed silanols could partially broke and give recondensation. By this, short-time reactions product geometric and sharp morphology, when long time hydrothermal reactions bring to more spherical shapes.
- **Effects of stirring:** at last, the key point of micrometric morphology generation is the absence of stirring. In fact, if the reaction mixture is stirred vigorously, first particle seeds formed cannot regular grow because they are in fast motion. To obtain defined shapes it is so necessary to let reactants in quiescent conditions and give time to particle seeds to coordinate the surfactant structure and assume defined geometries.

Basing on synthetic procedures reported in literature, we have focused our attention on four micrometric shapes: gyroids, hollow tubes, hexagonal fibres and spheres.

4.5.2 Synthesis of morphological mesoporous silica

All synthesis of morphological silica were performed in water solution starting from commercially available reactants. Surfactant (hexadecyltrimethylammonium chloride, C_{16}TMACl) was purchased in a 25% wt aqueous solution. Synthesis was conduced in acid conditions using hydrochloric acid (HCl). Tetraethyl orthosilicate (TEOS) was used as silica precursor. During silica condensation stirring is switched off to give time to particles to assume the final shape without risk to damage objects in formation.

4.5.2.1 Synthesis of gyroids

Gyroid is the most easy and quick shape to obtain. Molar ratios for this synthesis are the following:[16]

C_{16}TMACl 0.11 : HCl 3.5 : TEOS 0.13 : H_2O 100

Chemicals were mixed under vigorous stirring and reaction proceeds at room temperature. Silica particles start to condense after the silica precursor addition and condensation step is complete after 12h. Silica was collected by filtration and washed with water to remove surfactant excess and acid species stopping the reaction. Removal of surfactant was performed in a two step process to avoid damages to morphology. First, surfactant was removed by washing in refluxing ethanol using a Kumagawa apparatus for 48h, followed by a double calcination at 540°C for 6h to remove completely the surfactant. The heating was slow to avoid massive template decomposition and the formation of large amounts of gaseous species, that could break silica pore walls.

Gyroidal shape is an interesting case of morphogenesis. In fact, silica channels tend to close themselves in circular structures originating the final shape as illustrated in figure 4.4.

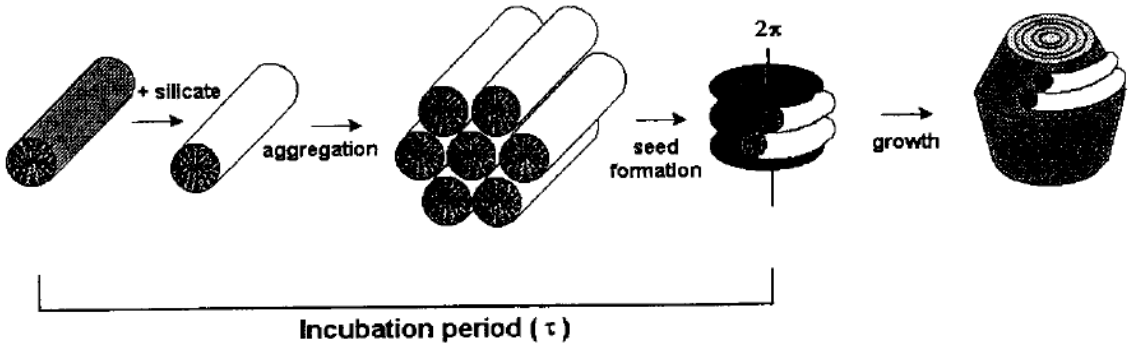

Figure 4.4

Scheme of formation of gyroidal particles [16]

Since gyroid dimension is of few micrometers, it is evident that they cannot be generated only by the bending of an unique linear channel pattern, but they are originated from a first seed and around it other cylindrical micellar structures condense.

4.5.2.2 Synthesis of hollow tubes

Hollow tubular shapes of silica show the unique characteristic to posses a central cavity, of micrometric diameter, besides the nanometric porosity. This internal empty space could be useful to trap large molecules, such as proteins, or for other applications.

Synthesis of hollow tubes requests the use of a certain amount of formamide reactant. Function of formamide is not clear: it could be used as a method to control pH of the final mixture or it can interact with the surfactant supramolecular structure, as described in paragraph 4.5.1, introducing controlled defects that bring to the structure bending.[17]

Molar ratios for this synthesis are:

C_{16}TMACl 0.11 : HCl 7.8 : Formamide 10.2 : TEOS 0.13 : H_2O 100

Excepted for TEOS, all chemicals were mixed and let under stirring for 48h. This induction time is necessary to homogenize the mixture, it let diffuse formamide in all the solution, to form liquid crystal structures. After this time TEOS is added and reaction proceeds for other 72h at room temperature. Silica was then collected by filtration and the powder was washed with water to remove surfactant excess and the other reactants stopping the reaction. As the gyroidal shape, surfactant removal was performed by a washing in ethanol for 48h followed by a double calcination at 540°C for 6h.

In the tube shape, nanoporous channels are disposed around the axis of central cavity, disposed on planes perpendiculars to this axis or slightly twisted to form helical structure. This disposition suggests that formation of the tube could be explained by a bending process of linear channels, as illustrated in figure 4.5.

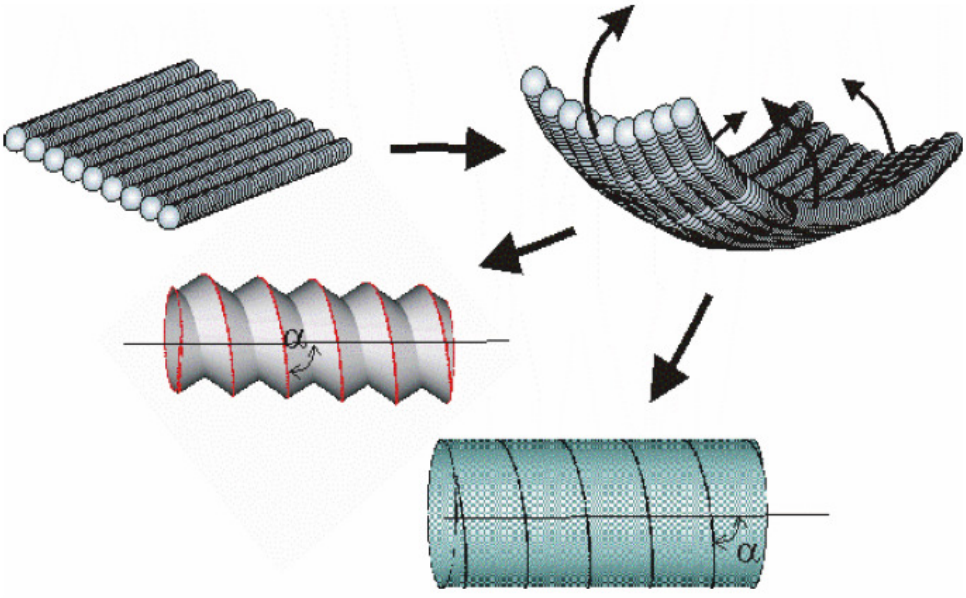

Figure 4.5

Scheme of channel bending during hollow tube or helical structures formation [17]

In rare cases, this synthesis brings to the formation of "Archimedian Screw" structures, originated by high twisting during liquid crystal bending. These objects have attracted the attention of numerous research groups, because they could be used to interact with chiral or biological molecules using their proper chirality. There is a deep study to understand how helical structures are formed in solution and, in particular, how obtain them without using a chiral surfactant.[18] Unluckily, in the proposed synthesis it has not still understood what is the key factor to switch from hollow tubes to these porous helical systems.

4.5.2.3 Synthesis of spheres

Nanometric and micrometric silica spheres, obtained by colloidal synthesis, are well known material for hard template synthesis or mechanical reinforce applications. With hexagonal packed channel structure it is possible to obtain mesoporous silica spheres with very uniform shape and micrometric dimensions. Spherical mesoporous silica synthesis requests long time because particles need to condense among themselves. In fact, during the synthesis silica particles assume first gyroidal shapes and only later

gyroids condense to give spherical structures.[19] Molar ratios of reactants are the following:

C_{16}TMACl 0.11 : HCl 0.9 : TEOS 0.13 : H_2O 100

Reactants were mixed together and, once added silica precursor, reaction mixture was heated at 80°C for a time of nine days. After this time, precipitated silica was collected by filtration and washed with water to remove unreacted chemicals. Surfactant inside pores was then extracted by a washing in ethanol for 48h in a Kumagawa apparatus, then silica was calcinated twice by heating at 540 °C for 4h.
Mesoporous silica spheres show very smooth particle surfaces and a narrow particle size distribution (see below in silica characterization paragraph). It is not clear how nanometric channels are disposed in the space, but it is assured by TEM measurements that they are extended to all the particle without poreless cores.

4.5.2.4 Synthesis of hexagonal fibres

Long silica fibres with hexagonal section are obtained when channel elongation is preferred to lateral condensation of different channels and hexagonal system shows low bending degree. This kind of growth could be obtained with high acidity conditions, so that repulsion with surfactant polar heads becomes so great that micellar bending is energetically unfavourable.[20] Molar ratios for this synthesis are:

C_{16}TMACl 0.02 : HCl 7 : TEOS 0.03 : H_2O 100

Reactants were mixed under stirring and, after silica precursor addition, stirring was stopped to consent silica particles nucleation and growth. Synthetic mixture was then heated at 60 °C for three days until silica precipitation.
A similar synthesis, starting from following molar ratios:

C_{16}TMACl 0.22 : HCl 9 : TEOS 0.13 : H_2O 100

involve instead a reaction time of 15 minutes at 4 °C.[21] In both cases, silica was collected by filtration, washed with water and surfactant was extracted by washing in Kumagawa with ethanol for 48h followed by a double calcination at 540 °C. Both the two procedures bring to hexagonal-section fibers, but in the first one these particles have length of tens of micrometers, when in the low temperature synthesis the length is only few micrometers.

Fibers with long mesostructured channels have an interesting shape for transport applications or as matrices to obtain linear and parallel nanometric filaments in metal or other materials, while short fibers show interesting photonic applications with opportune dyes.[22]

4.5.3 Characterization of mesoporous silicas

The five synthesized silica samples were analyzed with the following techniques, XRD, adsorption and SEM microscopy, and collected data were compared to highlight differences due to the morphology. By X ray diffraction (see figure 4.6) it is clear that all samples show an intense peak at about 2.5 2θ degrees, that corresponds to a distance of 3.53 nanometers. There are not signals at higher degree values, index that the mesostructure has a short-range order degree, with a relative number of defects that avoid higher order reflections. This is probably due to the acidic synthesis conditions, that bring to a less ordered structures than those obtained in basic solutions.

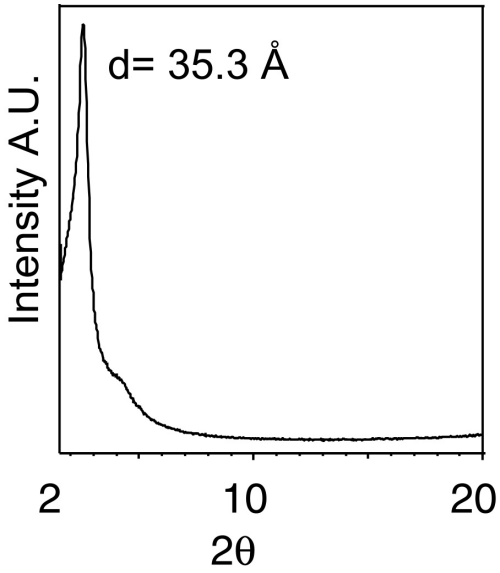

Figure 4.6

XRD pattern of gyroidal mesoporous silica

The distance associated to the mesoporous peaks is not really the physical distance between two pore centers in the hexagonal packing. As illustrated in figure 4.7, this distance is greater and can be calculated starting from the experimental data using the geometrical relationship:

$$a = \frac{d}{\cos 30°} = \frac{2d}{\sqrt{3}}$$

giving the final distance of 4.08 nm.

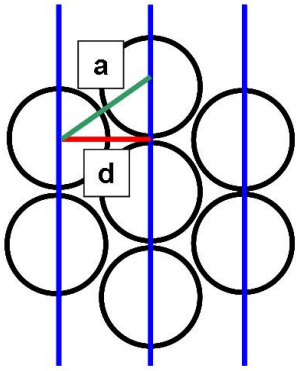

Figure 4.7

Scheme of hexagonal packed channels with relationship between diffraction planes (blue lines) with associate distance (d) and centre-to-centre distance (a)

Actually, mesoscopic order is independent from micrometric morphology. By adsorption measurements, instead, it is possible to see evident differences. All obtained isotherms are typical of mesoporous systems, but BET calculations give different results.

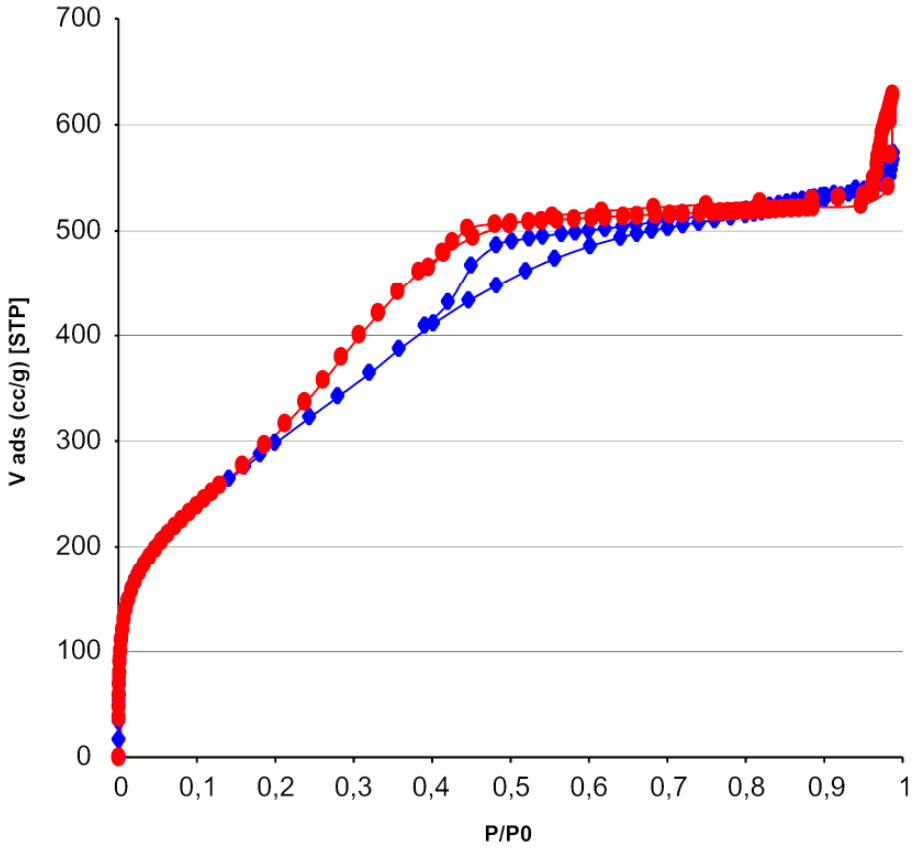

Figure 4.8

Nitrogen adsorption isotherms on gyroidal (red) and hollow tubular samples (blue)

Morphology	**Gyroids**	**Hollow tubes**	**Spheres**	**Short fibers**	**Long fibers**
BET surface area (m^2/g)	1140	1120	500	340	250

Table 4.1

BET surface area of the silica samples

As explained in table 4.1, gyroids and hollow tubes have very similar surface areas, of about 1200 m^2/g, while spherical particles and hexagonal fibers give a lower value. This

difference could be explained considering a partial occlusion of pores after recondensation, in the case of spheres, or the difficult accessibility to all parts of the channels in the case of hexagonal fibers. Furthermore, by BJH calculations it has been possible to calculate adsorption pore diameter, 3.2 nm, that, to XRD data, consents to estimate the pore wall thickness of about 1nm.

SEM images of the five samples give a direct view of micrometric morphology, as reported in figure 4.9:

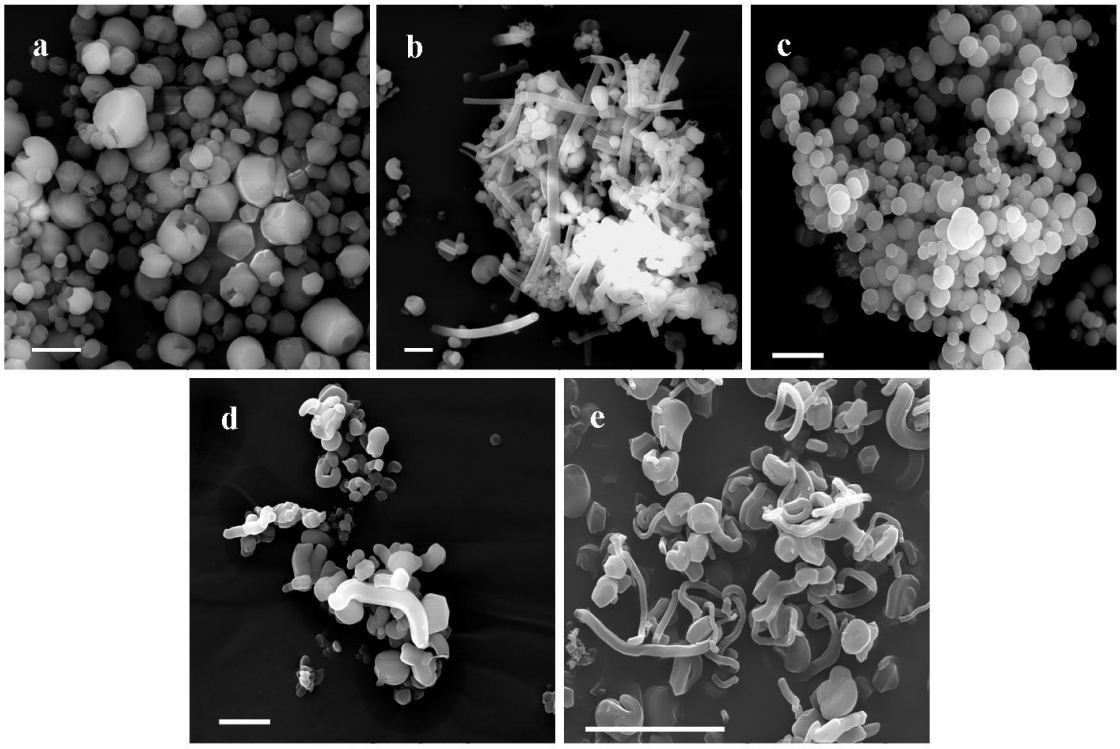

Figure 4.9

SEM images of synthesized morphological silica samples:
a) Gyroids; b) Hollow tubes; c) Spheres; d) Short fibers; e) Long Fibers
the reported scale bars correspond to 10 μm

By SEM images we can see that gyroids, tubes and spheres are homogeneous, while the two fibers samples present a very variegated and non homogeneous morphologies. Considering this as a signal of irregular properties, we have chosen to avoid to use these two samples for following steps of polymerization and carbonization. Despite other samples are more uniform, single particle size could be very different, in a range of 1-5 μm. From SEM images we can estimate silica particle size and deduce dimensional

distribution. We have not studied hollow tubes distribution because they have two dimensional parameters, diameter and tube length, and casual disposition on SEM images makes difficult to estimate precisely these parameters when the single particle is disposed diagonally respect to the SEM lens. Spheres and gyroids, instead, could be both approximated to spherical geometry, then they could be measured in whatever disposition. Distribution of these samples are reported in figure 4.10:

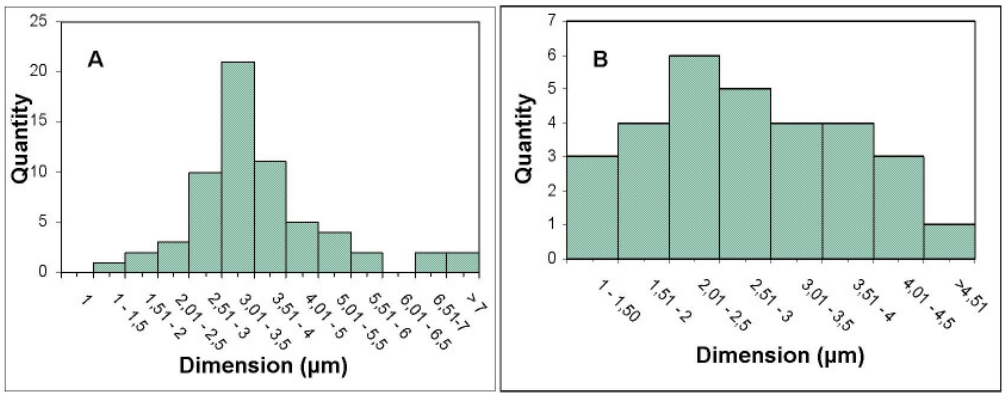

Figure 4.10

Distribution of particle size in gyroidal and spherical samples

Gyroids show very narrow distribution peaked around 3 µm size, while spheres have a quite uniform distribution between 2 and 4 µm. These results show that gyroids have the most narrow particle size distribution, even though their shapes are not perfectly the same, showing some little differences in their geometry. On the other hand, spheres, have the most homogeneous morphology, but with variable dimensions. It is not completely clear if particle size or the specific geometry can influence adsorption properties of the single object. To study this relationship, however, it shall be necessary to separate particles with different shapes or dimensions in the same sample, but this is very difficult particles tend to form small aggregates jointed by strong interactions among them. These aggregates cannot be easily separated, so also with selective filtrations with membranes of well-defined porosity we have not obtained a size-particle selection.

In conclusion, we have synthesized five silica samples with different morphologies, gyroids, spheres, tubes, short and long fibers, finding that mesoporous order is independent from micrometric morphology. This is instead very important for surface area, probably because of a different accessibility to pores or different channel configuration. Depending on the homogeneity of samples, three of them, gyroids, tubes and spheres, have been used as matrices to obtain polymeric and carbon nanocomposites, as will be described in chapter following chapters.

4.6 References:

1) a) J.S. Beck, J.C. Vartuli, W.J. Roth, M.E. Leonowicz, C.T. Kresge, K.D. Schmitt, C.T.W. Chu, D.H. Olson, E.W. Sheppard, S.B. McCullen, J.B. Higgins, J.L. Shlenker; *J. Am. Chem. Soc.* **1992***, 14*, 10834-10843; b) C.T. Kresge, M.E. Leonowicz, W.J. Roth, J.C. Vartuli, J.S. Beck; *Nature* **1992***, 359*, 710-712

2) G. A. Ozin, A. C. Arsenault, L. Cademartiri, *Nanochemistry* **2009**, RSC Publishing.

3) P. Selvam, S.K. Bhatia, C.G. Sonwane; *Ind. Eng. Chem. Res.* **2001**, *40*, 3237-3261

4) V. Meynen, P. Cool, E.F. Vansant; *Microporous and Mesoporous Materials* **2009**, *125*, 170-223

5) a) C.J. Brinker, Y. Lu, A. Secunger, H. Fan; *Adv. Mater.* **1999**, *11*, 579-585; b) W. Ying, D. Zhao; *Chem. Rev.* **2007**, *107*, 2821-2860; c) F. Hoffmann, M. Cornelius, J. Morell, M. Froeba; *Angew. Chem. Int. Ed.* **2006**, *45*, 3216-3251

6) K. Moller, T. Bein; *Chem. Mater.* **1998**, *10*, 2950-2963

7) X.S. Zhao, S.M. Chong, G.Q. Lu in *Nanoporous Materials, Science and Engineering*, (G.Q. Lu and X.S. Zhao editors), Series of chemical engeneering, Vol.4, Imperial college Press, London, **2004**, 392-426

8) S. Angelos, E. Johansson, J.F. Stoddart, J.I. Zink; *Adv. Funct. Mater.* **2007**, *17*, 2261-2271

9) a) W. Zhou, P. Gao, L. Shao, D. Caruntu, M. Yu, J. Chen, C.J. O'Connor; *Nanomedicine: Nanotechnology, Biology and Medicine* **2005**, *1*, 233-237; b) S. Giri, B.G. Trewyn, V.S.Y. Lin; *Nanomedicine* **2007**, *2*, 99-111; c) A. Sousa, K.C. Sousa, E.M.B. Sousa; *Acta Biomaterialia* **2008**, *4*, 671-679

10) G. Macchi, F. Meinardi, P. Valsesia, R. Tubino; *Int. J. Photoenergy* **2008**

11) a) H. Yang, D. Zhao; *J. Mater. Chem.* **2005**, *15*, 1217-1231; b) M. Tiemann; *Chem. Mater.* **2008**, *20*, 961-971

12) U. Ciesla, F. Schüth; *Microporous and Mesoporous Materials* **1999**, *27*, 131-149

13) a) H. Yang, N. Coombs, Ö. Dag, I. Sokolov, G.A. Ozin; *J. Mater. Chem.* **1997**, *7*, 1755-1761; b)H.P. Lin, Y.R. Cheng, S.B. Liu, C.Y. Mou; *J. Mater. Chem.* **1999**, *9*, 1197-1201; c) J. Zhang, Z. Liu, B. Han, Y. Wang, Z. Li, G. Yang; *Microporous and Mesoporous Materials* **2005**, *87*, 10-14; d) A.M. Mendoza, J. Warzywoda, A. Sacco Jr.; *J. Porous Mater* **2006**, *13*, 37-47

14) a) S. Mann, G.A. Ozin; *Nature* **1996**, *382*, 313-318; b) G.A. Ozin; *Acc. Chem. Res.* **1997**, *30*, 17-27; c) H. Yang, N. Coombs, G.A. Ozin; *Nature* **1997**, *386*, 692-695

15) I. Sokolov, Y. Kievsky; *Studies in Surface Science and Catalysis* **2005**, *156*, 433-442

16) S.M. Yang, H. Yang, N. Coombs, I. Sokolov, C.T. Kresge, G.A. Ozin; *Adv. Mater.* **1999**, *11*, 52-55

17) S.M. Yang, I. Sokolov, N. Coombs, C.T. Kresge, G.A. Ozin; *Adv. Mater.* **1999**, *11*, 1427-1431

18) a) S. Yang, L. Zhao, C. Yu, X. Zhou, J. Tang, P. Yuan, D. Chen, D. Zhao; *J. Am. Chem. Soc.* **2006**, *128*, 10460-10466; b) J. Wang, W. Wang, P. Sun, Z. Yuan, B. Li, Q. Jin, D. Ding, T. Chen; *J. Mater. Chem.* **2006**, *16*, 4117-4122

19) H. Yang, G. Vovk, N. Coombs, I. Sokolov, G.A. Ozin; *J. Mater. Chem.* **1998**, *8*, 743-750

20) J. Wang, C.K. Tsung, W. Hong, Y. Wu, J. Tang, G.D. Stucky; *Chem. Mater.* **2004**, *16*, 5169-5181

21) Y. Kievsky, I. Sokolov; *IEEE Transaction on Nanotechnology* **2005**, *4*

22) I. Sokolov, Y. Y. Kievsky, J. M. Kaszpurenko; *Small* **2007**, *3*, 419-423

CHAPTER 5

Periodic mesoporous organosilica

Periodic mesoporous organosilica (PMO) is a new and interesting class of hybrid materials with organic groups directly linked to a porous silica structure. There are different methods to obtain these hybrid structures, such as post-synthesis grafting or co-condensation methods but, in last years a new and more reproducible method was presented to obtain homogeneous structures by condensation of organic molecules with two or more silyl groups. The key point of these materials is the possibility to obtain regular structures with different organic groups, such as alchilic, double bonded or aromatic systems inserted in the walls of porous material. This lets to obtain many different structures that interact in different way with guest molecules and so the possibility to synthesize materials for a large variety of applications with the same method.[1]

In this chapter we will discuss about synthetic strategies, organic precursors and general properties of periodic mesoporous organosilica. A specific paragraph will be dedicated to a special family of organosilica with high degree of order: crystal-like periodic mesoporous organosilica. At the end of the chapter, moreover, we will illustrate the experiments performed to obtain a *p*-phenylene organosilica system with crystal-like structure.

5.1 Synthetic strategies for mesoporous hybrid systems

Hybrid organic-inorganic materials have been attractive for long time. Possibility to join great versatility and reactivity of organic molecules with stability and mechanical properties of inorganic matter was an interesting challenge for scientific community. In the specific case of nanoporous materials, possibility to change polarity of pore walls with different types of organic groups could open to a series of possible applications such as optimized materials for chromatographic separations, molecular storage and confined reactions.[1] The first target of synthesis methods, however, it was to obtain

porous structures that were ordered and homogeneous, because known methods, such as xerogel synthesis, bring to a disordered and often poreless materials, without the possibility to control system geometry.

To obtain porous, regular structures with organic functionalities three principal ways have been developed:

1. Post-synthesis grafting on regular porous silica matrices.
2. Co-condensation of silica precursors and organic-functionalized siloxanes.
3. Condensation of organosilanes molecules (single-source precursor method).

5.1.1 Post-synthesis grafting

As previously described, periodic mesoporous silica has a determinate number of unreacted silanol groups on pore walls. They can be exploited to link to the structures other molecules or chemical species.[2] This process, also named grafting, has three principal targets: to change walls polarity and adsorption properties using organic groups, to eliminate these unreacted silanol groups (passivation) or finally the introduction of specific organic functionalities. Chemical species used as common reactants for the grafting process are chloroorganosilanes, alkoxyorganosilanes and sylazanes (or sylamines). Among them, chloroorganosilanes are hard to control and give rise to unwanted polymerization reactions, so the other two species are preferable. Another possible way to perform grafting is to work with easy conversion of silanols in chlorosilane groups by exposition to chlorination reagents, such as CCl_4, $SiCl_4$, $SOCl_2$, $TiCl_4$ or PCl_5, to perform successive reactions with $HNEt_2$ (to give first silylamides) followed by reactions with functionalized alcohols.[3]

The great advantage of this process is that it works on a pre-existent structure, so there are not risks to have a poreless material. Nevertheless, samples obtained by this method are not completely homogeneous. In fact, grafting molecules are strong reactive and not specific, with the tendency to react fast with silanol groups near the pore opening, where there is the first contact between reactants. Once molecules are grafted, pore opening size decreases, so remaining reactant could not reach all pore surface, but remain confined near the external surface. To avoid this problem, two possible solutions could

be to start from a silica with large pores to leave enough open space to consent diffusion, or to use less reactive silanes leaving a longer reaction time.

By these characteristics, grafting method is overall used for low-coverage surface modification, using small amounts of grafting agents, such as catalytic scaffolds, or for specific applications that request only a functionalization near the pore opening, such as open-close devices or similar.

5.1.2 Co-condensation

Co-condensation is a direct synthesis method where tetraalkoxysilanes (TEOS or TMOS) condense in presence of trialkoxyorganosilanes ($RSi(OR')_3$, where R is an organic group and R' a methyl or a ethyl group) or silsequioxanes ($((R'O)_3Si\text{-}R\text{-}Si(OR')_3$, where R is an organic group and R' a methyl or a ethyl group) in presence of a templating agent.[4] Since organic functionalities are direct components of the silica matrix, pore occlusion is generally not a problem and they are more homogeneously distributed in the structure. However, increasing the quantity of organic-functionalized silanes, respect to the silica precursors, comports a gradually decreasing of mesoscopic order in the final material. This is due to local defects generated by organic groups, that are included in surfactant apolar phase and locally change the templating structure, it is also due to the different condensation geometry of these molecules, that posses only three silanols instead of four. These facts fix a superior limit of 40% of organosilanes, over that there is no more ordered structure. In common synthesis, this percentage is typically between 5 and 15%.[5] Other problems for this method, that are strictly connected to those described, are the slow decrease of surface area, due to the lost of structural order, and the fact that final proportion of organic groups is smaller than starting ratio. This difference is due to problems of phase auto-segregation that happens when ratios between organosilanes and silica precursors become great and cause separated condensations.

Considering all these aspects, co-condensation is a method to obtain systems with few organic groups homogeneously distributed in the structure. Materials produced by this way show interesting catalytic and adsorption properties, different from pure-silica systems. An ideal application could be to use these materials as scaffolds for post-

synthetic grafting starting from reactive organic groups introduced during the synthesis.[6]

5.1.3 Single-source precursor

This synthesis method is very similar to the synthetic method used for periodic mesoporous silica. The main difference is that instead of tetraalkoxysilane as silica precursor, a silsequioxane is used.[7] Silsequioxanes posses general structure $(R'O)_3Si\text{-}R\text{-}Si(OR')_3$, where R' is generally a methyl or ethyl group and R is an organic group that could be alchilic, arylic, polyconjugated, etheroaromatic and so other. Surfactants used for this type of synthesis are the same that for silica synthesis and, also in this case, it is possible to obtain different pore structures, such as parallel, hexagonal packed channels or three-dimensional systems with cubic symmetry. Materials obtained by this way are completely homogeneous and formed by organosilanes. Organic groups constitute pore walls, so pore occlusion is avoided, and they are accessible by the environment. Because of the large variety of silsequioxane precursors, with different organic groups, and different structures, these systems show a large number of possible applications, both as adsorptive and purification systems, based on interaction of guest molecules with specific organic groups, and as supports for post-synthesis reactions that involve organic molecules included in pore walls.[8]

Major difficulties of this approach come from precursor synthesis and general synthesis conditions. In fact, most of these precursors are not commercially available and synthesis and purification are difficult, often because there are no references in literature. Once obtained a new precursor, moreover, it is necessary to find synthesis conditions for a regular and periodic structure, because each organic core influences surfactant liquid crystal phase interacting with apolar phase in a unique manner, so often the same procedure is not efficacy for two different precursors. To find the ideal synthetic conditions is so necessary to perform a large number of experiments.

5.2 Periodic mesoporous organosilica synthesis

Synthesis of periodic mesoporous organosilicas can be divided in two successive steps: synthesis of precursor, if not commercially available, and synthesis of the porous structure.

There are different silsequioxane precursors, but the general procedure to synthesize them involve silylation of an halogen-substituted organic molecule and most common pathways to perform this type of reaction are three: Grignard reactions, reactions with alchillithium and catalytic reactions.[9] Each of these reactions starts from organic cores with halogen atoms in the position where must be bonded the silyl group. Common used halogens are bromide and iodine. This second is more reactive and is used overall for large, polyaromatic systems that are very stable and react with difficulty. The three reactions are characteristics of organic chemistry and specific for each precursor, so it is better to remand the synthesis description to single cases.

Synthetic procedure for periodic mesoporous organosilica is, as previously said, very similar to synthesis route for periodic mesoporous silica and it needs the presence of a template agent and acid or basis catalysis to start precursor hydrolization and condensation. Common template agents are hexa- and octadecyltrymethylammonium salts, with alchilic chain of sixteen and eighteen carbon atoms, respectively Brij systems, diblock copolymers with a short hydrophilic group and a long hydrophobic chain, and triblock polyethylenoxyde-polypropylenoxide-polyethylenoxide copolymers.[10] Actually, with ammonium salts and Brij copolymers there is the formation of hexagonal structures, the first in basic conditions ant the other in acid media, while with triblock copolymers cubic phases are more common. Differently from the case of silica, once obtained the structure, surfactant cannot be removed by thermal degradation, that shall decompose also organic linkers, so it is necessary to perform an extraction by washing with surfactant solvents, normally acid ethanol is used. Periodic mesoporous organosilica is generally obtained as powder. In literature there are, until now, only few examples of thin films and monolithic aspect.[11]

Until now, we have illustrated general synthesis procedures, using only one type of organic linker. Nevertheless, it is possible to use two or more silsequioxane molecules in the same time to obtain a periodic mesoporous organosilica with both organic bridges

in the structure. These systems are interesting for the possibility to obtain functional materials with more than one functional group. As in hybrid materials, two different functionalities could joint their properties to obtain high performance materials with unique characteristics that are quite different from the simple sum of single precursor properties. Examples of mixed organosilica materials are benzene/tiophene or ethane/propylethylenediamine mixed systems.[12] Synthetic procedure to obtain these mixed systems is the same of those for mono-precursor, but it is necessary to take in consideration synthetic conditions of each one of precursors. As previously explained, each precursor needs specific conditions of pH, temperature an surfactant type, so it is not easy to mix two precursors that request very different conditions. Normally, in this type of synthesis, molecules with similar characteristics are used, and the presence of both organic linkers could be verified by solid state NMR techniques. About mixed systems there is an interesting open question: how are spatially disposed the two organic cores. There are two main possible answers: the two species are mixed homogeneously in pore walls or they could be arranged in micro-domains mono-precursor. Unlucky, this question can't be answered easily, overall if the two precursors are very similar.

5.3 Periodic mesoporous organosilica with crystal-like pore walls

In 1999 Yoshima-Ishii et al. performed a periodic organosilica synthesis using 1,4-bis(triethoxysilyl)benzene (BTEB) and 2,5 bis(triethoxysilyl)thiophene (BTET) as precursors in presence of cetylpiridinum chloride as template agent in acid medium. This was the first time that a periodic mesoporous organosilica with aromatic linkers was obtained.[13] However, it is only in 2002 that Inagaki et al. obtain a periodic mesoporous organosilica with crystal-like walls using only benzene precursor. In XRD pattern two series of diffraction peaks appeared for the first time: one associable to mesoscopic order, and the other typical of *molecular* order. Comparing distances associated to these peaks with molecular dimensions, they found a precise correspondence.[14] Further studies demonstrated that in the new-synthesized organosilica benzene groups were organized in a high regular pattern, with a series of organic and inorganic layers along pore axes, as described in figure 5.1.

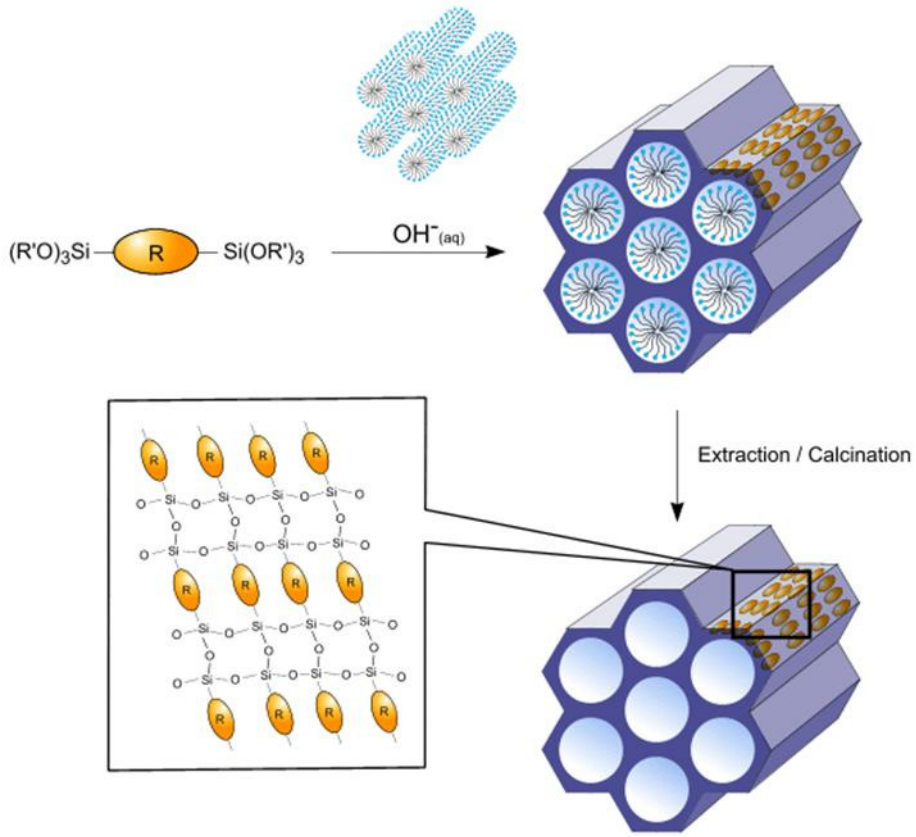

Figure 5.1

Synthesis and structure of periodic mesoporous silica with crystal-like walls [1]

This material class was called "crystal-like" periodic mesoporous organosilica, because the organic bridges do not have to possess a strict translational symmetry. In fact, organic bridges could be a little twisted along the channel axis and, furthermore, organic units can be slightly tilted with respect to each other. Benzensilica was the first example of crystal-like material. After Inagaki's paper, other authors reported synthesis of molecular ordered organosilica using, meta-disilylbenzene, diphenyl, ethylene or para-divinylbenzene organic bridges,[15] as illustrated in figure 5.2.

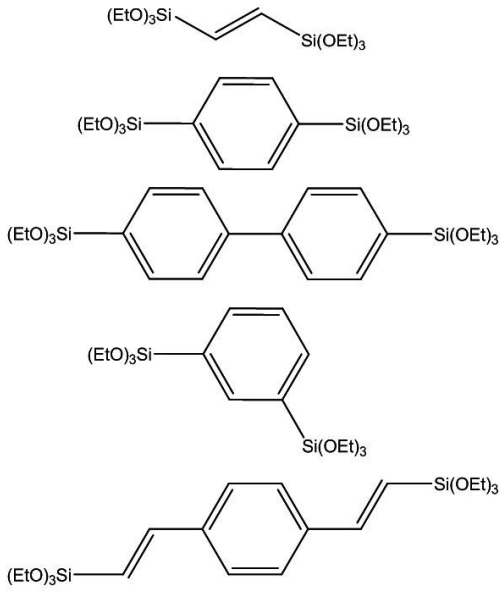

Figure 5.2

Organosilica precursors able to give periodic mesoporous organosilicas with crystal-like walls

Because synthesis procedure is not different from those of other periodic mesoporous organosilicas, the organization at molecular level could be associated to silsequioxane precursor properties. Analyzing nature and structure of molecules able to give crystal-like structures, it is possible deduce that a precursor for a crystal-like structure must show three important characteristics:

1. It must be enough rigid to maintain a regular distance between silyl terminals.
2. It must have an opportune geometry to pack near other molecules in regular patterns.
3. It must be able to give interactions with other precursor molecules, such as π-π correlations.

These are fundamental requirements, but not all molecules that satisfy these conditions are able to produce crystal-like organosilica, it is not clear if this is due to necessity of particular synthesis conditions, not still found, or to undiscovered other necessaries characteristics. Crystal-like materials are very interesting for their high structural order that, often, brings to general better properties, like surface area and pore size, respect to simply periodic mesoporous organosilica.

5.4 Periodic mesoporous organosilica applications

Periodic mesoporous organosilica found his main application as adsorbent media, scaffold for post-synthesis reactions and vessels for confined reactions and molecules storage. However, the presence of organic linkers change drastically interaction between pore walls and guest molecules, opening new application ways, most of which are depending from organic linker nature. Systems with aromatic linkers, for example, are able to use their π electrons to interact with other aromatic or halogen substituted molecules and to stabilize them.[16] By this way, these systems result to be ideal media to capture and sequester a large variety of pollutant chemicals, such as benzene, in air purification devices. Other applications involve the presence of double bonds or polyconjugated systems to capture and neutralize free radical species. Organic linkers are, furthermore, ideal groups for post synthetical functionalization.[14,17] In fact, it is easy to use double bonds and aromatic groups to perform classical synthesis of organic chemistry, such as halogenation, Dies-alder reactions and so other. One particular case is the bromination, that could be an easy and quick method to introduce selective sites for functional groups grafting. The introduction of functional groups in a regular structured matrix could be a first step to create functional devices or to introduce active centers to perform reactions in confined space. Crystal-like structures, in this case, show interesting properties, because grafted organic groups are at the same distance one by the others and this could be a first step to obtain particular nanomachines that request high structural order. Furthermore, materials with chiral organic linkers could possess well-organized helicoidal structure, where chiral groups are organized in a twisted geometry along channel axis.[18] This type of symmetry is very interesting and should be ideal to separate racemic mixtures of optical active molecules.[19] In fact, due to the specific chiral pore space, only one enantiomer could be stabilized and stored, while the complementary cannot enter or is excluded to favourite other interactions. An important application, is the creation of materials for optical applications. Changing organic bridges and using linkers with variable conjugation extension, it is possible to obtain porous material with different adsorption properties and, sometimes, different colors.[20]

These are applications reported in literature until now. Since the research on new organic linkers and periodic structures is still in progress, it is possible to find new fields of application for each specific new periodic mesoporous organosilica.

5.5 Periodic porous organosilica obtained by multi-silylated precursors

We have limited our discussion to silsequioxane precursors with two silyl groups, but in principle it is possible to have molecules with more than two silyl groups ready to condense. These molecules could create complex and regular structures, depending on their geometry.[21] Until now, porous materials with this type of precursors have been obtained, but are often more micro- than mesoporous, even though the presence of template agents. Nevertheless, these materials could represent a new horizon for porous organosilica systems, because they are able to co-condense with mono-substituted silsequioxanes to obtain porous material with high surface area and large pore size, belonging to mesoporous range. The complexity of formed structures and the possibility to condense with other types of precursors to obtain an hybrid matrix make these materials very interesting and opened to different studies.

5.6 Phenylene PMO

In our work we have synthesized and characterized a particular example of periodic mesoporous organosilica with crystal-like pore walls: phenylene organosilica. This material show a very regular structure both in mesoscopic than in molecular range, and has been further characterized with adsorption of different gases and vapor species.

5.6.1 Synthesis of 1,4 bis(triethoxysiliyl)benzene

1,4 bis(triethoxysilyl)benzene (BTEB) was prepared via a Grignard reaction on the *p*-dibromo precursor. Grignard reaction uses magnesium to generate a Grignard reactive on the aromatic ring, as illustrated below

$$Br\text{-}Ph\text{-}Br + 2Mg \rightarrow BrMg\text{-}Ph\text{-}MgBr$$

The reactive attaches then an electronpauper atom, in this case the silicon of TEOS, to give a double substitution:[22]

$$BrMg\text{-}Ph\text{-}MgBr + 2\ Si(OR)_4 \rightarrow (RO)_3Si\text{-}Ph\text{-}Si(OR)_3 + Mg\ salts$$

Grignard reaction is very sensitive to presence of water, because it reacts fast with the Grignard stopping the reaction. For this reason, reaction was performed in nitrogen atmosphere and solvents and reactants were dried before use.

The reaction starts from a molar ratio of 0.62 Mg/2.00 TEOS/0.20 dibromobenzene.[9] Magnesium and TEOS were mixed in Tetrahydrofuran (THF) under nitrogen with a catalytic amount of iodine and brought to reflux. A solution of 1,4 dibromobenzene in THF was added dropwise in 2h to the reaction vessel, and the final mixture was refluxed for 2h. The gray mixture was cooled and THF was removed under vacuum. Hexane was added to extract the product from the remaining Magnesium salts. After filtration, hexane was removed under vacuum, leaving a brown oil, which was distilled at reduced pressure yielding the BTEB clear colourless oil.

The product was then analyzed by solution NMR to confirm the formation of the precursor.

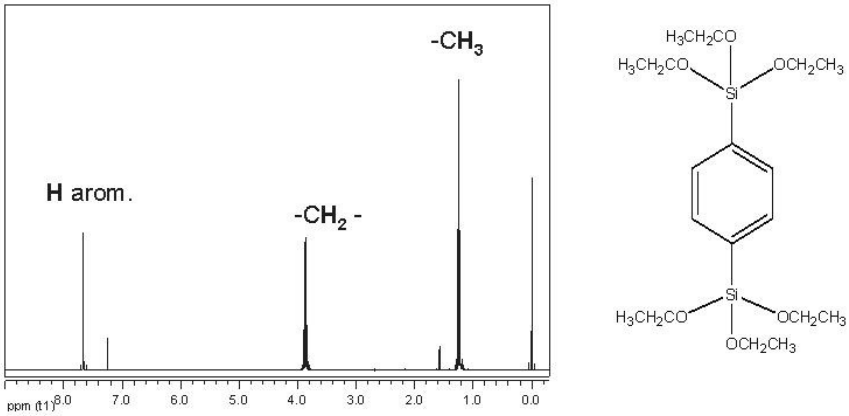

Figure 5.3

^{1}H NMR spectrum of bis-(Triethoxysilyl)benzene. Main signal are aromatic hydrogens (7.66 ppm), methylene hydrogens (3.85 ppm) and methyl hydrogens (1.24 ppm)

5.6.2 Synthesis of phenylene PMO

P-phenylensilica was prepared with a template synthesis in basic aqueous solution using octadecyltrimethylammonium bromide (C_{18}TMABr) as surfactant. The molar ratios of the reactants are:[14]

C_{18}TMABr 0.96 : BTEB 1 : NaOH 4.03 : H_2O 559.23

C_{18}TMABr was dissolved in the sodium hydroxide solution at 60-70 °C to ensure the complete dissolution, and then BTEB was added dropwise to the solution under vigorous stirring at room temperature. The mixture was treated with ultrasounds for 20 min to improve dispersion, stirred at room temperature for 20 h and then kept at 95 °C for 20 h under static conditions. The white precipitate was recovered by filtration and dried, then surfactant was removed washing about 1g of powder in 250 ml of ethanol and 9 g of 36% hydrochloride aqueous solution at 70 °C for 8 h.

Before to be analyzed, collected powders were outgassed under vacuum at 160°C to remove completely ethanol.

5.6.3 Characterization of p-phenylensilica

Obtained samples were investigated with X-ray diffraction, adsorption measurements and thermogravimetric analysis.

XRD pattern shows two distinct families of peaks: one in the range of 1-3 2θ-degree associated to mesoscopic order of channels, and the other, between 5 and 20 2θ-degree, associated to the crystal-like disposition of benzene rings. The mesoscopic signals give a distance of 4.57 nm, corresponding to a lattice constant of 5.28 nm,[23] when molecular-scale signals are associated to a typical distance of 7.6 Å. In the molecular range a broad peak is also present. This peak is generally associated to an amorphous part in the structure.

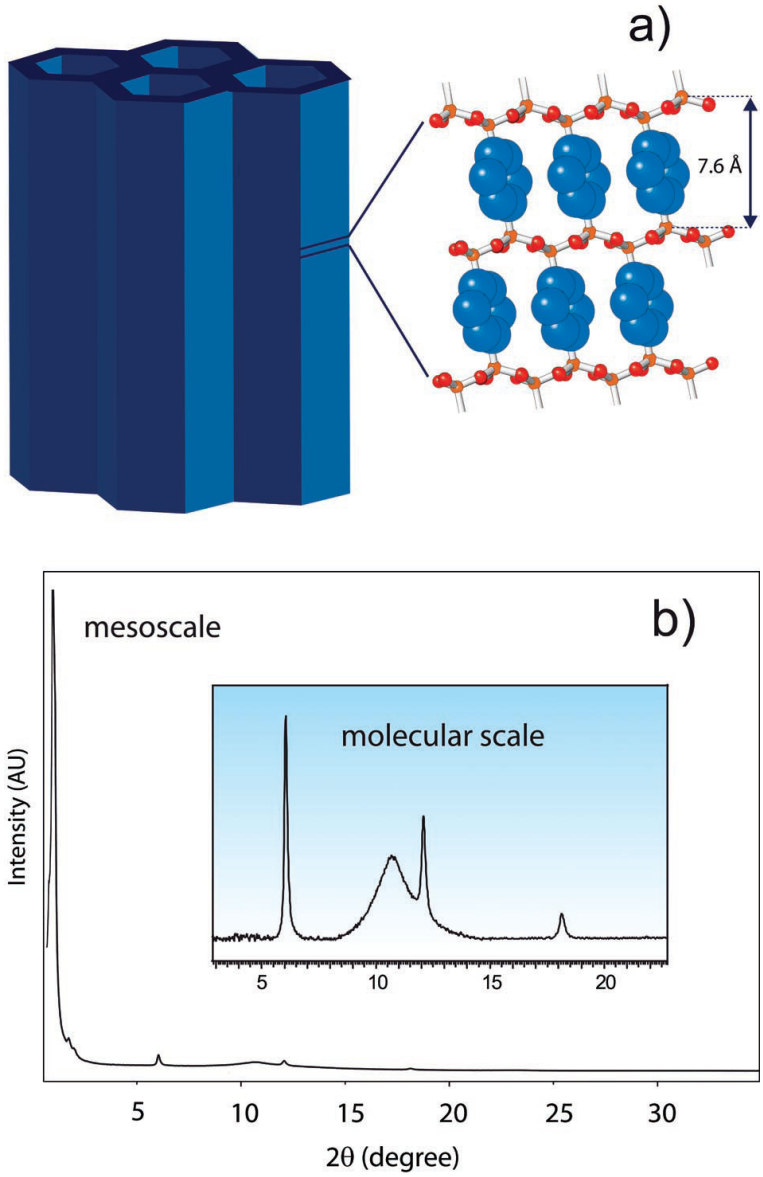

Figure 5.4

Representation of molecular order in *p*-phenylensilica (a) and X-ray diffraction pattern with both the molecular and the mesoscale order (b)

BET calculation gives a surface area of 780.4 m^2/g, while BJH methods finds a total pore volume of about 0.78 cm^3/g. TGA analysis show a weight loss, associated to the degradation of the organic part, of 35 % and a thermal stability over 500 °C.

On this porous structure different gases and chemical vapors have been adsorbed.

Observed chemical vapors have been Benzene, hexafluorobenzene, cyclohexane and ethanol, while gases have been carbon dioxyde, methane, oxygen and nitrogen.

Adsorption experiments have been performed at different temperatures, as reported in figures 5.5 and 5.6.

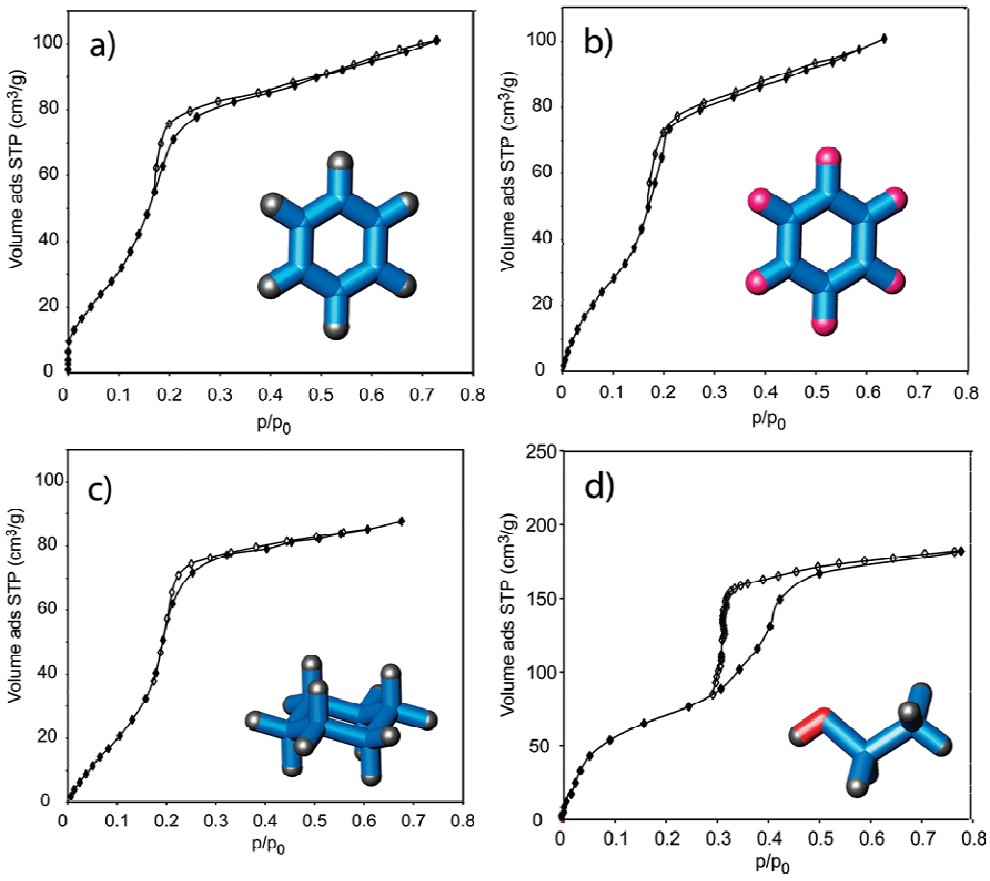

Figure 5.5

Adsorption isotherms on *p*-phenylensilica of:

a) benzene (room temperature), b) hexafluorobenzene (room temperature),

c) ciclohexane (room temperature) and d) ethanol (273 K)

Vapor adsorption isotherms are all of type IV, typical of mesoporous systems, and with small hysteresis, index of absence of ink-bottle pores. Adsorbed quantities for benzene, hexafluorobenzene and ciclohexane are quite similar (about 4 mmol/g) and this could mean that strong π-π interactions, between aromatic rings on pore walls and guest molecules, are not present. Actually, there is a little difference at the begin of the curve. This could mean that guest molecules interact strong with pore walls at low pressures, while at higher pressures interactions among guest molecules are preferred. Isotherm of ethanol, instead, present a different shape and a larger hysteresis, reaching an adsorbed

value of about 8.7 mmol/g (40% by weight). This affinity is probably due to the double hydrophilic-hydrophobic interaction with organic aromatic rings and inorganic silica layers.

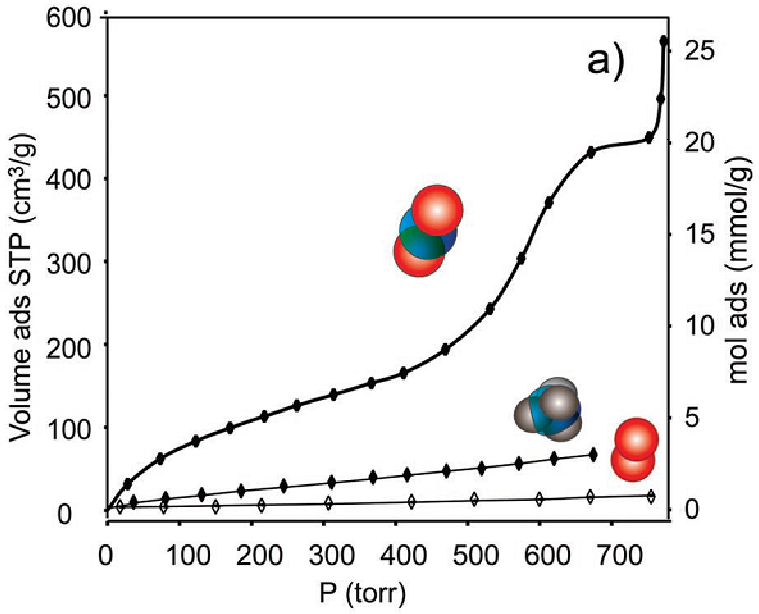

Figure 5.6

Adsorption isotherms of different gases on *p*-phenylensilica.

From the top: carbon dioxide (195 K), methane (195 K) and oxygen (273 K)

By gas adsorption measurements, we can see that the matrix has generally adsorptive properties greater than common inorganic zeolites with 1D channel system (methane uptake of 56 cm^3/g versus correspondent 49 cm^3/g for MCM-41 silica). Moreover, carbon dioxide adsorption at 195 K reaches the remarkable value of 20 mmol/g, corresponding to 88% by weight. Taking into account the density of liquid CO_2 at its boiling point and comparing the re-calculated pore volume (0.85 cm^3/g) with that calculated from nitrogen adsorption, we demonstrated a virtual 100% filling of the nanochannels. The absence of hysteresis indicates easy accessibility to the nanochannels and this fact, confronting the high adsorption values with those smaller of oxygen and negligible of hydrogen, make the *p*-phenylensilica an ideal candidate as a system for purification of carbon dioxide mixtures with oxygen and hydrogen.

On this structure, we have performed advanced 2D solid state NMR analysis to characterize the relationships between the organic cores and the inorganic bands.[24]

Monodimensional ^{29}Si and ^{1}H NMR experiments give informations about structure integrity. As shown in figure 5.7 (see below), in Silicon spectra there are only T species signals, attributed to silicon atoms directly linked to a carbon nucleus. Absence of Q signals, typical of silicon atoms linked with four oxygens, indicate that the Si-C covalent bond is stable in synthesis conditions and that there has been not cleavage.

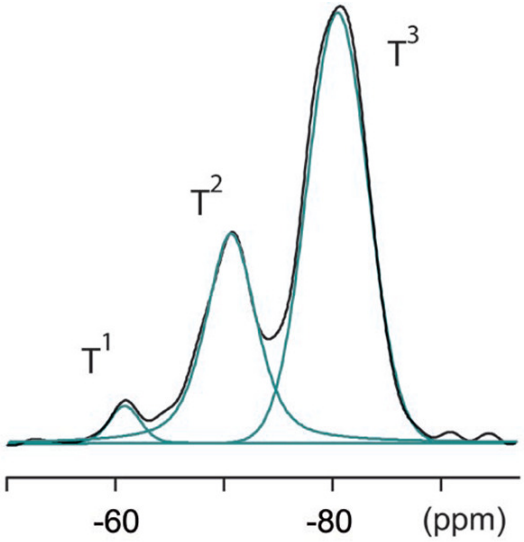

Figure 5.7

^{29}Si solid state NMR spectrum of *p*-phenylensilica matrix

The three T peaks are associated to species of different condensation. The number of condensed silanol groups is indicated at the exponential, so T^3 species are full-condensed while T^2 and T^1 have respectively one and two uncondensed groups. Intensity of single peaks are 64.9% (T^3, -80.5 ppm), 32.3% (T^2 , -70.4 ppm) and 2.8% (T^1, -60.9 ppm) to indicate a good condensation degree. Uncondensed silanol species are also visible in monodimensional proton spectrum, as silanol proton signal (1.8 ppm), with the signal associated to aromatic protons (6.8 ppm):

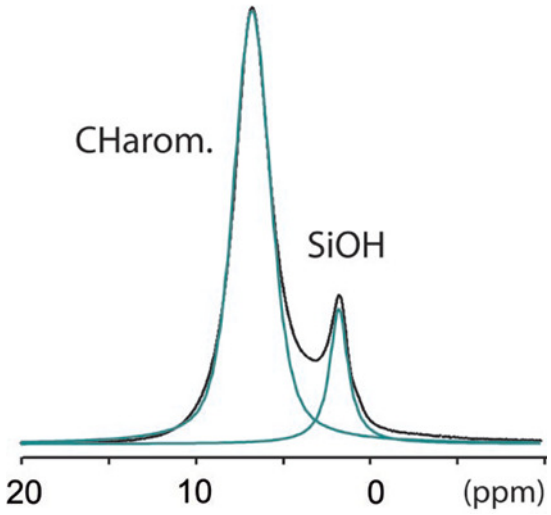

Figura 5.8

^{1}H solid state NMR of *p*-phenylensilica matrix

Monodimensional spectra have been used to interpretate the 2D spectra ^{1}H-^{29}Si and ^{1}H-^{13}C.

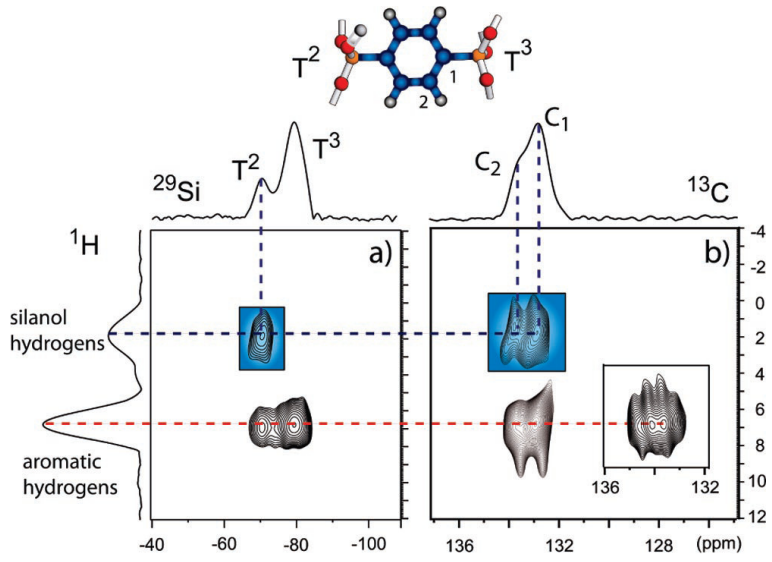

Figure 5.9

2D solid state NMR spectra ^{1}H-^{29}Si (a) and ^{1}H-^{13}C of *p*-phenylensilica matrix

In bidimensional spectra are clearly visible the correlation between the aromatic linker and the silica structure, as indicated by cross peaks between aromatic hydrogen atoms and T^3 silicon species and, at the same time, carbon atoms correlate with silanol

hydrogens. Moreover, at short contact times, near to 100 μs, aromatic hydrogens revealed two separated carbon signals at 134.3 and 133.5 ppm, as illustrated in the insert in figure 5.9. Following the dynamics of signal intensity at variable contact times we can associate each signal to the correspondent protonated and non protonated carbon nuclei. The presence of only two resonances confirms the highly symmetric arrangement of the *p*-phenylene group in the ordered walls.

In conclusion, we have synthesized and characterized a highly regular hybrid structure with molecular order and high surface area that shows interesting adsorption properties useful for gas storage and purification.

5.7 References:

1) F. Hoffmann, M. Cornelius, J. Morell, M. Froeba; *Angew. Chem. Int. Ed.* **2006**, *45*, 3216-3251

2) R.K Iler, U.S. Patent 2, *645*, 149 (Dupont), **1953**

3) a) W.J. Herzberg, W.R. Erwin; *J. Colloid Interface Sci.* **1970**, *33*, 172-177; b) R. Anwander, I. Nagl, M. Widenmeyer, G. Enghelhardt, O. Groeger, C. Plam, T. Röser; *J. Phys. Chem. B* **2000**, *104*, 3532-3544; c) Y.C. Liang, R. Anwander; *J. Mater. Chem.* **2007**, *17*, 2506-2516; d) M.G.L. Petrucci, A.K. Kakkar; *Chem. Commun.* **1995**, 1577-1578

4) a) S.L. Burkett, S.D. Sims, S. Mann; *Chem. Commun.* **1996**, 1367-1368; b) D.J. Macquarrie; *Chem. Commun.* **1996**, 1961-1962; c) M.H. Lim, C.F. Blanford, A. Stein; *J. Am. Chem. Soc.* **1997**, *119*, 4090-4091

5) a) O. Olkhovyk, M. Jaroniec; *J. Am. Chem. Soc.* **2005**, *127*, 60-61; b) R.M. Grudzien, S. Pikus, M. Jaroniec; *J. Phys. Chem. B* **2006**, *110*, 2972-2975

6) a) R.J.P. Corriu, A. Medhi, C. Reyé, C. Thieuleux; *Chem. Mater.* **2004**, *16*, 159-166; b) R.J.P. Corriu, A. Medhi, C. Reyé, C. Thieuleux; *Chem. Commun.* **2002**, 1382-1383; c) R.J.P. Corriu, A. Medhi, C. Reyé, C. Thieuleux; *Chem. Commun.* **2003**, 1564-1565; d) R.J.P. Corriu, A. Medhi, C. Reyé, C. Thieuleux; *New J. Chem.* **2003**, *27*, 905-908; e) J. Alauzun, A. Mehdi, C. Reyé, R.J.P. Corriu; *J. Mater. Chem.* **2007**, *17*, 349-356; f) J. Alauzun, A. Mehdi, C. Reyé, R.J.P. Corriu; *New J. Chem.* **2007**, *31*, 911-915

7) a) S. Inagaki, S. Guan, Y. Fukushima, T. Oshuna, O. Terasaki; *J. Am. Chem. Soc.* **1999**, *121*, 9611-9614; b) B.J. Melde, B.T. Holland, C.F. Blanford, A. Stein; *Chem. Mater.* **1999**, *11*, 3302-3308; c) T. Asefa, M.J. MacLachlan, N. Coombs, G.A. Ozin, *Nature*, **1999**, *402*, 867-871

8) a) K. Nakajima, I. Tomita, M. Hara, S. Hayashi, K. Domen, J. N. Kondo; *Adv. Mater.* **2005**, *17*, 1839-1842; b) K. Nakajima, I. Tomita, M. Hara, S. Hayashi, K. Domen, J. N. Kondo; *Catal. Today* **2006**, *116*, 151-156; c) X. Zhou, S. Qiao, N. Hao, X. Wang, D. Zhao, G.Q. Lu, *Chem. Mater.* **2007**, *19*, 1870-1876

9) K.J. Shea, D.A. Loy, O. Webster; *J. Am. Chem. Soc.* **1992**, *114*, 6700-6710

10) a) M.B. Kapoor, S. Inagaki; *Bull. Chem. Soc. Jpn.* **2006**, *79*, 1463-1475; b) S. Fujita, S. Inagaki; *Chem. Mater.* **2008**, *20*, 891-908

11) a) S.S Park, B. An, C.S. Ha; *Microporous and Mesoporous Materials* **2008**, *111*, 367-378; b) H. Zhong, G. Zhu, J. Yang, P. Wang, Q. Yang; *Microporous and Mesoporous Materials* **2007**, *100*, 259-267; c) Y. Goto, N. Mizoshita, O. Ohtani, T. Okada, T. Shimada, T. Tani, S. Inagaki; *Chem. Mater.* **2008**, *20*, 4495-4498

12) a) M.C. Burleigh, S. Jayasundera, M.S. Spector, C.W. Thomas, M.A. Markowitz, B.P. Gaber; *Chem. Mater.* **2004**, *16*, 3-5; b) M.A. Wahab, I. Kim, C.S. Ha; *J. Solid State Chem.* **2004**, *177*, 3439-3447; c) J. Morell, M. Güngerich, G. Wolter, J. Jiao, M. Hunger, P.J. Klar, M. Froeba; *J. Mater. Chem.* **2006**, *16*, 2809-2818

13) C. Yoshina-Ishii, T. Asefa, N. Coombs, M.J. MacLachlan, G.A. Ozin; *Chem. Commun.* **1999**, 2539-2540

14) S. Inagaki, S. Guan, T. Oshuna, O. Terasaki; *Nature* **2002**, *416*, 304-307

15) a) M.P. Kapoor, Q. Yang, S. Inagaki; *J. Am. Chem. Soc.* **2002**, *124*, 15176-15177; b) Y. Yang, A. Sayari, *Chem. Mater.* **2007**, *19*, 4117-4119; c) A. Sayari, W. Wang; *J. Am. Chem. Soc.* **2005**, *127*, 12194-12195; d) M. Cornelius, F. Hoffmann, M. Froeba; *Chem. Mater.* **2005**, *17*, 6674-6678; e) Y. Xia, W. Wang, R. Mokaya; *J. Am. Chem. Soc.* **2005**, *127*, 790-798; f) Y. Xia, R. Mokaya; *J. Mater. Chem.* **2006**, *16*, 395-400; g) Y. Xia, Z. Yang, R. Mokaya; *Chem. Mater.* **2006**, *18*, 1141-1148; h) Y. Xia, R. Mokaya; *J. Phys. Chem. B* **2006**, *110*, 3889-3894

16) A. Comotti, S. Bracco, P. Valsesia, L. Ferretti, P. Sozzani; *J. Am. Chem. Soc.* **2007**, *129*, 8566-8576

17) a) A. Kushel, S. Polartz; *Adv. Funct. Mater.* **2008**, *18*, 1272-1280; b) M. Ohashi, M.P. Kapoor, S. Inagaki; *Chem. Commun.* **2008**, 841-843

18) J. Morell, S. Chatterjee, P.J. Klar, D. Mauder, I. Shenderovich, F. Hoffmann, M. Froeba; *Chem. Eur J.* **2008**, *14*, 5935-5940

19) A. Kuschel, H. Sievers, S. Polarz; *Angew. Chem. Int. Ed.* **2008**, *47*, 9513-9517

20) M. Cornelius, F. Hoffmann, B. Ufer, P. Behrens, M. Froeba; *J. Mater. Chem.* **2008**, *18*, 2587-2592

21) a) K. Landskron, G.A. Ozin; *Science* **2004**, *306*, 1529-1532; b) W.J. Hunks, G.A. Ozin; *Adv. Funct. Mater.* **2005**, *15*, 259-266

22) J. Howarth, *Core Organic Chemistry*, John Wiley & Sons, England, **1998**

23) Considering geometrical properties of hexagonal channel system, planar distance of X-ray diffraction must be multiplied for $2/3^{1/2}$. See paragraph 4.5.3 for more details

24) S. Bracco, A. Comotti, P. Valsesia, B.F. Chmelka, P. Sozzani; *Chem. Commun.* **2008**, 4798-4800

CHAPTER 6

Polymeric nanocomposites and shape replica process

A composite material is a system constituted by two or more different materials, also named phases, that interact with each other. If single phases have nanometric dimensions, we can define them nanocomposite materials. In nanocomposites, interactions occur between single molecules and are generally weak such as dispersive forces, hydrogen bonds or dipole-dipole interactions. To increase system stability, it is often necessary to have a large number of these weak interactions that is generally obtained by extending the interfaces.[1] Consequently, a large number of nanocomposites has a host-guest system structure, where a principal phase with large surface area, named matrix, includes and interacts with a second phase through its high surface.

Polymeric nanocomposites are a two-phase systems in which polymer chains interact intimately with an inorganic matrix, often a porous silica. They were historically studied as a method to reinforce mechanical properties of bulk polymers. Inorganic matrices have been dispersed in polymeric material as anti-flame systems and to avoid polymer abrasion or deformation by mechanical stress.[2] The use of nanoporous silica or carbon systems, instead to nanosized particles, bring to a better interaction between the two materials, due to intercalation of polymer chains in matrix pores, and by consequence to an homogeneous dispersion.

To prepare polymeric nanocomposites, polymer and matrix could be mechanical mixed to obtain an homogeneous compound or the polymer could be directly synthesized inside matrix pores by an *in situ* polymerization.[3] This second process has bring to a large number of different applications, such as the use of polymeric nanocomposites to control molecular weight, to maintain active centres for preparation of block copolymers and to obtain porous polymeric systems by a reverse replica process.[4-6]

In recent years, our group has demonstrated that use of a silica matrix with defined micrometric morphology brings to the generation of polymeric micro-objects with

defined nanometric structure and the same micrometric shape of the matrix by a shape replica process.[7]

In this chapter we will discuss our works on preparation and study of polymeric nanocomposites obtained using different kinds of monomer left to diffuse in silica matrices with various shapes, as a key point for silica-to-polymer shape replication.

6.1 Intrapore chemistry

Preparation of host-guest systems by *in situ* polymerization is a typical example of the use of nanoporous materials as reaction vessels for chemical reactions in confined spaces. The series of reactions conduced inside matrix pores could also be named intrapore chemistry.[8]

The narrow, controlled pore size distribution in the ordered mesoporous silica systems and the large pore openings have added a new dimension to intrapore chemistry that was previously focused on microporous zeolitic materials. In fact, mesopores could host small structures, as large as few nanometers, such as metal clusters or polymer fibrils. This discovery has stimulated research in areas that include fundamental studies of sorption and phase transitions in confined spaces, ion exchange, the formation of intrachannel metal, metal oxide, and semiconductor clusters, and inclusion of various metal complexes and other guests. The internal surface reactivity of the mesoporous hosts has been exploited by covalently anchoring a number of functional groups to the channel walls, including attachment of ligands that are used for the formation of bulky metal complexes. An alternative approach to grafting the mesoporous internal walls is developing; that is, co-condensation of framework precursors with metal sources that are covalently bound to a functional group. Finally, intrachannel reactions even include polymerization of preadsorbed monomers, thus leading to confined filaments of common polymers as well as conducting materials such as carbon. Intriguing applications of these systems include catalysis with large substrate molecules, formation of novel nanocomposites, and separation.

Inclusion chemistry in periodic mesoporous hosts, so, regards a large number of applications such as sorption and phase transitions; ion exchange and complexation; metal and semiconductor clusters and wires; oxide and sulphide clusters; inclusion of

metal complexes and other guests; covalent grafting of ligands and functional groups; hybrid materials obtained by in situ co-condensation; and, in the case in examination, polymerization in mesoporous channels.[9-15]

6.2 Polymerization in mesoporous silica

Confined polymerization in porous matrices are well known since 1982.[16]

Amorphous silica particles and zeolites have been used in polymer composites, but few articles described the exploitation of mesoporous systems like MCM-41 for the preparation of such nanocomposites.

The first work in literature that reports an *in situ* polymerization in a mesoporous silica was published by T. Bein in 1994.[17] In this work he used MCM-41 silica as vessel to perform confined polymerization of aniline to obtain conductive polymer filaments.

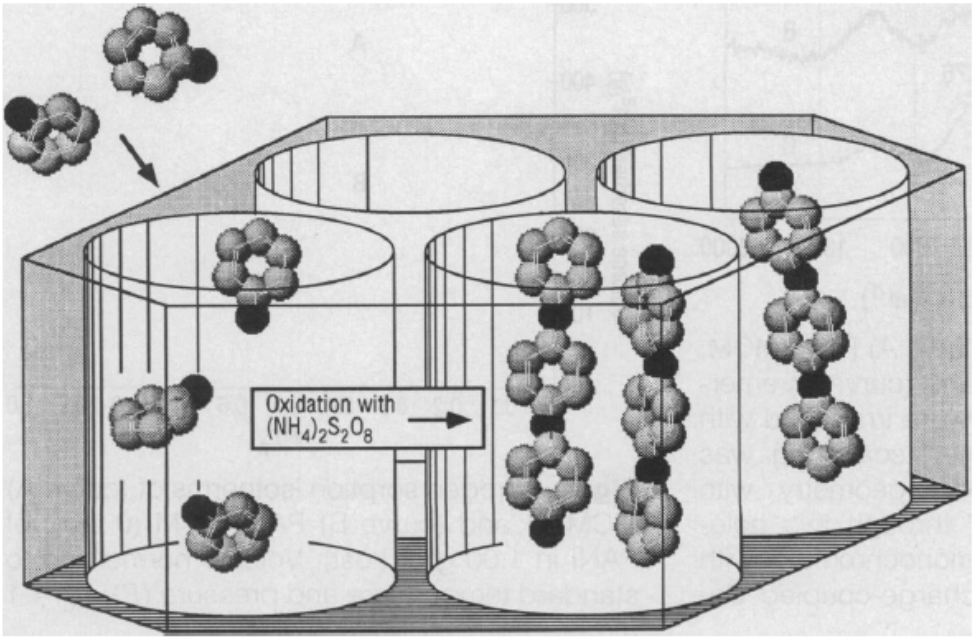

Figure 6.1

Reaction scheme for the encapsulation of polyaniline in the channels of MCM-41 [17]

Polymerization was started by immersion of the system filled with monomer in an aqueous solution of peroxydisulfate and electronic adsorption spectra showed typical transition of emeraldine systems. Based on this, a large number of other works about confined polymerization in mesochannels was published in following years. The aims

of these works were to exploit the highly regular pore pattern and silica properties to obtain functional materials. In fact, the regular system of large channels in MCM hosts offers unique opportunities for the preparation of new nanostructured materials and the feasibility of forming polymer networks within the internal pore structure of these materials was demonstrated. Confined polymerization was achieved through adsorption and subsequent polymerization of monomers in the host. The monomers were introduced into the dehydrated and evacuated hosts from the vapor phase to avoid the formation of polymer layers on the external surface. Polymerization proceeded via radical initiation with high yield and resulted in nanocomposites with high polymer content. Thus, Llewellyn et al. adsorbed styrene, vinyl acetate, and methyl methacrylate (MMA) into MCM hosts with different pore sizes and studied the effect of confinement on polymer growth. An increase in chain length of PMMA with decreasing pore size of MCM-41 was associated with inhibited termination processes in the channels.[18]

In a related study, the adsorption of MMA in MCM-41 was also performed by Aida et al.[4] These authors observed that PMMA grown in the mesoporous channels of MCM-41 can exceed the bulk molecular weight by an order of magnitude; the chain length was controlled by the stoichiometry between the monomer and initiator. Differently from previous cited works, in this case the monomer was diffused into the silica channels by liquid phase, helping the diffusion with a series of freeze-and-thaw cycles to eliminate gas trapped inside the pores. By this method it was possible to let diffuse the radical initiator, generally benzoyl peroxide, peroxydisulphate or azo-bis isobutyronitrile (AIBN), dissolved in the monomer.[4,19,20] By this method, it is possible to let diffuse into the silica monomers with high molecular weight, for example styrene, and then perform confined polymerizations.

Another chance gift from confined polymerization process is to use silica matrices to avoid the polymerization end step, maintaining “live” active centres.[5] In fact, in controlled environment radical chain ends could not joint themselves or transfer the active radical to silica walls or other species. By this way, it is possible to think to use extended silica matrices to perform successive confined polymerizations with different monomers, generating defined block copolymers.

Once obtained the polymeric nanocomposite, polymer could be extracted from silica matrix by washing with an opportune solvent and then collecting it by precipitation, or

directly collecting it by filtration after silica dissolution by etching in HF solution. Otherwise, nanocomposites could be used for post synthesis applications.

Some examples of these post-synthetic applications are generation of conductive polymers in silica nanochannels or fabrication of carbon nanofibers with defined diameter.[17,21] In the first case, confined polymers still show possibility to support charge carriers by microwave conductivity measurements. Conductivity is about one half respect to the bulk polymer, nevertheless nanocomposites with linear nanometric silica channels could be thought as nanometric electrical cables. Another candidate for conductive nanostructures is graphitic carbon, because it is chemically stable and exhibits high conductivity. One of the most common methods to realize carbon structures with graphitic fragments is the pyrolysis at high temperatures in non-oxidative atmosphere of polyacrylonitrile. It has been demonstrated that it is possible to obtain confined polyacrylonitrile in nanometric silica channels and use it to obtain conductive graphitic carbon structures of nanometric dimensions. For a more detailed discussion about polyacrilonitrile we will remand on the next chapter.

At last, a new, twist method to use confined polymerization was reported by Mallouk, Ozin and co-workers.[6] These authors form a polymer mould of the channel structure of MCM-41, followed by dissolution of the host in HF: phenol-containing MCM-41 was treated with formaldehyde vapour and HCl gas at elevated temperatures to form a cross-linked phenolic resin. After extraction from the host, polymer mesofibers that can visualize the length of mesoporous channels were recovered.

Figure 6.2

Transmission electron micrograph of extracted polymer mesofibers.

Scale bar reported corresponds to 100 nm [6]

This work was the first example of attempt to replicate the regular structure of porous silica matrix with an organic material. This experiment brings to the reverse replica process to obtain porous carbons and to the shape replica process described below.

6.3 Shape replica process

The specific functions of macroscopic objects are often modulated by their shape and design. On a smaller scale, the attainment of microscopic objects endowed with a well defined shape enables novel functional properties on a diversity of hierarchical scales.[22] A strategy to realize high performance innovative materials is the fabrication of ordered composite materials with a finely tuned structure at the nanoscale, nevertheless morphological control at the micrometric scale is still rare.

First examples of shape modelling at micrometric level were reported by Ozin and coworkers about synthesis of silica particles with defined micrometric morphology, but the shaping of plastic matter on the micrometre scale was still limited to simple forms that are typically obtained as inverse replicas of channel-like cavities and colloidal crystals.[23,24] This limitation could be, in principle, overcome by transferring the shape pattern from one material to another.

In 2006, our group present a first work where mesoporous silica particles with defined micrometric morphology were used as a mould to obtain porous micro-objects in polystyrene, that maintain the shape of starting silica matrices by a process named direct shape replica.[7] Polymer micro-objects were obtained by confined polymerization of styrene using AIBN as radical initiator, followed by silica dissolution with HF solutions. Despite the dramatic material change, the morphotypes remained fully preserved throughout the process, the plastic micro-objects being recognizable clones of the parent silica shapes. The mechanism of shape replica process is schematically illustrated in figure 6.3:

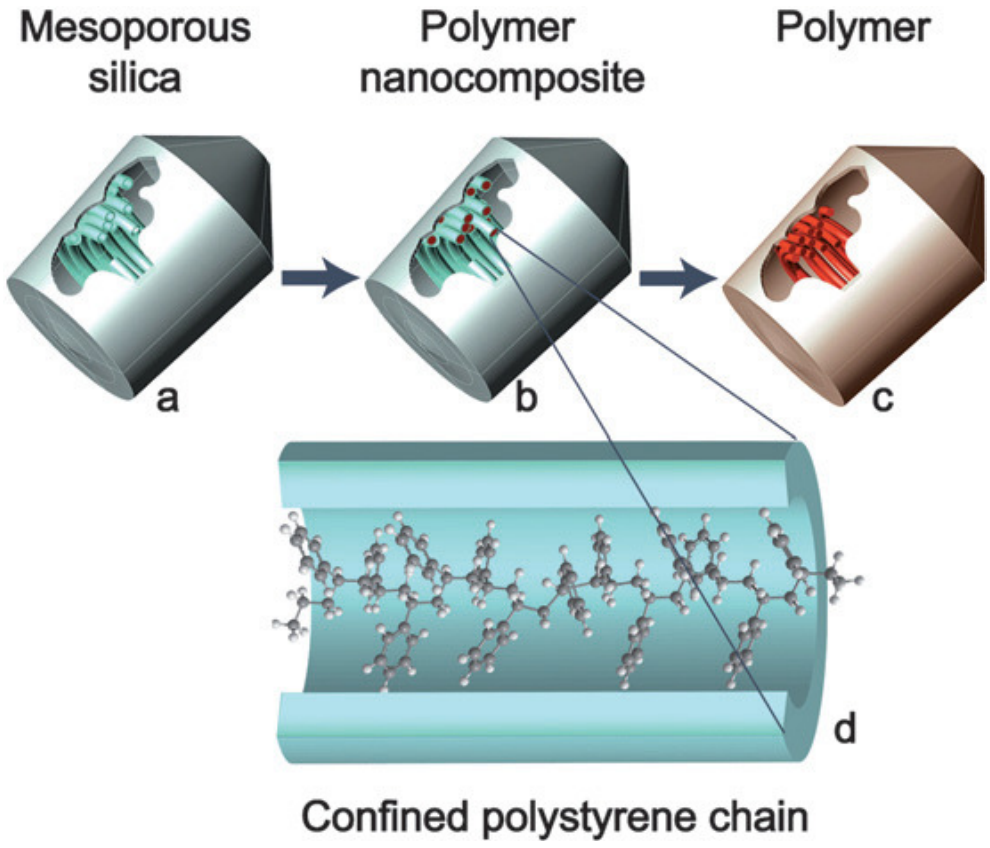

Figure 6.3

Schematic representation of shape replica process. The micrometric shape is retained in each step, starting from morphological mesoporous silica (a), passing from polymeric nanocomposite (b) until the final polymeric micro-object (c).

On the bottom (d) a representation of polystyrene chain confined in the nanometric silica channel [7]

The nanocomposite adducts play an active role as mediators for the replica process from self-generated silica objects to polymer reproductions and assume the architecture of a geometrical solid of micrometric dimensions. The realization of an extensive polymer–silica interface is pivotal to the success of the plastic-object fabrication. In fact, only a material consisting of two distinct phases so intimately entangled can explain the success of a replica process in which the morphology of the original material is entirely transposed to a polymeric material that fully retains its shape. This intimae interaction could be investigated by 2D hetcor NMR experiments (see below).

Polymeric micro objects retain both micrometric morphology and memory of silica nanometric structure, as demonstrated by TEM imaging:

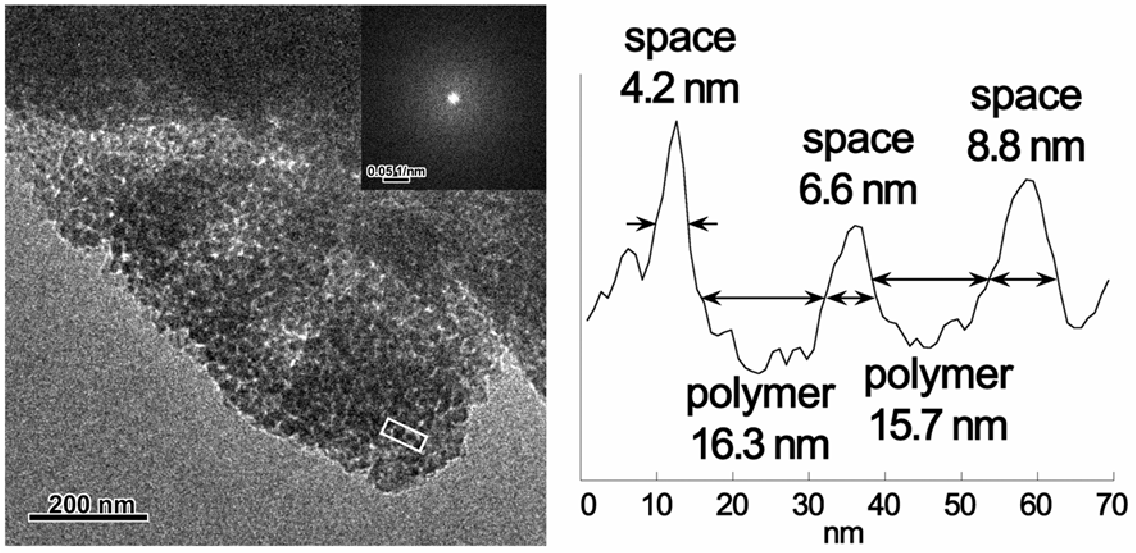

Figure 6.4

TEM image of extracted polymer micro-object. On the right, reconstruction of profilometer analysis performed on the area evidenced in the TEM image [7]

Obtained polymeric micro-objects maintain 60% of their porosity after compression at 1,500MPa for 30 min. The extended polymer surface can be modified, as shown by the efficiency of a mild sulphonation reaction with concentrated H_2SO_4 at room temperature (substitution degree of 1.8 mmol g−1). The remarkable change of surface pH and hydrophilicity permitted the anchorage of chemicals: water-soluble dyes for laser and diagnostic applications could be linked to the material.

The successful process of transformation of micrometric objects from one material into another with complete shape retention opens up new ways to realize micro-objects tailor-made to a given design, the final goal being to combine shape factors with chemical reactivity to modulate properties of the end products. Morphological control over individual polymer particles has never been achieved to such a level of complexity and accuracy. In fact, the shape of mesoporous silica is retained on micrometresized scale, imprinting it onto standard polymers. The combined control over shape and porosity promises novel applications of plastic matter on the microscale. Owing to the ductility and weldability of plastic matter, the miniaturized objects can be used as building blocks for microfabrication, and can be assembled into micromachines. Biological macromolecules such as DNA were encapsulated in the plastic tube-shaped objects, giving great potential for biomedical applications.

In this PhD work we have used shape replica process using different vinyl monomers, such as polystyrene or polymethylmethacrylate, to obtain porous polymeric micro objects with different micrometric morphologies. Interactions between polymeric and silica phase were deeply investigated with advanced 2D solid state NMR experiments, to point out the key factors of the replica process.

6.4 Polymerization in morphological silica samples

We have performed different *in situ* polymerizations in morphological mesoporous silica using different monomers, such as styrene, methylmethacrylate and acrylonitrile. Aim of this work is the realization of nanocomposites to obtain shape replica effect with different morphologies. Here below are reported the results of polystyrene and polymethylmethacrylate, while for polyacrylonitrile nanocomposites we will remand to the next chapter.

6.4.1 In situ polymerization process

Despite used monomer or morphology of silica, synthesis method to obtain polymeric nanocomposites was the same. Monomers were purified by distillation at room temperature and reduced pressure to remove stabilizer contained in commercial reactants. As radical initiator, commercial azo-bis isobutyronitrile (AIBN) was used

without purification. A mixture of fresh distilled monomer and AIBN, present at 0.7% weight respect to monomer, was outgassed two times by freeze and thaw cycles and then transferred with a cannula under vacuum on the silica matrix, previously dried under vacuum at 160 °C overnight. Once covered silica with the liquid mixture, the sample was outgassed three times with freeze and thaw cycles and then leaved at low temperature and dark for some days to leave time to the mixture to fill completely the matrix pores. Sample was then collected by filtration and radical initiator thermally activated at 100 °C under nitrogen flux for three hours and half.

6.4.2 Nanocomposites characterization

As-obtained nanocomposites were characterized by differential scanning calorimetry (DSC) to verify the effective formation of nanocomposites and the absence of external polymer. In the case of polystyrene and polymethylmethacrylate, external polymer is visible by the presence of glass transition phenomenon, when confined polymer does not show that because polymer chains do not have enough space for collective motions and to change their state:

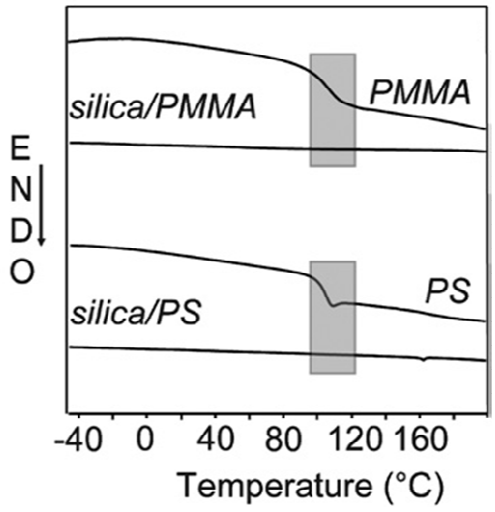

Figure 6.5

DSC analysis conduced on polymeric nanocomposites and bulk polymers.

In evidence the disappearance of the glass-transition phenomena in the nanocomposite samples

If external polymer is present, the sample was washed in refluxing chloroform overnight, collected by filtration and analyzed again until disappearance of glass transition signal. Of course, in this case DSC alone is not enough to demonstrate the effective formation of nanocomposite. It is necessary to confirm the presence of polymer by solid state NMR techniques or thermogravimetric analysis (see below).

Once removed external polymer, nanocomposites have been analyzed with adsorption measurements, thermogravimetric analysis and advanced solid state NMR techniques.

Adsorption measurements of N_2 and benzene vapors (see figure 6.6) indicate a reduction of the free space within the silica pores by the presence of polymeric chains and they again show an adsorption IV-type curve, typical of mesoporous materials. The adsorption profile of silica particles grown under quiescent conditions usually shows a smoother step than those obtained under conventional conditions.[25]

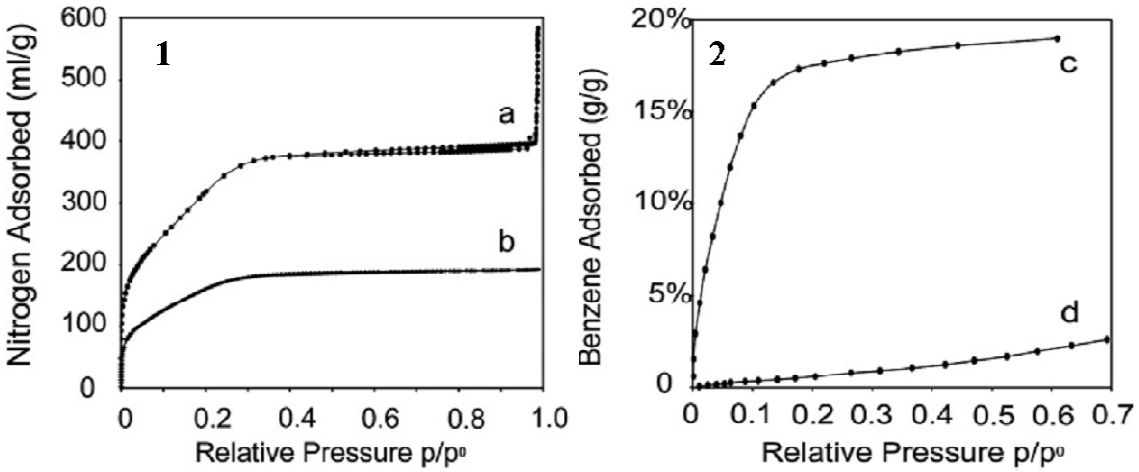

Figure 6.6

Nitrogen (1) and benzene (2) adsorpion isotherms of gyroidal silica matrix (a,c) and polymeric nanocomposite (b,d)

The surface area was evaluated with the BET method that shows, for gyroidal nanocomposites, a decrease to 612 m^2/g, half of that found for the empty silica matrix, while the total volume is 0.28 cm^3/g in capacity, demonstrating the incorporation of polymers inside the silica mesochannels. The shape of the N_2 isotherm follows the same pattern as that of the mesoporous silica particles and there is no decrease in the pore diameter dimension. The small nitrogen molecules are allowed to enter and explore

polymer-free chambers in the nanochannels by percolating through defects in the inorganic structure. In the case of benzene vapors, the reduction of adsorption is dramatic (see figure 6.6 2): the pattern is typical of a material showing low porosity. This could be attributed to the larger size of benzene molecules, that hinds their diffusion since the percolation ways are occluded by the polymer.

TGA trace demonstrates that polystyrene and polymethylmethacrilate fill respectively 66% (20% weight loss) and 86% (30% weight loss) of the available intrachannel space.

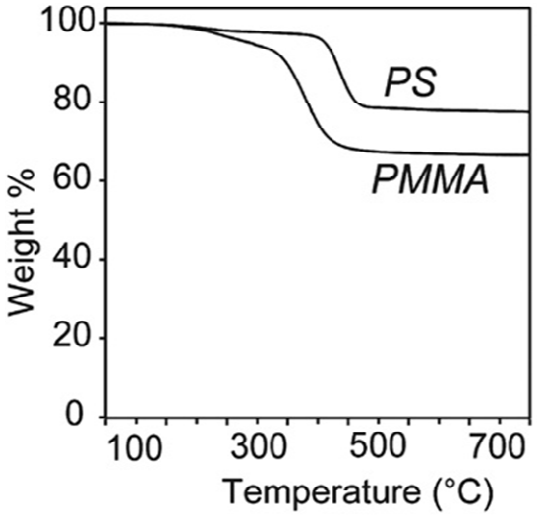

Figure 6.7

TGA analysis on polymeric nanocomposites: polystyrene (top) and polymethylmethacrylate (down)

The nanocomposite with polystyrene shows a complete decomposition of the polymer at a temperature of 500°C, that is much higher than the typical decomposition temperature of the bulk polystyrene, indicating the matrix acts as a protective shell for the polymer. The specific density of the polystyrene nanocomposite, measured by He picnometry, is decreased to 1.91 g/cm^3 starting from a value of 2.1 g/cm^3 for silica micro-objects, confirming the inclusion of 20% by weight of polymer (assuming polystyrene density of 1.04 g/cm^3).

^{13}C fast-MAS CP NMR experiments performed on nanocomposite samples highlight polymer formation and the absence of residual monomer. In fact, in these spectra only characteristic peaks of the three polymers are observed. With 2D solid state NMR

measurements, instead, we can see directly the intimae correlation between confined polymer and pore walls, as indicated in figure 6.8:

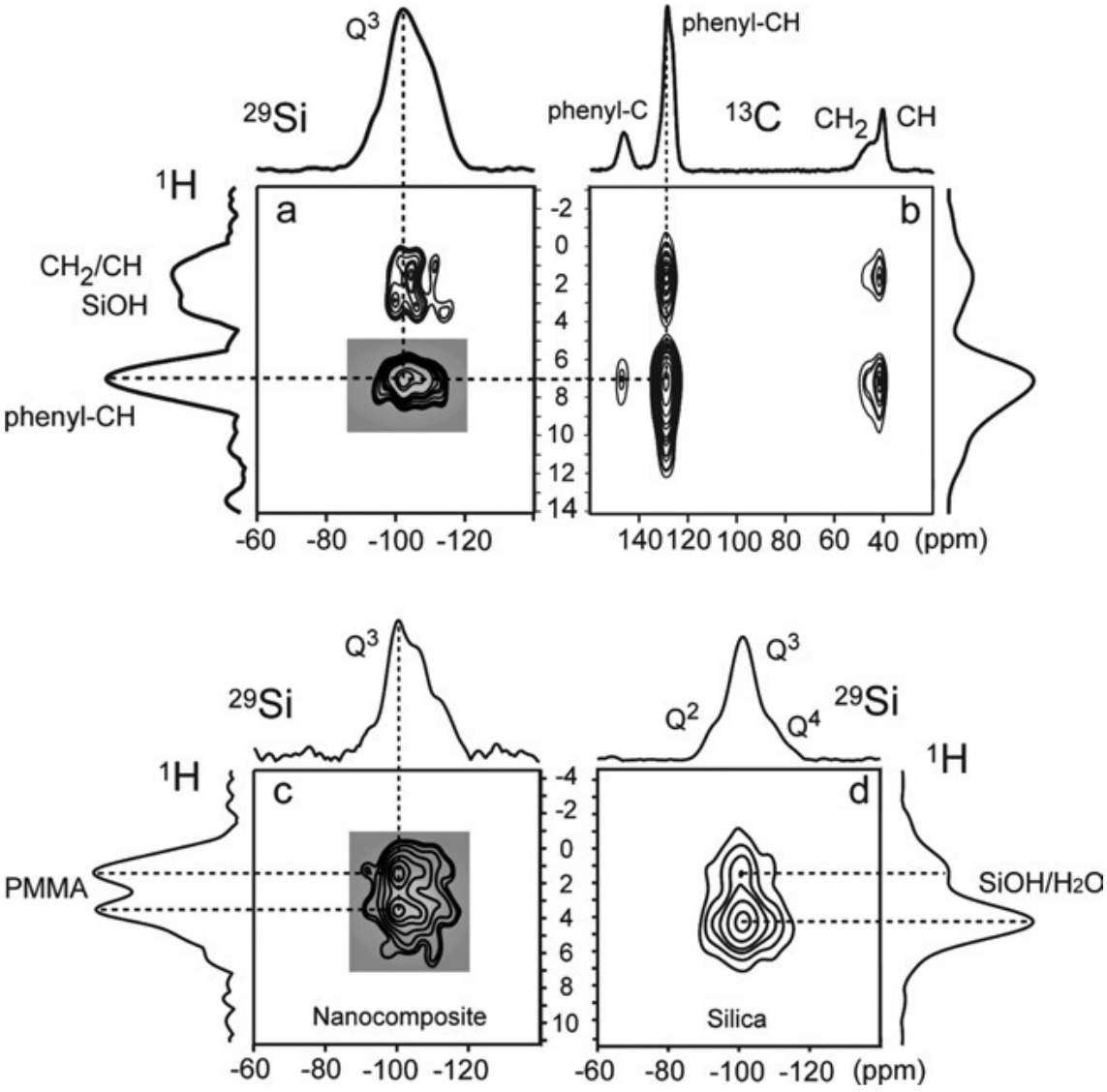

Figure 6.8

2D hector NMR experiments performed on polymeric nanocomposites with styrene (top) and polymethylmethacrylate (down)

In these ^{1}H-^{29}Si HETCOR spectra we can observe intense cross-peaks due to strong dipole-dipole interactions, occurring at short distances, between polymer hydrogen atoms and silicon of silanol groups lining the mesochannel walls of the silica matrix. In particular, we can observe correlation signals between Q^3 species (-102.2 ppm) and CH/CH_2 (1.4 ppm) and phenyl CH (7.1 ppm) in the case of polystyrene; between Q^3

species (-100.6 ppm) and protons in a range of 1.7-3.6 ppm in the case of polymethylmethacrylate. This relationship cannot occur for distances greater than 1 nm and this means that polymer and matrix have an intimae spatial correlation.[26]

6.4.3 Silica matrix dissolution and shape replica effect

Nanocomposite has been washed at low temperature in a aqueous solution of HF (26% wt) to dissolve silica matrix. The polymer was then collected by filtration, dried and analyzed with TGA and DSC analysis, adsorption measurements, solution NMR and SEM microscope. First of all, by SEM images we can see that micrometric morphology is retained both in nanocomposite and polymeric objects:

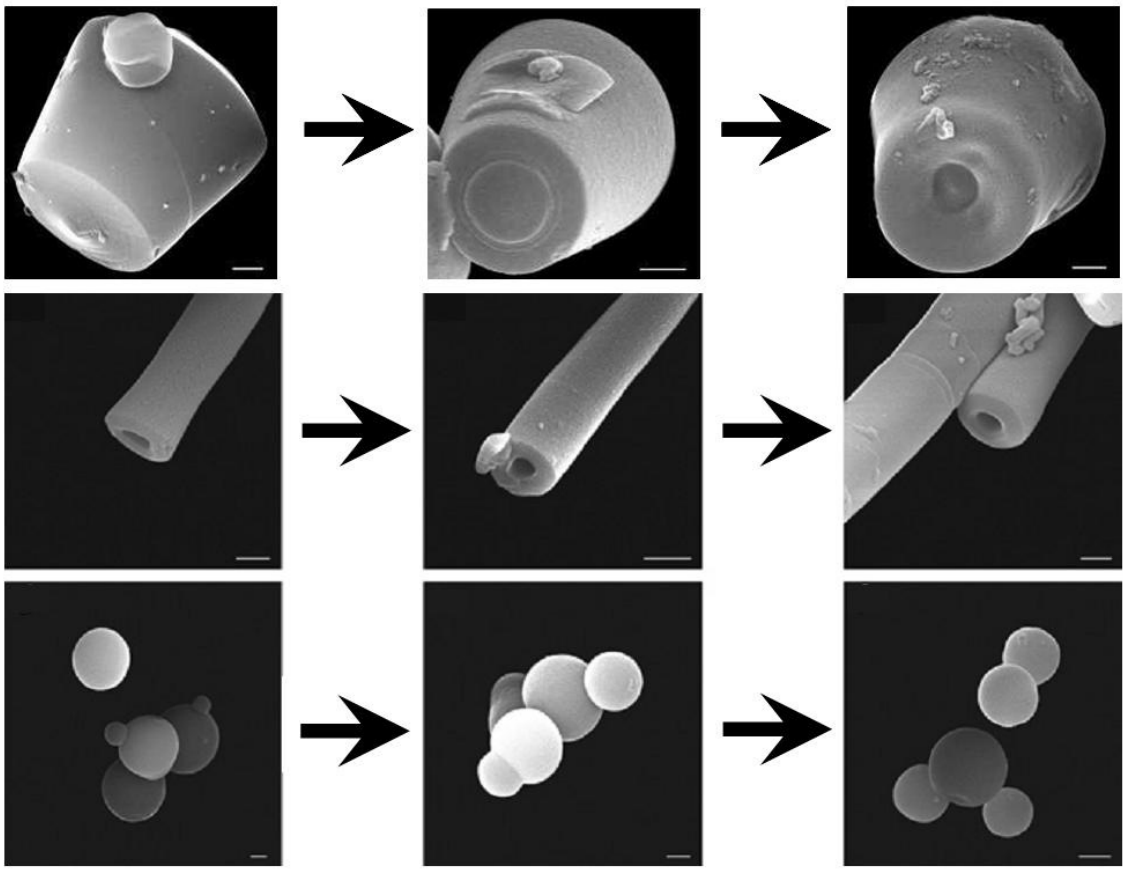

Figure 6.9

SEM images of morphological mesoporous silica particles (left), polymeric nanocomposites (middle) and polymeric micro-objects (right) with different morphologies. Reported scale bars correspond to 1 μm

Confronting single objects with the same morphology, we can see that silica dissolution does not influence object dimensions. BET analysis indicates that polymeric micro-objects have a surface area of about 70 m^2/g and TGA weight losses show a complete sample degradation over 450°C, index that silica dissolution was complete.

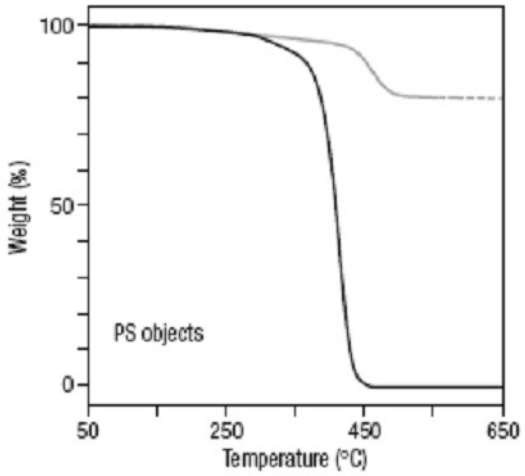

Figure 6.10

TGA analysis performed on extracted polymeric objects (black line) compared with nanocomposite (grey line). To note the complete degradation of polymer objects

Solution NMR analysis confirms that polymers are atactic, since pores are too large to impose specific configuration. DSC analysis, instead, shows very interesting phenomenon.

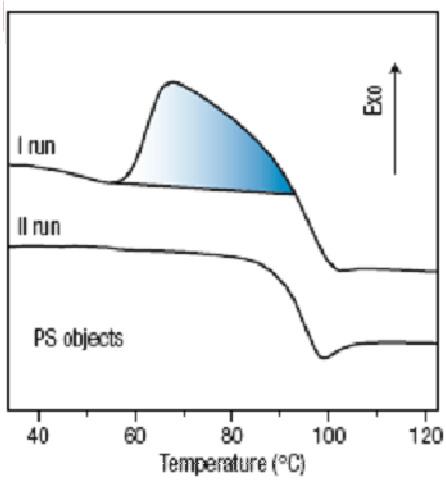

Figure 6.11

DSC analysis on extracted polymers. Clear visible in the I run the large exothermic peak associated to the structural collapse of polymer fibrils

This technique reveals the rare metastable state of PS and PMMA. In fact, a large exotherm precedes glass transition due to the release of excess surface energy from the nanoporous polymer network, that progressively collapses to the dense bulk (ΔHexo. of PS = 8 J g−1; ΔHexo. of PMMA = 6 J g−1). The second DSC run, showing only the glass transition, is typical of a conventional bulk polymer of high molecular weight, indicating an irreversible switch after thermal treatment above glass transition (100 ◦C for PS and 110 ◦C for PMMA). Increasing the temperature, the thermal agitation causes the chain–bundles to progressively associate into fibrils, as indicated by the DSC exotherm. Chain–bundle association already occurs at room temperature, contributing to the overall dimensional stability of the polymer network and the construction of a robust nanoscopic framework that could sustain the microscopic polymeric architecture.

In conclusion, we have performed confined polymerization of different monomers in mesoporous silica matrices with different micrometric morphologies. These polymeric nanocomposites have been used to obtain porous polymeric micro-objects with well defined porosity and shape by shape replica effect.

6.5 References:

1) a) R. Simonutti, A. Comotti, S. Bracco, P. Sozzani; *NATO Science Series, II: Mathemathics, Physics and Chemistry* **2002**, *76*, 159-163; b) B. Pukanszky; *Eur. Pol. J.* **2005**, *41*, 645-662; c) F. Ciardelli, S. Coiai, E. Passaglia, A. Pucci, G. Ruggeri; *Polymer International* **2008**, *57*, 805-836; d) J. Mozco, B. Pukanszky; *J. Ind. Eng. Chem.* **2008**, *14*, 535-563

2) D. Schmidt, D. Shah, E.P. Giannellis; *Current Opinion in Solid State & Materials Science* **2002**, *6*, 205-212

3) a) F.W. Billmeyer, jr., *Textbook of polymer Science, 3rd edition*, John Wiley & Sons, New York, **1984**; b) Q.T. Nguyen, D.G. Baird; *Advances in Polymer Technology* **2006**, *25*, 270-285; c) A.D. Pomogailo; *Inorganic Materials* **2005**, *41*, S47-S74; d) J. Pyun, K. Matyjaszewski; *Chem. Mater.* **2001**, *13*, 3436-3448

4) S. Ogino, T. Aida, K.A. Koyano, T. Tatsumi; *Macromol. Rapid. Commun.* **1997**, *18*, 991-996

5) T. Uemura, K. Kitagawa, S. Horike, T. Kawamura, S. Kitagawa, M. Mizuno, K. Endo; *Chem. Commun.* **2005**, 5968-5970

6) a) S.A. Johnson, D. Khushalani, N. Coombs, T.E. Mallouk, G. A. Ozin; *J. Mater. Chem.* **1998**, *8*, 13-14; b) J.Y. Kim, S.B. Yoon, F. Kooli, J.S. Yu; *J. Mater. Chem.* **2001**, *11*, 2912-2914

7) P. Sozzani, S. Bracco, A. Comotti, P. Valsesia, R. Simonutti, O. Terasaki, Y. Sakamoto; *Nature Materials* **2006**, *5*, 545-551

8) K. Moller, T. Bein; *Chem. Mater.* **1998**, *10*, 2950-2963

9) a) J.M. Baker, J.C. Dore, P.J. Behrens; *J. Phys. Chem. B* **1997**, *101*, 6226-6229; b) K. Morishige, K. Nobuoka; *J. Chem. Phys.* **1997**, *107*, 6965-6969; c) K. Morishige, H. Fujii, M. Uga, D. Kinukawa; *Langmuir* **1997**, *13*, 3494-3498; d) K.J. Edler, P.A. Reynolds, F. Trouw, J.W. White; *Chem. Phys. Lett.* **1996**, *249*, 438-443

10) a) M. Hartmann, A. Pöppl, L. Kevan; *J. Phys. Chem.* **1996**, *100*, 9906-9910; b) A. Pöppl, M. Hartmann, L. Kevan; *J. Phys. Chem.* **1995**, *99*, 17251-17258

11) a) R. Ryoo, C.H. Ko, J.M. Kim, R. Howe; *Catal. Lett.* **1996**, *37*, 29-33; b) U. Junges, W. Jacobs, I. Voigt-Martin, B. Krutzsch, F. Schüth; *J. Chem. Soc., Chem. Commun.* **1995**, 2283-2284; c) U. Junges, F. Schüth, G. Schmid, Y. Uccida, R. Schlögl; *Ber. Bunsen-Ges. Phys. Chem.* **1997**, *101*, 1631-1634; d) B.P. Perline, K.D. Schmitt, J.C. Vartuli; U.S. Patent 5.270.273, Dec. 14, **1993**

12) a) B.J. Aronson, C.F. Blanford, A. Stein; *Chem. Mater.* **1997**, *9*, 2842-2851; b) J.V. Walker, M. Morey, H. Carlsson, A. Davidson, G.D. Stucky, A. Bulter; *J. Am. Chem. Soc.* **1997**, *119*, 6921-6922; c) S. Ayyappan, N. Ulagappan; *Proc. – Indian Acad. Sci. Chem. Sci.* **1996**, *108*, 505-510

13) a) W. Böhlmann, K. Schandert, A. Pöppl, H.C. Semmelhack; *Zeolites* **1997**, *19*, 297-304; b) I. Honma, H. Sasabe, H.S. Zhou; *Mater. Res. Soc. Symp. Proc.* **1997**, *457*, 525-531; c) J.F. Diaz, K.J. Balkus Jr.; *J. Mol. Catal. B: Enzymatic* **1996**, *2*, 115-126

14) a) J.S. Beck, D.C. Calabro, S.B. McCullen, B.P. Pelrine, K.D. Schmitt, J.C. Vartuli; U.S. Patent 5.145.816, Sept. 8, **1992**; b) D.H. Olson, G.D. Stucky, J.C. Vartuli; U.S. Patent 5.364.797, Nov. 15, **1994**

15) a) S.L. Burkett, S.D. Sims. S. Mann; *Chem. Commun.* **1996**, 1367-1368; b) C.E. Fowler, S.L Burkett, S. Mann; *Chem. Commun.* **1997**, 1769-1770

16) a) M. Farina, G. DiSilvestro, P. Sozzani; *Makromolekulare Chemie, Rapid Communications* **1981**, *2*, 51-54; b) M. Farina, G. DiSilvestro, P. Sozzani; *Macromolecules* **1982**, *15*, 1451-1452; c) M. Farina, G. DiSilvestro, P. Sozzani; *Molecular Crystals and Liquid Crystals* **1983**, *93*, 169-181

17) C.G. Wu, T. Bein; *Science* **1994**, *264*, 1757-1759

18) P.L Llewellyn, U. Ciesla, H. Decher, R. Stadler, F. Schüth, K.K. Unger; *Studies in Surface Science and Catalyisis* **1994**, *84*, 2013-2020

19) K. Moller, T. Bein, R.X. Fischer; *Chem. Mater.* **1998**, *10*, 1841-1852

20) M. Choi, F. Kleitz, D. Liu, H.Y. Lee, W.S. Ahn, R. Ryoo; *J. Am. Chem. Soc.* **2005**, *127*, 1924-1932

21) a) C.G. Wu, T. Bein; *Science* **1994**, *266*, 1013-1015; b) R. Fernandez-Saavedra, P. Aranda, E. Ruiz-Hitzky; *Adv. Funct. Mater.* **2004**, *14*, 77-82

22) G.A. Ozin, A.C. Arsenault, L. Cademartini, *Nanochemistry, A chemical approach to Nanomaterials* 2nd ed., RCS Publishing, Cambridge, UK, **2009**

23) H. Yang, N. Coombs, G.A. Ozin; *Nature* **1997**, *386*, 692-695

24) a) M. Steinhart, J.H. Wendorff, A. Greiner, R.B. Wehrspohn, K. Nielsch, J. Shilling, J. Choi, U. Goesele; *Science* **2002**, *296*, 1997; b) V.M. Cepak, C.R. Martin; *Chem. Mater.* **1999**, *11*, 1363-1367; c) S.I. Moon, T.J. MacCarthy; *Macromolecules* **2003**, *36*, 4253-4255; d) Z. Yang, W.T.S. Huck, S.M. Clarke, A.R. Tajbakhsh, E.M. Terentjev; *Nature Materials* **2005**, *4*, 486-490; e) S.A. Johnson, P.J. Ollivier, T.E. Mallouk; *Science* **1999**, *283*, 963-965

25) S.M. Yang, I. Sokolov, N. Coombs, C.T. Kresge, G.A. Ozin; *Adv. Mater.* **1999**, *11*, 1427-1431

26) a) A.Comotti, S. Bracco, P. Valsesia, L. Ferretti, P. Sozzani; *J. Am. Chem. Soc.* **2007**, *129*, 8566-8576; b) S.S. Hou, T.J. Bonagamba, F.L. Beyer, P.H. Madison, K. Schmidt-Rohr; *Macromolecules* **2003**, *36*, 2769-2776; c) J.D. Epping, B.F. Chmelka; *Curr. Opin. Colloid Interface Sci.* **2006**, *11*, 81-117; d) A. Comotti, S. Bracco, R. Simonutti, P. Sozzani; *Chem. Commun.* **2004**, 768-769; e) P. Sozzani, S. Bracco, A. Comotti, M. Mauri, R. Simonutti, P. Valsesia; *Chem. Commun.* **2006**, 1921-1293

CHAPTER 7

Polyacrylonitrile and graphitic-like systems

Polyacrilonitrile is a polymer of acrylic family, used to produce common objects such as laboratory gloves or certain types of tissues. As omopolymer, it is white and brittle and is generally produced in fibers by electrospinning of dimethylformammide solutions. Often it is produced as copolymer, with styrene or itanoic acid, to give it better mechanical properties. Polyacrilonitrile is furthermore the most common precursor to create carbon fibers, because heating it over 700 °C in a non-oxidative atmosphere brings to the production of a large polyaromatic structure similar to a graphitic sheet. This is very interesting in industrial applications, because it is an easy method to produce rigid and mechanical resistant structures with good electrical characteristics in a simple way.[1]

In this chapter we will describe polyacrylonitrile structures and their evolutions as function of temperature. In particular, we will focus the attention on graphitic structures that could be obtained and on Raman analysis performed on these structures. In the second part of the chapter we will describe the study conduced on a class of polyacrylonitrile nanocomposites, obtained by *in situ* polymerization, and on the *p*-phenylen organosilica matrix, heating these samples at different temperatures and dissolving silica frameworks with hydrofluoric acid.

7.1 Polymer synthesis, chemical structure and general properties

Polyacrilonitrile is generally obtained by a radical process using AIBN or peroxydisulfate as radical initiators. In some works it was otherwise obtained by irradiation with light or microwaves to induce polymerization without the initiator.[2] Polymerization is fast, exothermic and, once initialized, it is self-activating due to the large heat release. By this type of reaction, obtained polymer is usually atactic, without spatial order of CN pendant groups. Nevertheless, bulk polyacrylonitrile shows an interesting XRD diffractogram, with two distinct peaks due to partial order.

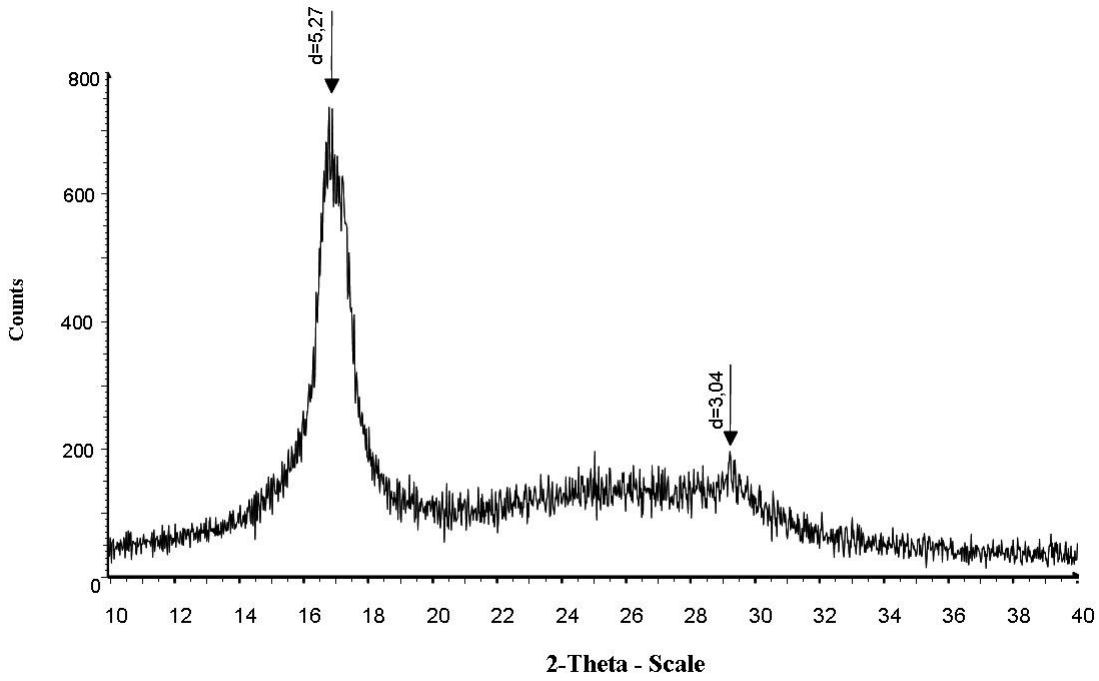

Figure 7.1

XRD diffraction pattern of bulk polyacrylonitrile

In differential scanning calorimetric analysis, however, the polymer does not show an exothermic phenomenon associable to fusion of crystalline phase, but two phenomena of glass transition, one at ~100 °C ant the other one at ~150 °C. These data could be interpreted considering the polymer having a supramolecular organization. In this model, polymer chains dispose themselves in columnar structures with polar CN groups towards the external. These columns are then organized in a regular hexagonal pattern.[3] By this model, the first, sharp peak (distance 5.27 Å), could be associated to hexagonal-packing of columnar phase, while the second, the broad one (distance 3.04 Å) is associated to the complete amorphous phase. In this case, the first glass transition is due to the chain motion of columnar phase, while the second is due to the collective motion of amorphous polymer chains. Transition of ordered phase happens at lower temperature, respect to that expected, because chains are less entangled and need low energy to move themselves.

7.2 Thermal evolution of polyacrylonitrile and Raman analysis

Polyarcylonitrile has very interesting thermal properties. In fact, heating the polymer at different temperatures the chemical structure changes as proposed in the following scheme:

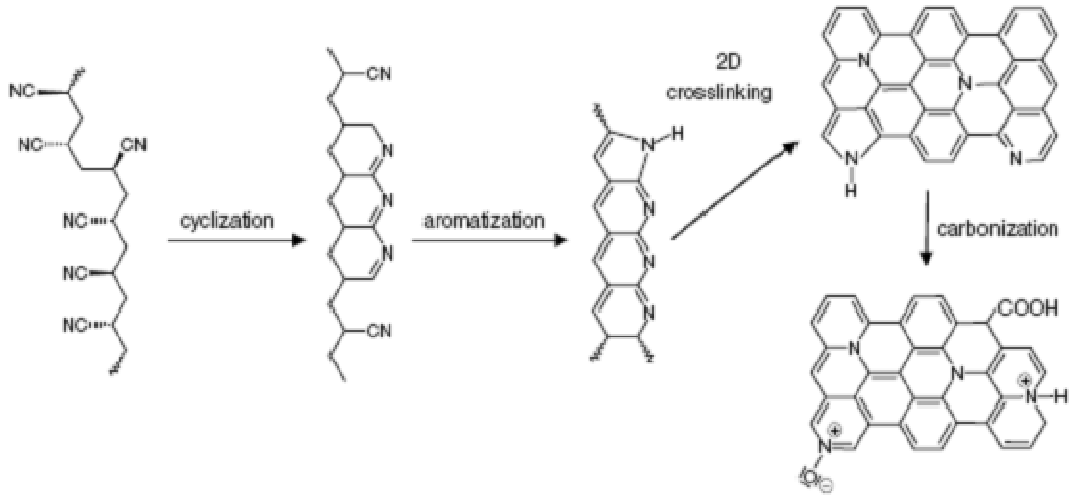

Figure 7.2

Scheme of thermal reactions of polyacrylonitrile [6]

The first reaction, the cyclization of CN groups in a polyconjugated structure, happens at about 270-300 °C, immediately followed by the aromatization step with loss of hydrogen molecules and the formation of a laddered aromatic structure.[4] At this level, presence of oxygen could bring to a formation of carbonyl species on structure corners. This reaction is also named stabilization and is commonly used in industrial applications to make the polymer more resistant to chemical etchants.[5] Heating at temperatures above 500 °C in non-oxidative atmosphere comports lateral condensation of laddered structures, with loss of hydrogen, as indicated in the scheme reported below.

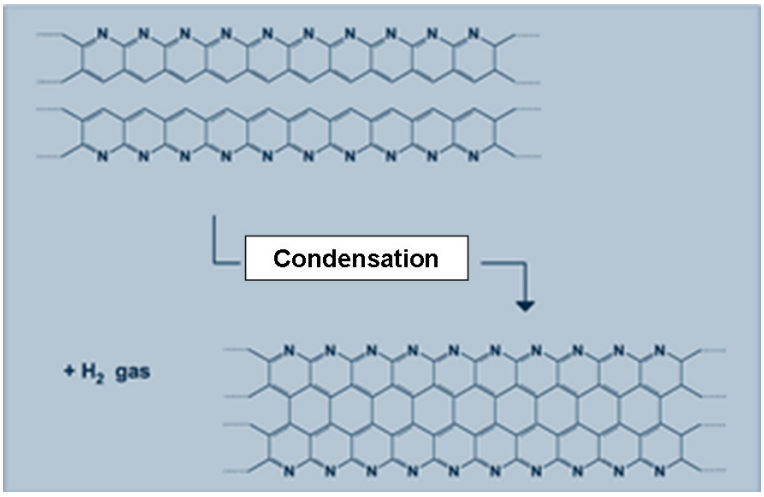

Figure 7.3

Scheme of first lateral condensation of laddered structures

Increasing again the temperature above 700 °C, ever in non-oxidative atmosphere, induces a successive lateral condensation with loss of different gaseous species, such as ammonia, cyanidric acid or nitrogen, that tend to eliminate nitrogen to generate an extended, aromatic graphitic-like structure.[6] About mechanisms that initiates these reactions there are many unsolved questions. Some authors indicate an amino-enamminic tautomerie as starting spark,[7] while other authors use a small quantity of oxygen to explain the first attach.[8] Whatever is the explanation, the exact process is not still fully understood.

Obtained graphitic-like systems are generally investigated by Raman analysis. These condensed structures show two characteristic vibrational modes.[9] The first mode, at about 1360 cm^{-1}, is named "breathing" mode or diamond-like mode (D band) and is associated to a coordinate motion of carbon atoms that enlarge and contract hexagonal rings as showed in figure:

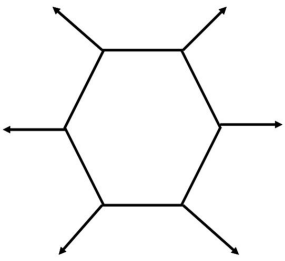

Figure 7.4

Scheme of breathing motion of carbon atoms

The second mode, between 1500 and 1630 cm^{-1}, is named "shear" mode or graphite-like mode (G band) and is associated to an alternate atom motion, as indicated in figure:

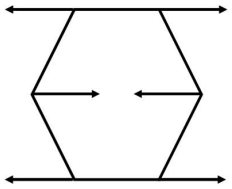

Figure 7.5

Scheme of shear motions of carbon atoms

These vibrational modes are both characteristics of large condensed aromatic systems and involve sp^2 carbon atoms. In fact, graphite-like motion is associated to a perfect and infinite plane, so it is generated by cores of aromatic structures. Diamond-like motion, instead, is typical of plane borders and defects, because ring expansion could happen only with free space disposable. Nevertheless, this mode is not associated to sp^3 carbon atoms, as the name could suggest, but needs a planar aromatic ring to be expressed. Because D band is strictly associated to plane borders, comparing intensities of the two signals in a Raman spectrum, it is possible to estimate the extension of graphitic-like systems by the empirical formulae:

- For L_a<20 Å: $\frac{I_d}{I_g} = C(\lambda)L_a^2$
- For L_a>20 Å: $\frac{I_d}{I_g} = \frac{2.4*10^{-10}\lambda^4}{L_a}$

Where L_a is the graphitization extension, I_d and I_g are the integrated intensities of, respectively, D and G bands, and λ is the used laser wavelength.[10]

7.3 Silica-polyacrylonitrile nanocomposites

Nanocomposites of silica and polyacrylonitrile can be exploited to obtain porous carbon materials or extended graphitic-like structures. In the first case, colloidal silica nanoparticles are dispersed in a monomer solution and, after polymerization and carbonization, dissolved using a HF solution.[11] Surface area of this type of systems could reach a value of about 30 m^2/g, compared with the 20 m^2/g of poreless carbon fibers. To obtain graphitic-like systems with controlled size, it is instead useful to synthesize polyacrylonitrile nanocomposites in a porous silica matrix. The first example of this type of nanocomposites was reported by Bein in 1994.[12] In his work, Bein uses a MCM-41 silica as matrix to perform a confined polymerization of acrylonitrile. Monomer was diffused by gas phase and polymerization was activated with an aqueous solution of potassium peroxydisulfate. Once obtained the nanocomposite, it was heated over 800 °C to induce graphitization. Raman analysis conduced on carbon-silica nanocomposite shows intense D and G bands, from which we can calculate a graphitic length of about 30 Å, compared with a length of about 24 Å calculated on a bulk sample treated with the same procedure. After this work, other works have been focused on preparation of polyacrylonitrile nanocomposites in porous glasses or other porous silica systems.[13] Aims of these works were to study the thermal properties of confined polyacrilonitrile, the influence of spatial confination on aromatic extension after carbonization and to obtain new porous carbon materials with graphitic fragments on the surface.

7.4 Investigation over thermal evolution of polyacrylonitrile nanocomposite

Polyacrylonitrile nanocomposites are synthesized by *in situ* radical polymerization in morphological mesoporous silica matrices and studied focusing the attention on thermal evolution of confined polymer. To better understand the effect of chain confinement, the results have been compared with those obtained on bulk polyacrylonitrile thermal treated with the same procedure than nanocomposites.

7.4.1 Preparation of silica-polyacrylonitrile nanocomposite and bulk polymer

Acrylonitrile was purified by distillation at room temperature and reduced pressure to remove stabilizer contained in commercial reactants. As radical initiator, commercial azo-bis-isobutyronitrile (AIBN) was used without purification. A mixture of fresh distilled monomer and AIBN, present at 0.7% weight respect to monomer, was outgassed two times by freeze and thaw cycles and then transferred with a cannula under vacuum on the silica matrix, previously dried under vacuum at 160 °C overnight. Once covered silica with the liquid mixture, the sample was outgassed three times with freeze and thaw cycles and then leaved at low temperature and dark for some days to leave time to the mixture to fill completely the matrix pores. Sample was then collected by filtration and radical initiator thermally activated at 100 °C under nitrogen flux for three hours and half.

This bulk sample, instead, was synthesized with a radical polymerization of a solution of AIBN in acrylonitrile 0,7% wt, heating at 110 °C for 3h and half under nitrogen flux. Polymer was then milled in a fine powder with a cryo-miller.

7.4.2 Nanocomposite characterization

The effective formation of nanocomposite could be seen directly by DSC analysis. In fact, polyacrylonitrile presents a characteristic exothermic peak between 250 and 300 °C, associated to the first thermal reaction of cyclization (see paragraph 7.2 for thermal reaction of polyacrylonitrile). In bulk polyacrylonitrile this peak is sharp and very intense, while in our sample this peak is broader, between 200 and 300 °C, with a little sharp signal.

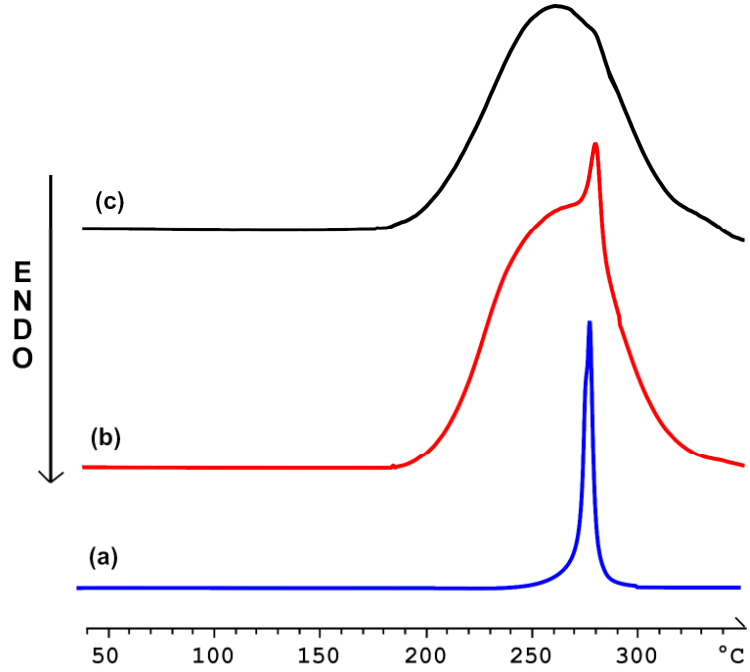

Figure 7.6

DSC analysis conduced on bulk polyacrylonitrile (a); as-obtained nanocomposite (b) and nanocomposite after washing with DMSO and methanol (c)

This sharp peak is associated to external polymer, while the broad signal is due to polyacrilonitrile inside the pores. In fact, according to literature, the confinement of chains changes cyclization dynamic, that start at lower temperatures.[14] External polymer was removed by washing in dimethyl sulfoxide (DMSO) at room temperature for about 3 hours, sample was then filtered, washed on the filter with methanol twice to remove residual DMSO and analyzed until complete disappearance of external polymer signal. Once removed external polymer, nanocomposites have been analyzed with adsorption measurements and thermogravimetric analysis.

BET analysis shows that surface area decreases in a range between 500 and 100 m^2/g, when pore volume becomes 0.2-0.02 cm^3/g. Confronting these data with TGA weight loss in air at 900 °C, that is of about 35%, it is possible to estimate that polymer fill silica channels of about 70-90% and that this filling is homogeneous, without empty spaces in the core of the particle. This data is also confirmed by the shape of adsorption isotherm of the nanocomposite, that maintains the typical pattern of mesoporous systems adsorption curves.

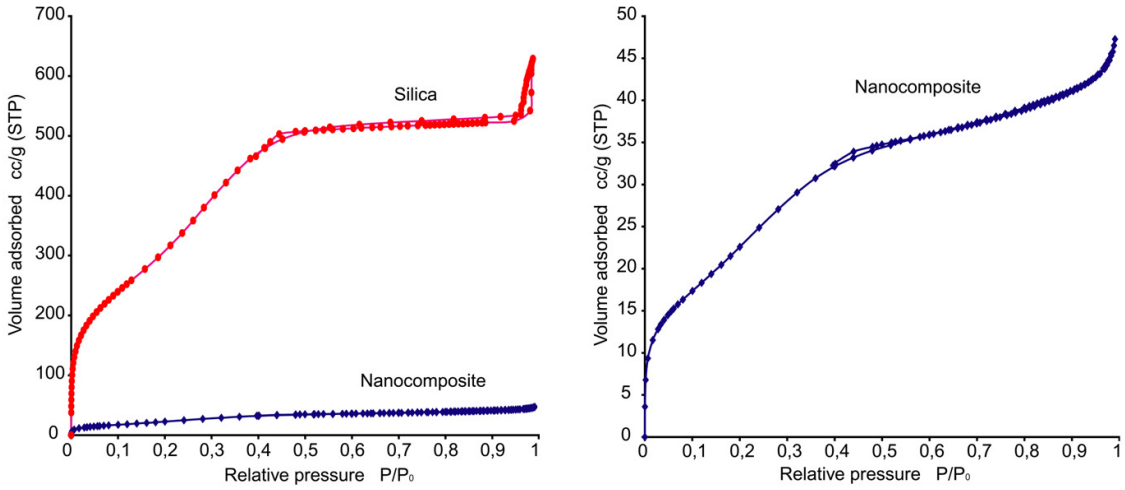

Figure 7.7

Nitrogen adsorption isotherms on silica and nanocomposite compared (left) and the expanded pattern of nanocomposite (right)

7.4.3 Thermal treatments

We have performed different thermal treatments, based on results of TGA analysis conduced on the nanocomposite in nitrogen atmosphere:

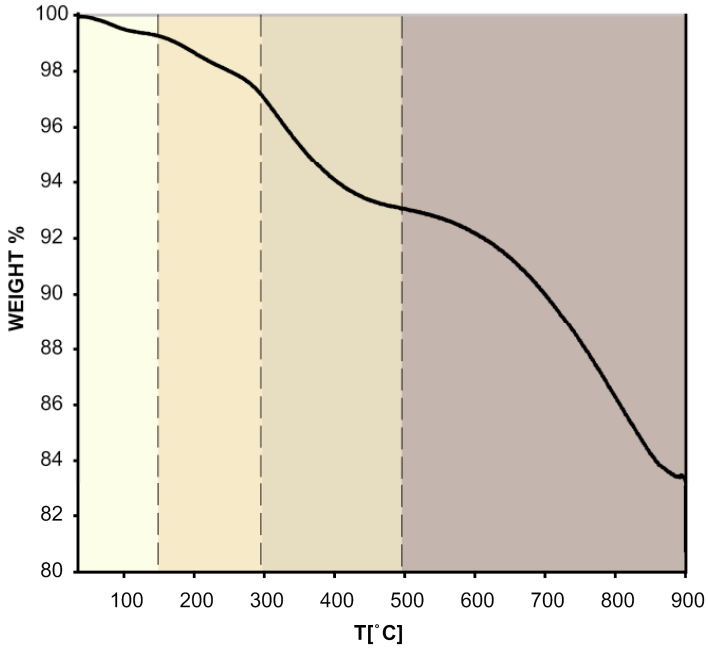

Figure 7.8

TGA analysis performed in nitrogen on polyacrylonitrile nanocomposite

Observing weight losses in TGA we have divided the temperature range in four zones using different weight losses: between ambient temperature up to 150°C, between 150 up to 300°C, between 300 up to 500°C and starting from 500 until over 900°C. By this separation, nanocomposite and polymer have been thermal treated up to 150, 300, 500 and 1100°C, generating two series of five samples. All thermal treatments have been performed in a non-oxidative atmosphere: nitrogen for treatments up to 300°C and argon for these up to 1100°C.

First evidence of efficacy of these treatments is the change of colour in the sample, as showed in figure 7.9:

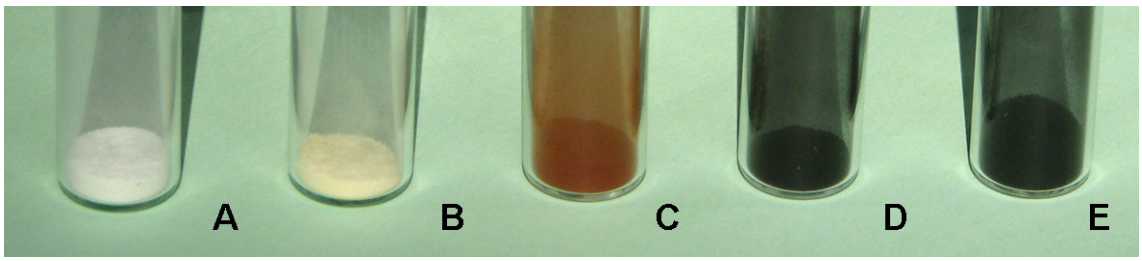

Figure 7.9

Colours of thermal treated nanocomposites: white (A, RT); light yellow (B, 150°C), brown (C, 300°C), dark brown (D, 500°C) and black (E, 1100°C)

As-obtained nanocomposite is white pearl, but the colour changes increasing temperature and it becomes light yellow (150°C), orange-brown (300°C), dark brown (500°C) and at last black (1100°C). This is a first difference respect to bulk polymer, because this becomes dark brown-black already after the thermal treatment at 300°C.

To understand the meaning of changes, ATR and Raman spectroscopic analysis was performed on the samples.

7.4.4 Spectroscopic analysis

ATR analysis were performed both on nanocomposites than on bulk polymer. Nevertheless, nanocomposite spectra show very intense silica signals, that surround completely polymer signals. Experiments conduced on bulk polymer, however, give the same useful and interesting informations on polyacrylonitrile structural evolution. Here

below are reported the ATR spectra performed on samples with peak assignation (reported in table 7.1).

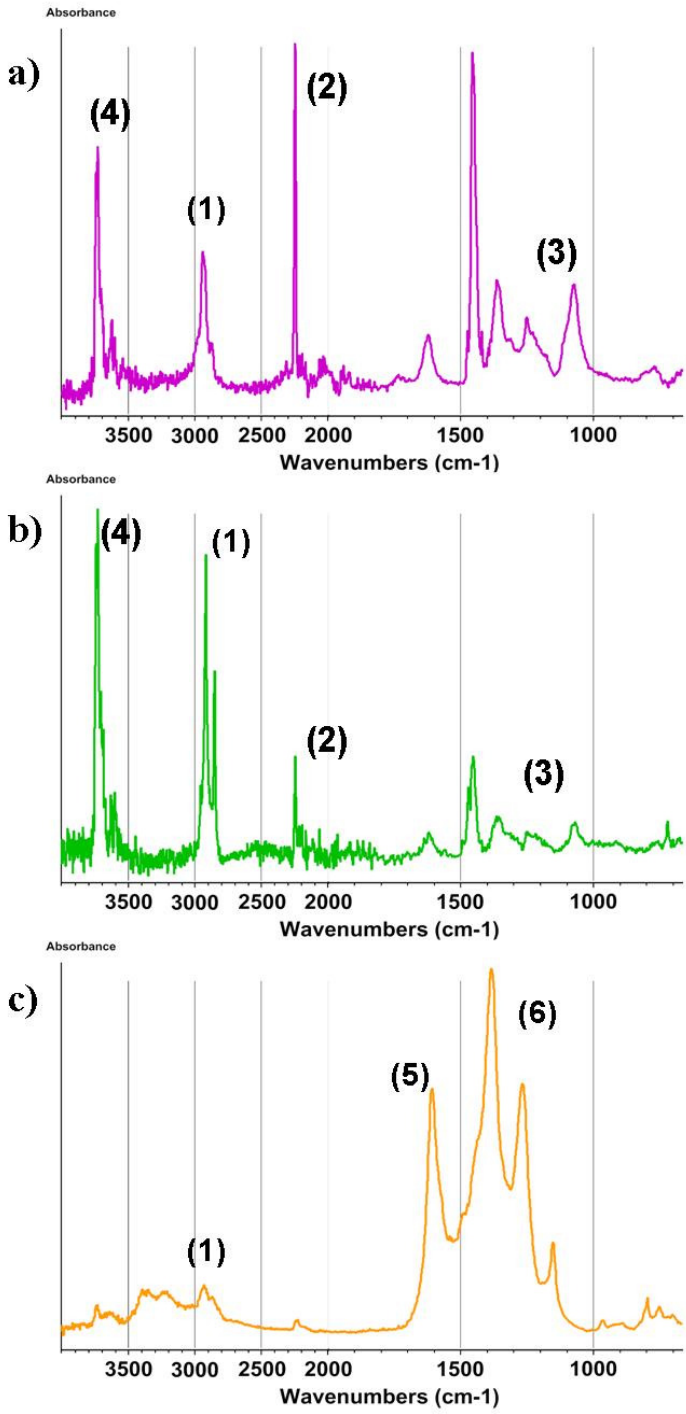

Figure 7.10a

ATR spectra of bulk polyacrylonitrile (a), polyacrylonitrile heated at 150°C (b) and 300°C (C)

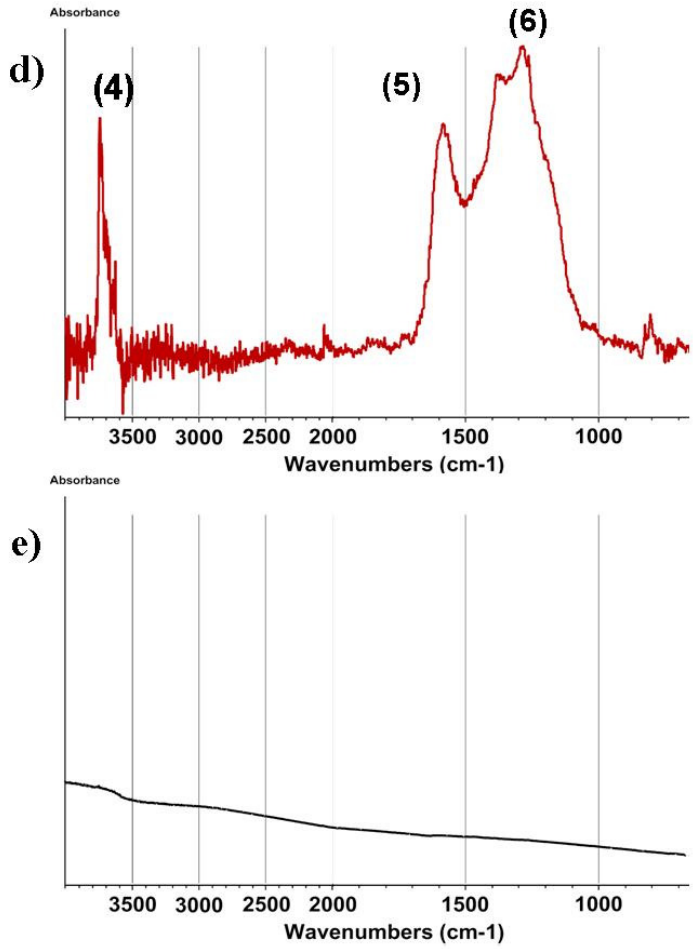

Figure 7.10 b

ATR spectra of bulk polyacrylonitrile heated at 500°C (d) and 1100°C (e)

Signal n°	**1**	**2**	**3**	**4**	**5**	**6**
Wavenumber (cm^{-1})	2940	2242	1220-1270 1345-1375 1440-1465	3750	1600	1377
Species	CH_2 stretching	C≡N stretching	CH motion	Amino groups (chain end)	C=C, C=N	Condensed laddered structures

Table 7.1

ATR peak assignation

A possible spectral interpretation is this: at 150°C signals of cyano groups, in the spectrum of non treated polyacrilonitrile, decrease quickly because of the begin of

cyclization process. At 300°C cyclyzation is complete, cyano peak is completely disappeared and there are signals associated to C=N and C=C, index of laddered structure formation. Evolution at 500°C comports a lateral condensation, that causes a gradual broadening of single signals due to evolution of IR inactive species. Finally, the carbonized sample does not show any signal, meaning that carbonization is complete and there are no more IR active groups.

To analyze the structure of these last two samples Raman analysis were performed.

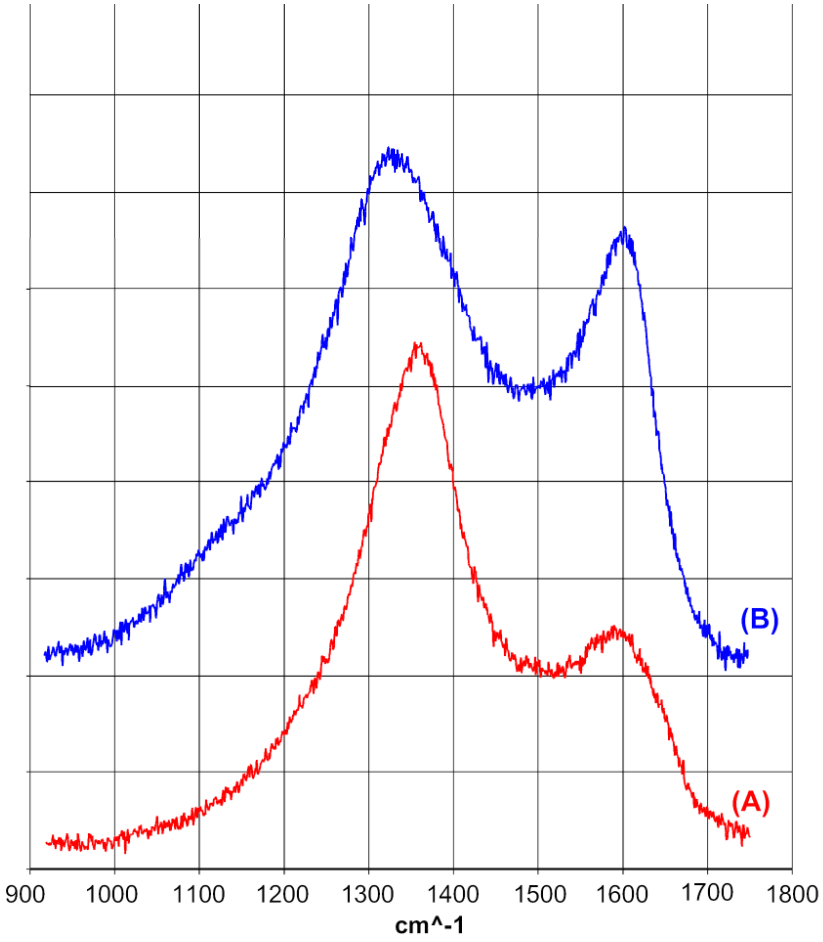

Figure 7.11

Raman analysis on nanocomposite heated at 500°C (A) and 1100°C (B)

In both the spectra are presents D and G bands, index of formation of an extended aromatic structure. This structure extension becomes larger increasing the temperature, as indicated by the intensification of G signal in the 1100°C spectrum. Applying the

empirical mathematical formula described in paragraph 5.2 on these spectra we could estimate the dimension of graphitic-like system:

Sample	I_d (area)	I_g (area)	I_d/I_g	L_a (nm)
Nanocomposite heated at 500°C	87.64	166.81	0.52	20.22
Nanocomposite heated at 1100°C	115.93	174.25	0.66	25.60

Table 7.2

Data calculated on Raman spectra. The laser wavelength used is 632.8 nm

There is an experimental evidence, according to literature[10], that graphitic-like systems obtained by heating confined polymers are larger than those obtained from bulk polymers. This fact could be explained by a pre-orientation of polymeric chains induced by channel geometry. In fact, during cyclization confined polymeric chains are forced by the channel walls to dispose themselves in a parallel symmetry, while in bulk polymer they can assume three dimensional spatial dispositions. Since lateral condensation needs laddered structures are parallel one respect each others, to generate covalent bondings by lost of hydrogen, those structures confined in nanometric channels are already in a favourable disposition. In bulk polymer, instead, structures must first move themselves in a parallel disposition and then condense. Since they are rigid systems, this motion is often very difficult.

7.4.5 Thermal treated nanocomposites characterization

TGA experiments have been performed on thermal treated samples to check the differences with non treated samples:

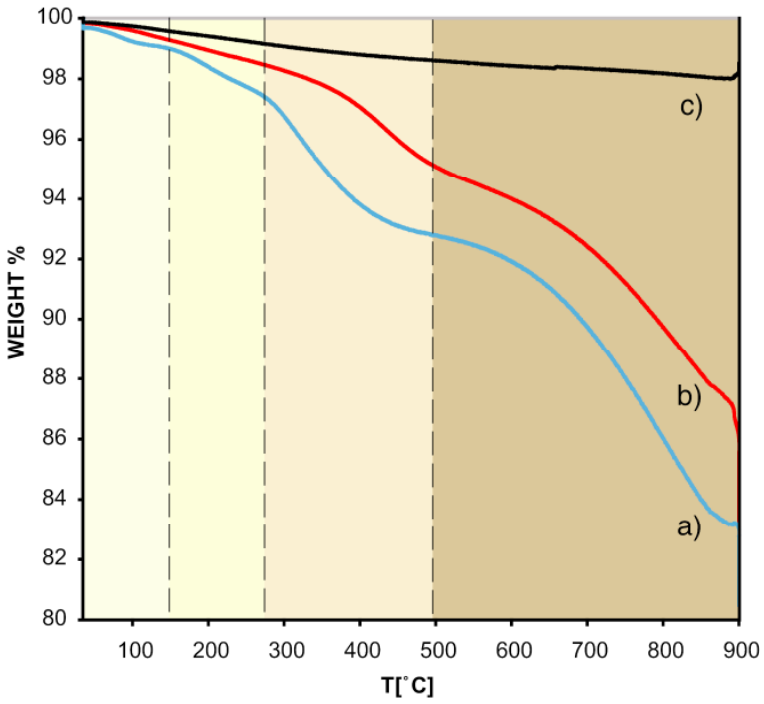

Figure 7.12

TGA analysis conduced on polyacrylonitrile nanocomposite (a),
on nanocomposite heated at 300°C (b) and on carbonized nanocomposite (c)

As illustrated in figure 7.12, nanocomposite thermal treated at 300°C does not show more weight losses before the treatment temperature. Furthermore, the curve after that temperature has the same behaviour than the curve of non-treated nanocomposite. The distance between them is exactly the first weight loss of the non treated nanocomposite. Concerning the carbonized sample, instead, it does not show relevant weight losses (the low loss visible could be attributed to the presence of a small amount of water and instrumental sensitivity).

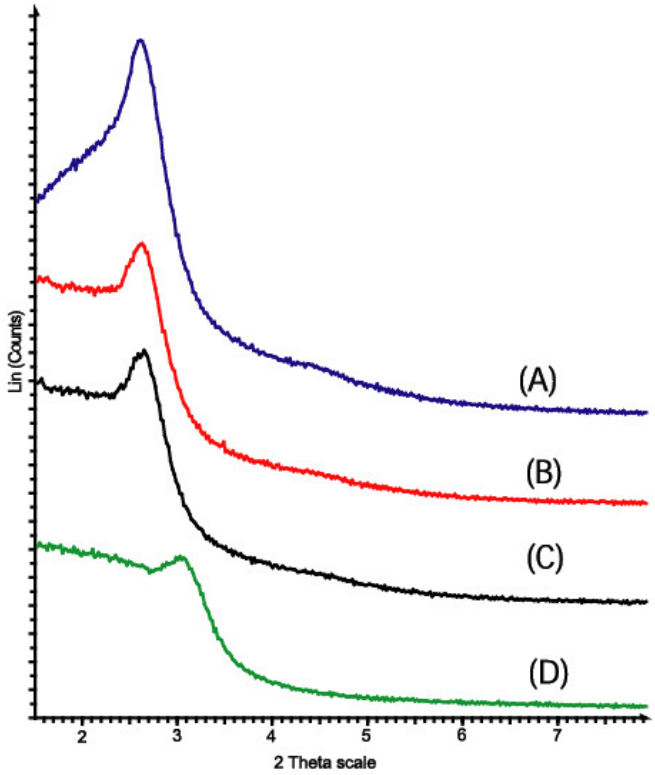

Figure 7.13

XRD patterns on pure silica matrix (a), nanocomposite (b) and nanocomposites heated at 300°C (c) and 1100°C (d)

XRD analysis indicates that thermal treatments up to 500 °C do not influence the periodic channel structure, while heating at 1100°C comports a shift of periodicity at a distance of 2.90 nm. This shift could be attributed to a channel shrinkage of 14% probably due to a furthermore condensation of the silica structure, as indicated by XRD experiments conduced on a silica sample heated at the same temperature.

At last, ^{13}C solid state NMR experiments are now in progress to check directly the structural evolution of polyacrylonitrile structure.

7.4.6 Silica matrix dissolution and shape replica effect

Samples obtained by carbonization process (or heated at 1100 °C) have been washed in a 26%wt HF aqueous solution to dissolve silica and to obtain porous carbon micro-objects with defined micrometric morphology. Washing was performed at low temperature to avoid unwanted reactions of graphitic system.

Like polymeric micro-objects, gyroids and hollow tubes carbon micro objects maintain the shape of the starting silica matrix:

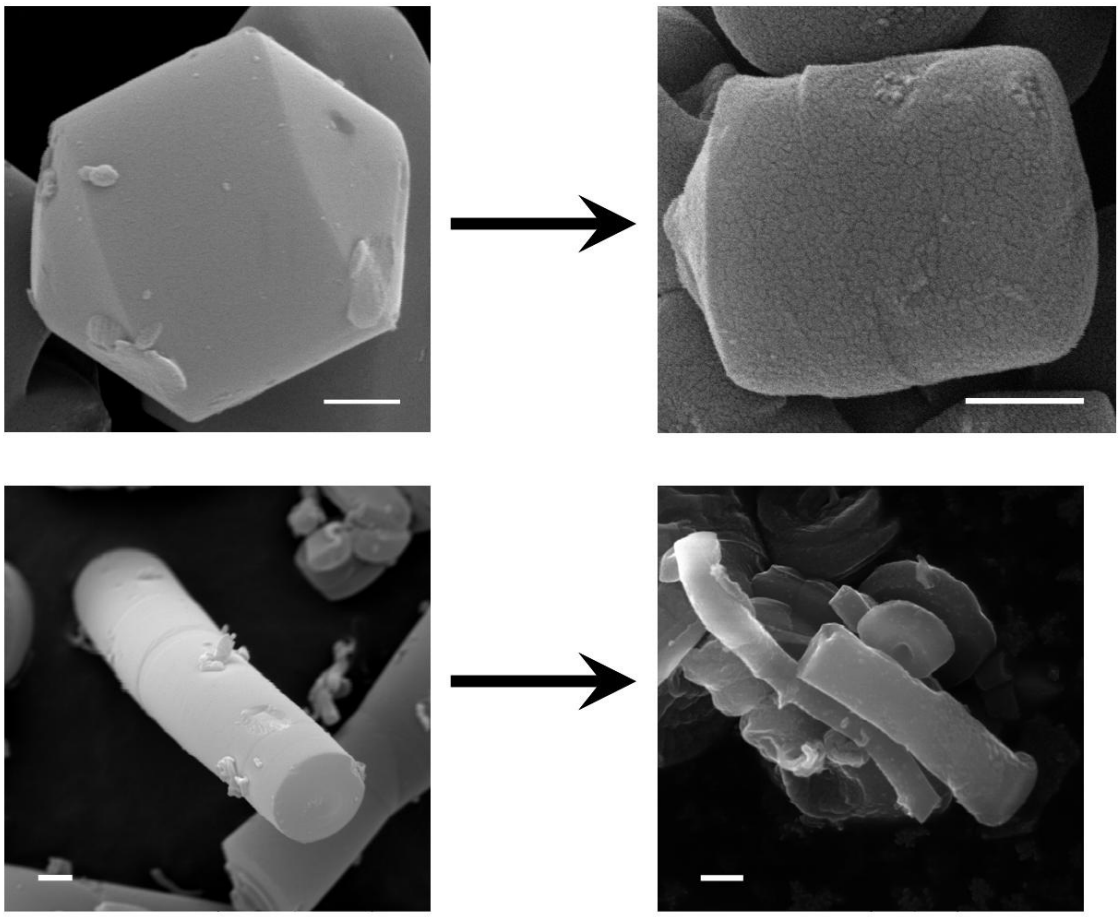

Figure 7.14

SEM images of morphological mesoporous silica particles (left) and correspondent porous carbon objects (right) obtained by replica-shape process

Scale bars reported correspond to 1 μm

Extracted objects have been analyzed with TGA measurements in nitrogen atmosphere and air, as indicated in figure 7.15.

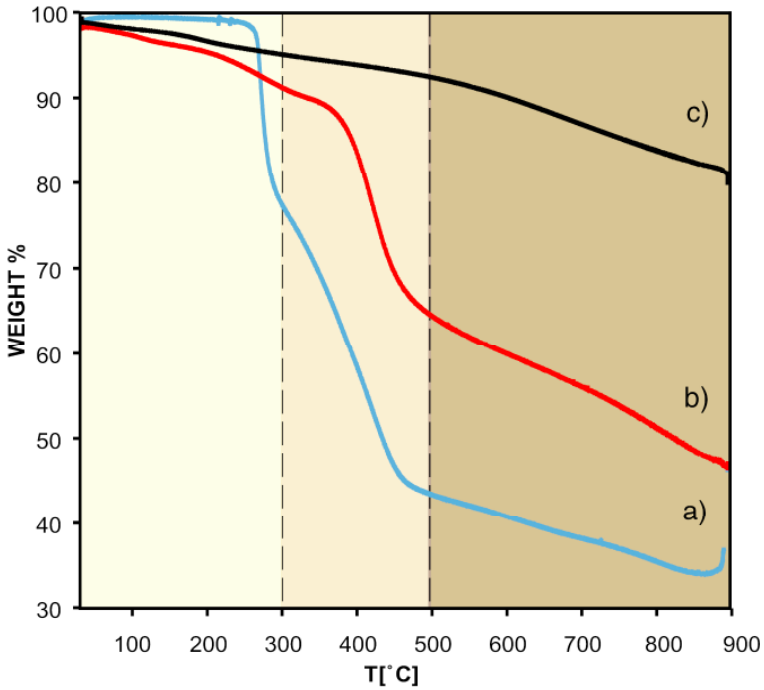

Figure 7.15

TGA analysis conduced on extracted polyacrylonitrile micro-objects (a), on polymer extracted from nanocomposite heated at 300°C (b) and from on carbonized nanocomposite (c) in nitrogen atmosphere

From analysis conduced in air, it is possible to understand that silica dissolution is complete, since the weight loss is complete. From analysis conduced in nitrogen atmosphere, instead, we can calculate the partial weight losses at each temperature: 20% until 300°C and 40% between 300 and 1100°C. The first weight loss could not be attributed to the only hydrogen release during aromatization process as suggested in literature. It is so probably the evolution of other volatile species, such as ammonia or cyanidric acid, generated at chain terminals to maintain the structure. In the same way, the second loss could be attributed to the generation of a large amount of gases or volatile species, such as hydrogen, ammonia, cyanidric acid, nitrogen and oligomeric fragments, during lateral condensation and graphitization processes.

Finally, adsorption measurements of nitrogen on extracted carbons give a BET surface area of about 1060 m^2/g. The adsorption isotherm, reported below, has the shape typical of microporous system:

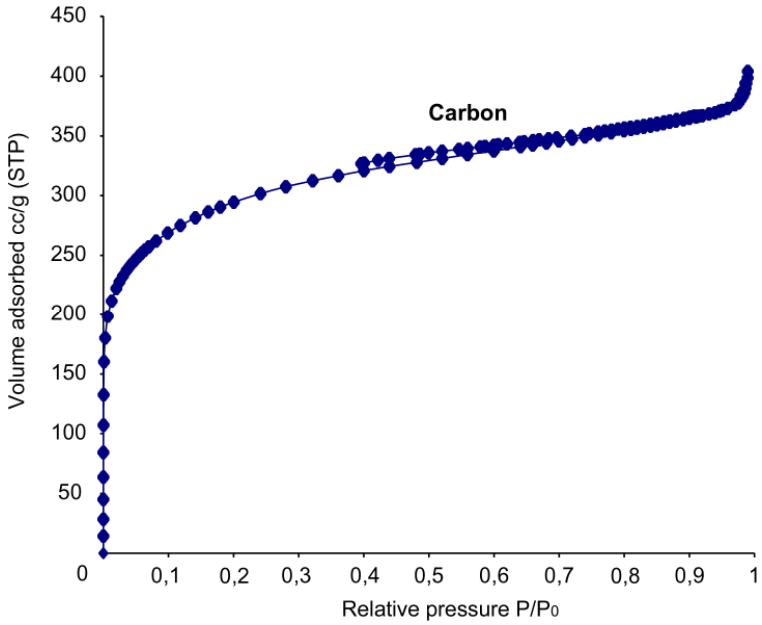

Figure 7.16

Nitrogen isotherm adsorption on extracted carbon micro-objects

The presence of microporosity, in this case, could be explained considering both the formation of gaseous species during thermal evolution and a probably generation of micro fractures due to silica matrix shrinkage.

7.5 Investigation over thermal evolution of p-phenylensilica system

We have also studied the thermal evolution of synthesized organosilica matrix using the same thermal treatments performed on polyacrylonitrile nanocomposites.

In fact, in literature are reported few works on organosilica carbonization to obtain stable silica-carbon nanocomposites.[15] In these works, nevertheless, there is not a discussion about formation mechanisms or final structures of carbon phase.

During thermal treatments, a first experimental evidence is that organosilica structure changes only over 500°C, when sample colour becomes black. This is in accord with TGA analysis, where the sample starts to lose weight only over 450-500°C. For this reason, we have focus our attention to obtain carbonized samples.

7.5.1 Thermal treatments on p-phenylensilica

We have performed two types of thermal treatments. The first one provides a first heating at 300°C in nitrogen flux followed by a carbonization at 900°C under argon atmosphere for 6h. The second is a thermal treatment at 1050°C under argon for 6h. In this second process the first heating step was omitted because there are no changes in the sample.

7.5.2 Characterization of carbonized samples

Carbonized samples were characterized by XRD, TGA, nitrogen adsorption, Raman and solid-state NMR analysis.

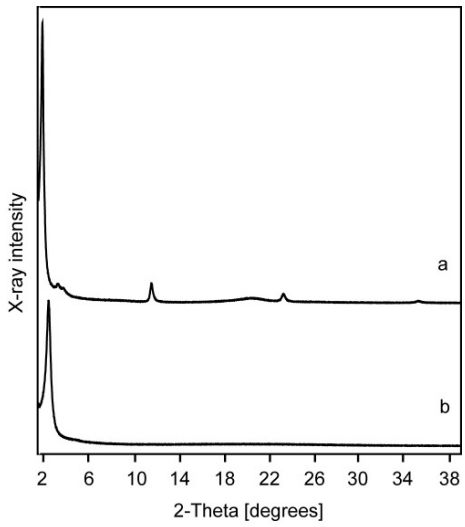

Figure 7.17

Confront between XRD patterns of *p*-phenylensilica matrix (a) and carbonized matrix (b)

XRD diffractograms clearly show that mesoscopic order is maintained, while the molecular order is completely lost. This loss is confirmed by ^{29}Si solid state NMR experiments, that show the presence of Q signals:

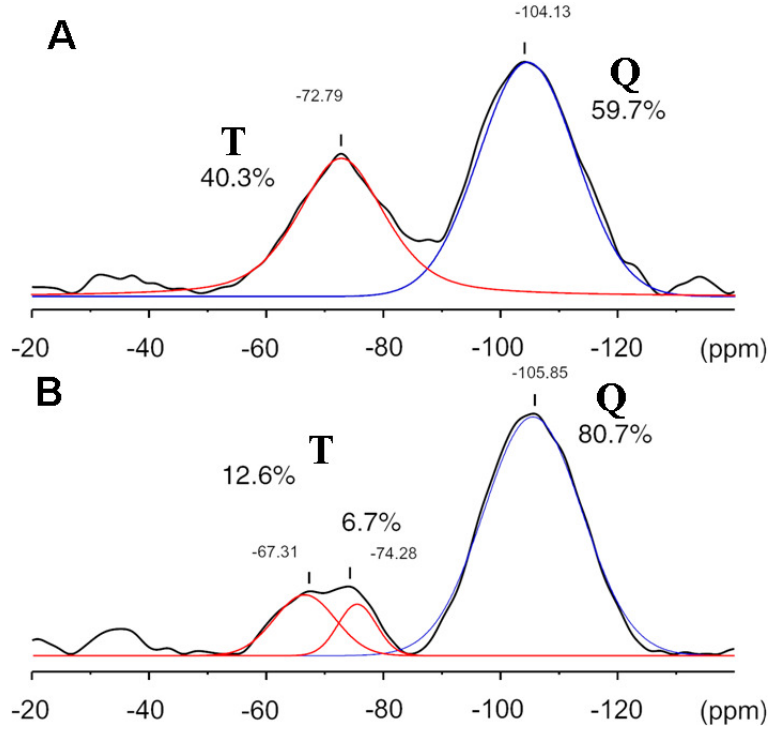

Figure 7.18

^{29}Si solid state NMR experiments conduced on sample heated at 900°C (A) and 1050°C (B)

These signals are due to cleavage of C-Si covalent bond during the carbonization process. Confronting intensity of Q peaks in the two spectra, 60% in the sample heated at 900°C, 80% in that heated at 1050 °C, we can suppose that during heating carbon re-arrange in a different structure. This, however, does not comport a structural collapse, because the mesoscopic peak is still present and the BET surface area remains about 700 m^2/g.

TGA measurements in nitrogen atmosphere do not show significant weight losses, index that the carbonization has been completed, while those performed in air show a weigh loss of about 30%. Confronting this datum with the weight loss in air of the non carbonized system (35%), we can estimate the weight loss during the carbonization of about 5%, confirmed by TGA measurements in nitrogen conduced on the non- treated matrix.

Raman analysis, instead, show both D and G band like carbonized polyacrylonitrile nanocomposites.

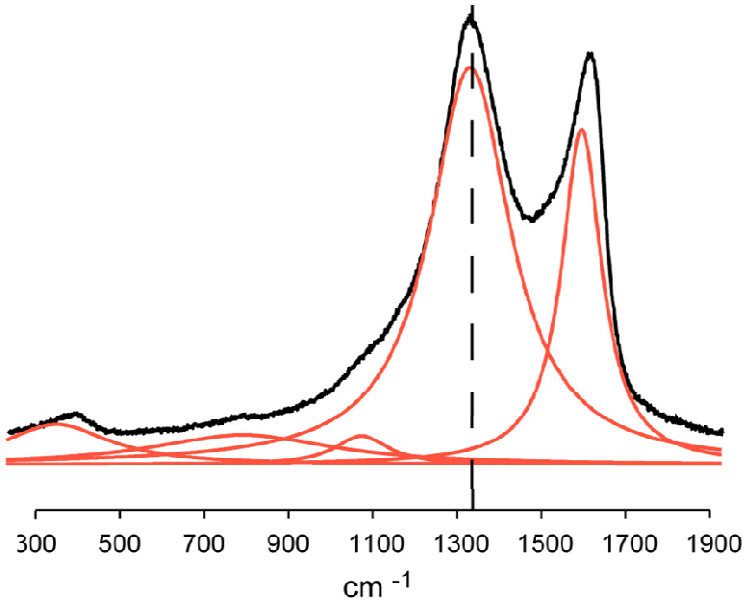

Figura 7.19

Raman spectrum obtained by carbonized *p*-phenylensilica matrix

The presence of a G band in these analysis suggests that single aromatic rings blend in a graphitic-like structure, probably by lateral condensation and hydrogen loss. This blending could be at the base of silicon-carbon cleavage denoted in ^{29}Si solid state NMR spectra. In the Raman spectra are also visible three defined shoulders at lower energy in the D band. These signals could be attributed to the presence of full-condensed silica structures inside the sample. This silica is generated by the cleavage of C-Si bonds and it is a confirmation of NMR data.

In conclusion, we have performed a series of thermal treatments on three different systems that show thermal evolution: bulk polyacrylonitrile, polyacrylonitrile-silica nanocomposite and an organosilica empty matrix. All of these systems show formation of extended aromatic structures and could be used as models to understand thermal evolutions of systems to obtain graphitic-like systems.

7.6 References:

1) a) A. Brokman, M. Weger, G. Marom; *Polymer Communications* **1980**, *21*, 1114-1115; b) C.L. Renschler, A.P. Sylwester, L.V. Salgado; *J. Mater. Res,* **1989**, *4*, 452-456; c) P. Wang, K. Hong, Q. Zhu; *Polymer* **1996**, *37*, 5533-5535; d) K.E. Perepelkin; *Fibre Chemistry* **2003**, *35*, 409-416

2) a) A.F. Porto, B.L. Sadicoff, M.C.V. Amorim, M.C.S. de Mattos; *Polymer Testing* **2002**, *21*, 145-148; b) C. Hou, R. Qu, J. Liu, L. Ying, C. Wang; *J. Appl. Polym. Sci.* **2006**, *100*, 3372-3376; c) I.F. Catta Preta, S.C. Sakata, G. Garcia, J.P. Zimmermann, F. Galembeck, C. Giovedi; *Journal of Thermal Analysis and Calorimetry* **2007**, *87*, 657-659

3) a) Z. Bashir; *J. Macromol. Sci. – Part B: Physics* **2001**, *40*, 41-67; b) Z. Bashir, S. Rastogi; *J. Macromol. Sci. – Part B: Physics* **2005**, *44*, 55-78

4) a) N. Grassie, R. McGuchan; *Eur. Polym. Journ.* **1970**, *6*, 1277-1291; b) W. Zhang, J. Liu, G. Wu; *Carbon* **2003**, *41*, 2805-2812

5) a) P. Wang, K. Hong, Q. Zhu; *Polymer* **1996**, *37*, 5533-5535; b) G.Wu, C. Lu, X. Wu, S. Zhang, F. He, L. Ling; *J. Appl. Polym. Sci.* **2004**, *94*, 1705-1709

6) a) T.J. Xue, M.A. McKinney, C.A. Wilkie; *Polymer Degradation and Stability* **1997**, *58*, 193-202; b) M. Surianarayanan, R. Vijayaraghavan, K.V. Raghavan; *J. Polym. Sci. A: Pol. Chem.* **1998**, *36*, 2503-2512; c) C. Weidenthaler, A.H. Lu, W. Schmidt, F. Schüth; *Microporous and Mesoporous Materials* **2006**, *88*, 238-243; d) Y.X. Wang, C.G. Wang, J.W. Wu, M. Jing; *J. Appl. Polym. Sci.* **2007**, *106*, 1787-1792; e) Y.N. Sazanov, A.V. Novoselova, G.N. Fedorova, E.M. Kulikova, A.V. Gribanov; *Russian Journal of Applied Chemistry* **2007**, *80*, 2124-2128

7) a) J. Shurz; *J. Polym. Sci.* **1958**, *28*, 438-439; b) W. Skody, J. Shurz, L. Bayzer; *Z. Phys. Chem (Leipzig)* **1959**, *210*, 35

8) a) H.F. Friedlander, L.H. Peebles jr., J. Brandrup, J.R. Kirby; *Macromolecules* **1968**, *1*, 79-86; b) L.H. Peebles jr., R.B. Thompson jr. J.R. Kirby, M.E. Gibson; *J. Appl. Polym. Sci.* **1972**, *17*, 3341-3351

9) a) F. Tunistra, J.L. Koenig; *J. Chem. Phys.* **1970**, *53*, 1126-1130; b) R.J. Nemanich, S.A. Solin; *Phys. Rev. B* **1979**, *20*, 392-401; c) L. Nikiel, P.W. Jagodzinski; *Carbon* **1993**, *31*, 1313-1317; d) L.G. Cançado, M.A. Pimenta, B.R.A. Neves, M.S.S. Dantas, A. Jorio; *Phys. Rev. Lett.* **2004**, *93*, 247401-1,4; e) E.B. Barros, H. Son, Ge.G. Samosonidze, A.G. Souza Filho, J. M. Filho, G. Dresselhaus, M.S. Dresselhaus; *Phys. Rev. B* **2007**, *76*, 035444-1,6; f) S. Reich, C. Thomsen; *Phil. Trans. R. Soc. Lond. A* **2004**, *362*, 2271-2288; g) K. Sato, R. Saito, Y. Oyama, J. Jiang, L.G. Cançado, M.A. Pimenta, A. Jorio, Ge.G. Samsonidze, G. Dresselhaus, M.S. Dresselhaus; *Chem. Phys. Lett.* **2006**, *427*, 117-121; h) A.C. Ferrari, J.C. Meyer, V. Scardaci, C. Casiraghi, M. Lazzeri, F. Mauri, S. Piscanec, D, Jang, K.S. Novoselov, S. Roth, A.K. Geim; *Phys. Rev. Lett.* **2006**, *97*, 187401-1,4; i) D. Graf, F. Molitor, K. Ensslin, C. Stampfer, A. Jungen, C. Hierold, L. Wirtz; *Solid State Comm.* **2007**, *143*, 44-46

10) a) P. Lespade, R. Al-Jishi, M.S. Dresselhaus; *Carbon* **1982**, *20*, 427-431; b) A.C. Ferrari, J. Robertson; *Phys. Rev. B* **2000**, *61*, 14095-14107; c) V.A. Davydov, A.V. Rahmanina, V. Agafonov, B. Narymbetov, J.P. Boudou, H. Szwarc; *Carbon*, **2004**, *42*, 261-269; d) L.G. Cançado, K, Takai, T. Enoki, M. Endo, Y.A. Kim, H. Mizusaki, A. Jorio, L.N. Coelho, R. Magalhães-Paniago, M.A. Pimenta; *Appl. Phys. Lett.* **2006**, *88*, 163106-1,3; e) M.A. Pimenta, G. Dresselhaus, M.S. Dresselhaus, L.G. Conçado, A. Joiro, R. Saito; *Phys. Chem. Chem. Phys.* **2007**, *9*, 1276-1291

11) a) L. Ji, C. Saquing, S.A. Khan, X. Zhang; *Nanotechnology* **2008**, *19*, 1-9; b) M. Jaroniec, J. Choma, J. Gorka, A. Zawislak; *Chem. Mater.* **2008**, *20*, 1069-1075

12) C.G. Wu, T. Bein; *Science* **1994**, *266*, 1013-1015

13) a) N. Sonobe, T. Kyotani, Y. Hishiyama, M. Shiraishi, A. Tomita; *J. Phys. Chem.* **1988**, *92*, 7029-7034; b) P. Enzel, J.J. Zoller, T. Bein; *J. Chem. Soc. Chem. Commun.* **1992**, 633-635; c) S. Esnouf, F. Beuneu, P. Enzel, T. Bein; *Phys. Rev. B* **1997**, *56*, 12899-12904; d) T. Kyotani, T. Nagai, S. Inoue, A. Tomita; *Chem. Mater.* **1997**, *9*, 609-615; e) P.R. Giunta, R.E. Bossio, A.E. Stiegman, A.G. Marshall; *Chem. Mater.* **2003**, *15*, 1289-1295; f) M. Kruk,

B. Dufour, E.B. Celer, T. Kowalewski, M. Jaroniec, K. Matyjaszewski; *J. Phys. Chem. B* **2005**, *109*, 9216-9225

14) a) P.R. Giunta, L.J. Van de Burgt, A.E. Stiegman; *Chem. Mater.* **2005**, *17*, 1234-1240; b) O. Ruzimuradov, G. Rajan, J. Mark; *Macromol. Symp.* **2006**, *245-246*, 322-324

15) a) J. Pang, V.T. John, D.A. Loy, Z. Yang, Y. Lu; *Adv. Mater.* **2005**, *17*, 704-707; b) J. Pang, L. Yang, D.A. Loy, H. Peng, H.S. Ashbaugh, J. Mague, C.J. Brinker, Y. Lu; *Chem. Commun.* **2006**, 1545-1547

CONCLUSIONS AND OUTLOOKS

This work has been focused on the study of nanostructured porous materials and their exploitation to obtain new porous materials with different chemical nature.

Mesoporous hexagonal silica with well-defined micrometric morphology has been synthesized using template synthesis in different environmental conditions of temperature, pH and reaction time. These systems have been characterized using X-ray diffraction, adsorption techniques and SEM imaging to define the effective pore dimension, the surface area value and the particle size distribution. They have been used as matrices to perform *in situ* polymerization of different vinyl monomers, such as styrene, methylmethacrylate and acrylonitrile. The effective formation of the nanocomposite and the intimate interactions between the polymeric phase and the silica matrix were investigated with a variety of techniques, such as differential scanning calorimetry (DSC), thermogravimetric analysis (TGA) and advanced 2D hetcor solid-state NMR techniques that highlight the spatial relationship between polymer and matrix atoms. This intimate interaction is the key point for the shape replica process. In fact, it is possible to obtain polymeric micro-objects with the retention of the micrometric morphology of the silica, in which they are formed. They show a well-defined porosity and a notable surface area. The surfaces of these objects could be chemically functionalized with a post-synthetic treatment and they could be used as supports to graft functional dyes, as separating medium for organic-separation chromatographic columns or, in the specific case of shapes with micrometric holes, to trap and store large biological molecules like DNA fragments. Since the polymer structure is metastable and collapses on heating, it could be sealed by irradiating the extremities.

A class of nanocomposites, those with polyacrylonitrile as polymer phase, has been further studied for its particular thermal properties to produce graphitic-like carbon structures. In fact, polyacrylonitrile can perform a series of internal reactions thermally activated, that start with the cyclization based on the reaction of cyano groups and the

formation of a laddered structure until lateral condensations and loss of nitrogen that bring to the formation of an extended graphitic structure. Nanocomposites have been heated in non-oxidative atmosphere at different temperatures and each step has been extensively investigated with spectroscopic ATR and Raman techniques to follow the evolution of confined polymer and comparing them with bulk polyacrylonitrile thermal treated in the same way. Confinement in nanometric spaces seems to favourite the polymer evolution steps, so that they start at lower temperatures, as demonstrated by DSC analysis; at the same time it limits successive structure evolution hindering the lateral extension of the graphitic-like system. By this, it is possible to obtain elongated graphitic-like fragments that are large only few nanometers. Moreover, during thermal evolution a progressive change of sample colour was observed. White room-temperature samples become darker at each heating step until black over 700°C. This seems to suggest the use of these systems like "molecular thermometers", to indicate the maximum temperature reached by a system.

Dissolution of silica matrix of carbonized nanocomposites generates a new class of porous carbon systems with graphitic-like pore walls, high surface area and well-defined micrometric morphology, as demonstrated by microraman spectroscopy, nitrogen adsorption and SEM imaging. These carbon objects could be used as gas-storage systems, as purification systems for gases and liquids or as matrices for generation of host-guest systems. Moreover, by SEM imaging without sputtering of gold, there are first evidences that these micro-objects have partial electron conductivity properties, probably due to the aromatic system of graphitic fragments.

The extension of the concept of hybrid carbon-silica material drove us to study the thermal evolution of a periodic mesoporous organosilica with aromatic organic bridges. The *p*-phenylensilica matrix has been synthesized through a template synthesis in basic aqueous solution starting from 1,4-bis(triethoxysilyl)benzene as precursor. The system was characterized by X-ray diffraction, adsorption of different gases and vapors and solid state NMR techniques. The XRD pattern clearly shows the high structural order of this system, that has both a well-defined mesoscopic pore order and a nanometric-level molecular order. In fact, aromatic rings are included in pore walls in regular disposition that alternates silica layers and organic bridges along the channel axis. This great structural order is also visible in NMR experiments, showing that the Si-C bond is not

cleaved during the synthesis and that there is a high degree of condensation. Gas and vapor adsorption shows the affinity of this system for polar molecules, such as ethanol, and in particular for carbon dioxide, reaching a virtual filling of 100%, while there are not evidences of adsorption of oxygen. *P*-phenylensilica could be an ideal system for purification of carbon dioxide gas mixtures or as sequestering agent for pollutant chemicals. The high regular disposition of organic groups could be further exploited in post-synthetic grafting of functional groups , i.e. sulphonation or nitration of aromatic rings.

Organosilica samples were carbonized and then characterized with X-ray diffraction, Raman spectroscopy, adsorption techniques and solid state NMR. During carbonization Si-C bonds cleave and the aromatic moieties become a graphitic-like structure. The system loses the molecular order, but maintains the period order on the mesoscale and its surface area and the total pore volume remain the same of non-carbonized sample. This process could be a valid alternative way to obtain porous carbon systems with tuneable surface area and pore volume with graphitic-like pore walls, that could be used, for examples, as high performance adsorption systems or lightweight scaffolds for catalysis support.

Topics proposed in this work are only few examples of structural control on the nanometric and micrometric level and of processes to obtain polymer and carbon systems with high surface area and defined nanometric structures. They could be exploited in the future for the realization of functional nanodevices.

Appendices

Appendix A

Adsorption measurements

Adsorption measurement is one of the most diffuse techniques to characterize porous materials and to estimate the surface area, the pore size, the porosity, the pore size distribution and the affinity for different molecules. Adsorption happens when a gaseous or vapour molecules interact with a solid surface, passing from the gaseous (or vapour) phase to an *adsorbed* state. In a typical adsorption measurement a solid is put in contact with a defined amount of a pure substance, or a mixture with known composition, to study the specific interaction between the two phases.

A first, necessary distinction must be done now between *adsorption* and *absorption*. In the first case gaseous molecules interact with the material surface, but do not diffuse in bulk material, while in absorption process interacting molecules penetrate through the surface and diffuse in the pore walls structure.

Concerning nanoporous materials, absorption phenomenon is generally rare and they are investigated only by adsorption techniques.

A.1 Definitions

To avoid ambiguities that can arise in reporting gas adsorption data and to formulate a standardization of procedures and terminologies, the International Union of Pure and Applied Chemistry (IUPAC) recommends to precise the following definitions, before starting to describe porous materials properties.[1]

The material onto which adsorption takes place is called *adsorbent*, while the substance to be adsorbed is called the *adsorpt* or *adsorptive*, before the adsorption process starts, and *adsorbate*, when it is in the adsorbed state. (Figure A.1)

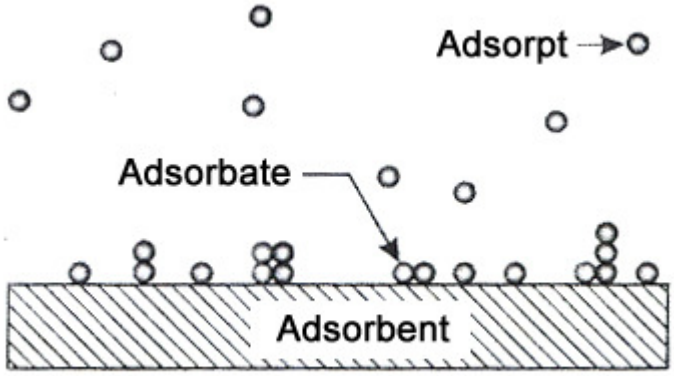

Figure A.1

Definition of adsorbent, adsorpt and adsorbate

The *adsorption process* is the enrichment of one or more components in an *interfacial layer*. This interfacial layer comprises two regions: the *surface layer* of the adsorbent and the *adsorption space* in which enrichment of the adsorptive can occur.

The term adsorption may also be used to denote the process in which adsorptive molecules are transferred to, and accumulate in, the interfacial layer. The term *desorption* denotes the converse process, in which the amount adsorbed decreases. Adsorption and desorption are often used adjectivally to indicate the direction from which experimentally determined adsorption values have been approached (e.g. adsorption and desorption curve). Adsorption *hysteresis* arises when the adsorption and desorption curves do not coincide.

When adsorption is dominated by physical interaction rather than chemical bonding, we talk about *physisorption*, otherwise if the adsorption energy is of the order of chemical binding energies we talk about *chemisorption*.

Physisorption is characterized by:[2]

- The sublimation energy is in the order of 20-40 kJ/mol;
- The adsorbate is still relatively free to diffuse on the surface and to rotate;
- The molecular structure of the solid does not change with physorption except for some molecular solids;
- An adsorption equilibrium is quickly established. When lowering the pressure the gas desorbs reversibly (except in porous solids).

While chemisorption is characterized by:[2]

- The sublimation energy is in the order of 100-400 kJ/mol;
- Often there are specific binding sites. The adsorbate is relatively immobile and usually does not diffuse on the surface;
- Even on covalent or metallic solids there is often a surface reconstruction;
- Due to the strong binding, the molecules pratically do not desorb.

At last, an important distinction must be done between *internal* and *external* surface. Generally, all protrusions and cracks wider than deep are considered external surface, while walls of voids deeper than large are considered internal surface.

A.2 Adsorption process

Adsorption in nanopores does not occurs always with the same process, but it is strictly related to the pore size. According to IUPAC nanopore classification,[1] we can separate adsorption in micropores from that in meso- and macropores. Micropores are characterized by a *filling* process, because they are very narrow and during adsorption they are directly filled in one-step process, while in the case of larger pores we can distinguish between a first *superficial* adsorption followed by a *capillary condensation*. In surface adsorption the adsorbate covers the pore surface with a single molecular layer (*monolayer* adsorption) or two or more layers (*multilayer* adsorption) still leaving an empty space. This space is then filled by the adsorbate during the capillary condensation, that is often associated to an hysteresis cycle. Capillary condensation term cannot be used for micropore filling.

For physisorption, the *monolayer capacity* (n_m) is usually defined as the amount of adsorbate needed to cover the surface with a complete monolayer of molecules. The *surface coverage* (θ) is defined as the ratio of the amount of adsorbed substance to the monolayer capacity.

The *surface area* (A_S) of the adsorbent may be calculated from the *monolayer capacity* ($n^a{}_m$ in moles), provided that the area (a_m) effectively occupied by an adsorbed molecule in the complete monolayer is known.

Thus,

$$A_S = n_m^a N_A a_m$$

Where N_A is the Avogadro constant. The *specific surface area* (a_S) refers to unit mass of adsorbent:

$$a_S = \frac{A_S}{m}$$

In the case of micropore filling, the interpretation of the adsorption isotherm in terms of surface coverage may lose its physical significance, for this reason, sometime, it may be convenient to define a *monolayer equivalent area* calculated from the amount of adsorbate required to fill the micropores.

Physical adsorption is generally enthalpically driven, with a global energetic stabilization given by the instauration of Van der Waals interactions between adsorbant and adsorbate.

A.3 Isotherms

The relation, at constant temperature, between the amount adsorbed and the equilibrium pressure of the gas is known as *adsorption isotherm*. It is determined experimentally and could be described by the adsorption function:[3]

$$\Gamma = f(p,T)$$

In a simply model, we can imagine the adsorbent medium as a grid of adsorption sites where only one molecule could be linked. Using the following approximations:

- All sites are equal
- Adsorption is not influenced by the number or the position of occupied sites
- Adsorbed molecules do not interact among them

we can suppose that all gas molecules adsorbed are in dynamic equilibrium with those already linked:

$$\mathrm{A(g) + M(sup)} \underset{k_D}{\overset{k_A}{\rightleftharpoons}} \mathrm{AM}$$

where k_A and k_D are respectively kinetic coefficients of the adsorption and desorption process:

$$v_A = k_A p_A N(1-\theta)$$

$$v_D = k_D N\theta$$

At equilibrium $k_A = k_D$, so calling K the ratio k_A / k_D:

$$\theta = \frac{Kp_A}{(1+Kp_A)}$$

K is the equilibrium constant and it is an index of the affinity of that gas for the solid and it is proportional to the inverse of temperature (in physical adsorption).

Quantities of gas adsorbed (n) on weight of adsorbent solid (m) is a function of the equilibrium pressure (p), of temperature (T) and of the nature of the adsorbate-adsorbent system (gas-solid).

For a particular gas type adsorbed on a solid, at constant temperature:

$$\Gamma = \frac{n}{m} = f(p)_T$$

and if the gas is under the critical temperature:

$$\Gamma = \frac{n}{m} = f\left(\frac{p}{p^0}\right)_T$$

where p^0 is the vapor pressure of the liquid adsorbed at temperature T.

A great variety of adsorption isotherm are experimentally observed and the official IUPAC classification divides them in six types (see figure A.2),[1] even if in most cases, at sufficient low surface coverage the isotherm reduces to a linear form, described by the Henry adsorption isotherm equation:

$$\Gamma = K_H \frac{p}{p^0}$$

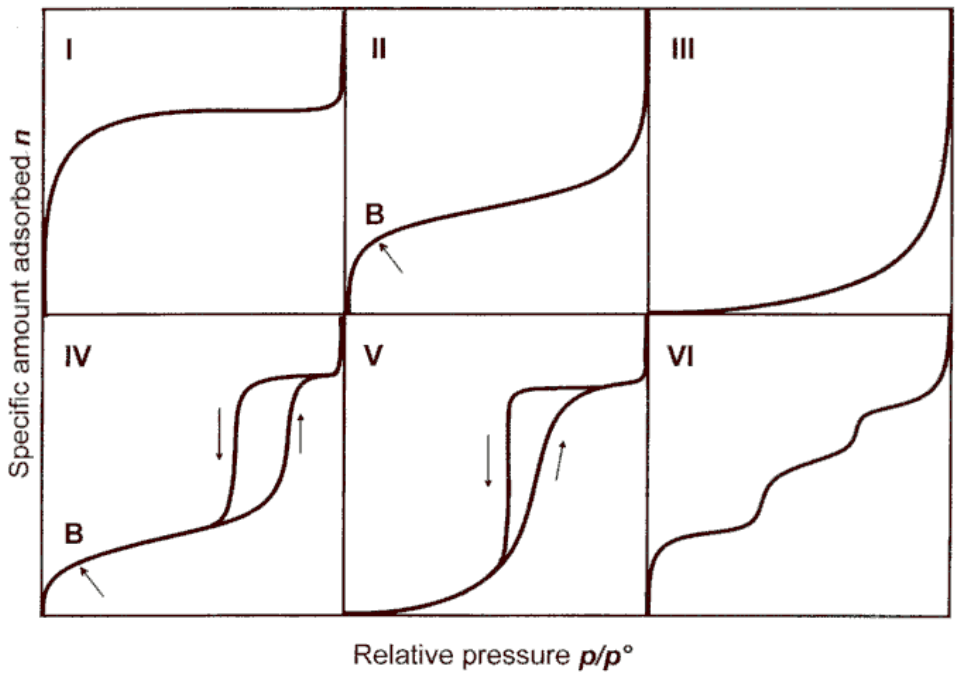

Figure A.2

Types of physisorption isotherms [1]

Single adsorption isotherms could be described as follows:[1,2]

- **Type I** isotherm or **Langmuir type** is concave to the p/p^0 axis and n^a approaches a limiting value as $p/p^0 \rightarrow 1$. It can be described by the Langmuir adsorption isotherm equation:

$$\frac{n}{n_m} = \theta = \frac{K_L P}{1 + K_L P} \quad \text{with} \quad \theta = \frac{\Gamma}{\Gamma_{mon}}.$$

  K_L is a constant and Γ_{mon} is the maximum amount adsorbed. This isotherm is given by microporous solids having relatively small external surfaces.

- **Type II** isotherm or **Freundlich type** is the normal form of isotherm obtained with a non-porous or macroporous adsorbent or with a porous material in which there are different adsorption sites, some having a high affinity and others having a low affinity for that specific adsorptive. The high affinity sites are occupied first and the point B indicates the stage at which monolayer coverage is complete and multilayer adsorption begins.

This isotherm is described by the Freundlich adsorption isotherm equation:

$$\Gamma = K_F P^q$$

where K_F and q (q<1) are constants.

- **Type III** isotherm is convex to the p/p^0 axis over its entire range and therefore does not exhibit a "Point B". This isotherm is not common but it is expected if the binding of the first monolayer is weaker than the binding of molecules to those already adsorbed; this is the case if the heat of adsorption is lower than the heat of condensation.
- **Type IV** isotherm or **BET type** is typical of mesoporous materials. The initial concave part is attributed to the adsorption of the monolayer followed by the multilayer adsorption before and then the capillary condensation with an hysteresis loop usually associated. When $p/p^0 \rightarrow 1$ condensation leads to macroscopically thick layers.

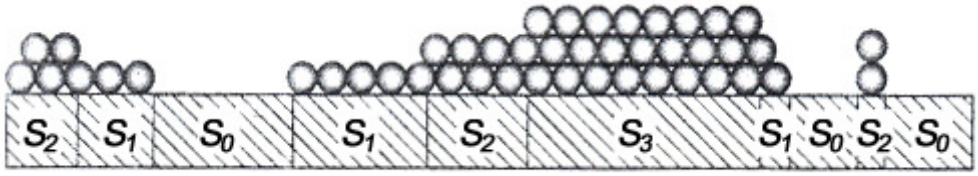

Figure A.3

BET model of multilayer adsorption

- **Type V** isotherm or **Sigmoid type** is uncommon and indicates cooperative effects. A molecule binds to the surface better if it can interact with e neighboring adsorbed molecule. As a consequence of this lateral interaction two-dimensional condensation occurs.
- **Type VI** isotherm or **Step type** is characterized by sharp steps depending on the system and the temperature. It represents stepwise multilayer adsorption on a uniform non-porous surface. The step-height now represents the monolayer capacity for each adsorbed layer.

A.4 Adsorption hysteresis

As previously described, hysteresis loops are associated to capillary condensation phenomena in meso- or macropore systems. An hysteresis loop is generated when the desorption and the adsorption curves do not correspond. This happens when adsorbant comes out from pores at a relative pressure lower than that of adsorption. Causes of hysteresis mechanism could be associated to thermodynamic or geometrical reasons.[2]
Thermodinamic mechanism is illustrated in figure A.4:

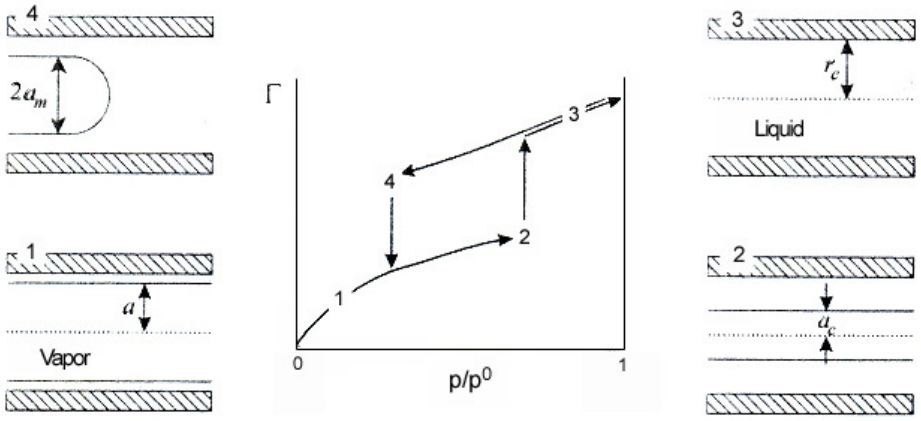

Figure A.4

Filling and emptying of a cylindrical solid pore with liquid from its vapor and the corresponding schematic adsorption/desorption isotherm [2]

As illustrated in figure, an adsorption process in a pore of radius r_c starts with the formation of a thin adsorbate layer that leaves an empty space of radius a (stage 1). Increasing the pressure the thickness of the adsorbate layer increases and, consequently, the free space radius decreases until reaching of a critical radius a_c and after that capillary condensation occurs and the pore is completely filled (stages 2 and 3). During desorption, liquid starts to evaporate, generating a meniscus of radius a_m that is greater than a_c and requests a lower pressure.
The topology of the pore network plays another role, as illustrated in figure A.5.

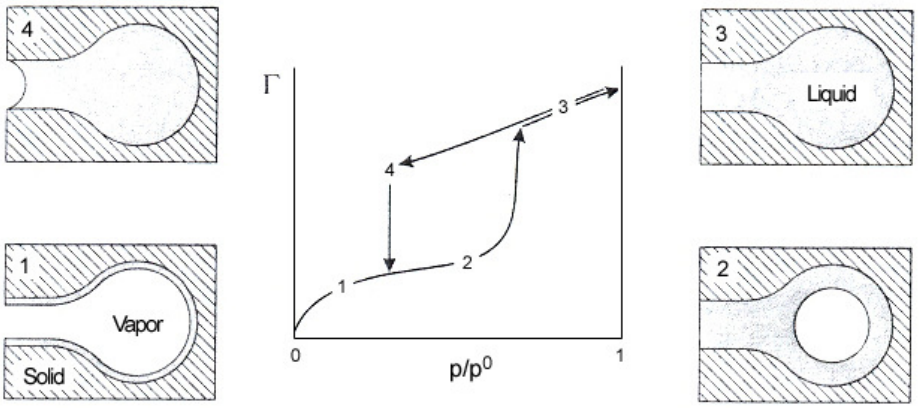

Figure A.5

Filling and emptying of a solid "ink bottle" pore with liquid from its vapor and the corresponding adsorption/desorption isotherm [2]

As illustrated in figure, hysteresis is generated by "ink bottle" pore geometry. In fact, during desorption vaporization can occur only from pores that have access to the vapor phase, and not from pores that are surrounded by other liquid-filled pores. There is a "pore blocking" effect in which a metastable liquid phase is preserved below the condensation pressure until vaporization occurs in a neighboring pore. The relative pressure at which vaporization occurs depends on the size of the pore, the connectivity of the network, and the state of neighboring pores.

By the same way, also adsorption is limited by small pore openings, as indicated in steps 1 and 2. In fact, after a first surface adsorption, in the narrow pore the critical radius is reached before the complete filling of the large pore and a capillary condensation happens. This generate a liquid membrane that slow down adsorbate diffusion and complete pore filling.

Despite the motivations of the process, there are four experimental hysteresis loops, illustrated in figure A.6.

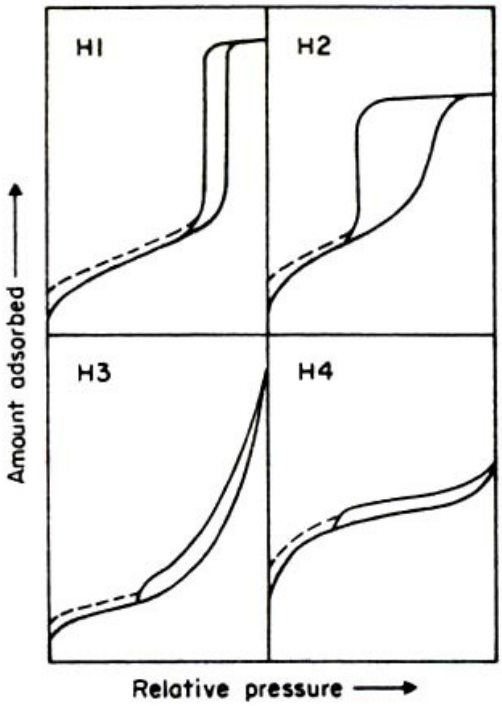

Figure A.6

Types of Hysteresis loops [1]

H1 and H4 types are the two extremes: H1 shows vertical, parallel branches in a narrow range, while H4 is quite horizontal and extended in a wide range of relative pressure. Hysteresis H2 and H3 are instead intermediate between the two.

Each loop could be associated to a well defined pore structure:

- **Type H1** is associated to a system with well-defined cylindrical-like pores or agglomerates or compacts of approximatively uniform spheres in fairy regular array.
- **Type H2** is typical of disordered systems with not defined distribution of pore size and shape.
- **Type H3** is generally due to aggregates of plate-like particles, as indicated by the absence of upper adsorption limit.
- **Type H4** is often associated with narrow slit-like pores and in the case of Type I isotherm it is indicative of microporosity.

With many systems, especially those containing micropores, low pressure hysteresis (dashed lines in Figure A.6) may be associated with the swelling of a non-rigid porous

structure or with the irreversible uptake of molecules in pores of about the same width as that of the adsorbate molecule or in some instances with an irreversible chemical interaction of the adsorbate with the adsorbent. In these systems the removal of the residual adsorbed molecules is then possible only if the adsorbent is outgassed at higher temperatures.

A.5 Experimental procedures

Adsorption measurements could be conduced exploiting gravimetric or volumetric methods.

In the first method the adsorbant material is placed on a microbalance and the quantity of adsorbed gas is calculated by the weight increase. Known the molecular weight of the adsorbate it is possible to calculate the number of moles and, so, the covered surface (see next paragraphs).

In the second method, instead, the amount of adsorbed gas is calculated from the pressure decrease in a sealed container caused by the sequestration of the adsorbate from gaseous phase. The volume of the container must be calibrated and constant, at a known temperature. A determined quantity of pure gas is admitted in the outgassed vessel containing the sample. As adsorption takes place, the pressure in the confined volume falls until equilibrium is established. The amount of gas adsorbed at the equilibrium pressure is given as the difference between the amount of gas admitted and the amount of gas required to fill the space around the adsorbent (*dead space*) at that pressure. The adsorption isotherm is constructed point-by-point by the admission to the adsorbent of successive charges of gas with the aid of a volumetric dosing technique and application of the gas laws. The volume of the dead space must be known accurately by a pre-calibration of the confined volume and subtracting the volume of the adsorbent. The amount of adsorbed gas can be expressed by its mass or volume (often given in STP per unit mass; STP: standard temperature and pressure, namely 273.15 K and 760 Torr or 101325 Pa).

In this work, we have used only volumetric methods.

A.6 Determination of surface area

Because the accessibility of pores depends on the size and shape of the gas molecules, the internal surface as determined by gas adsorption may depend on the dimension of the adsorptive molecules (*molecular sieve* effect).

Porosity is defined as the ratio of the volume of pores and voids to the volume occupied by the solid. If a cylindrical pore geometry can be assumed, the *average pore diameter* of a porous materials can be calculated by the following relation:

$$D_{4V/s} = \frac{4V_p}{(S_{total} - S_{ext})}$$

The total surface area S_{total} can be calculated either from the BET-method, from t-plot or α_s comparison plot methods.[4-6]

Among all, the Brunauer-Emmett-Teller (BET)[4] gas adsorption method has become the most used standard procedure for the determination of the surface area of porous materials, in spite of the oversimplification of the model on which the theory is based. This is the BET equation in the linear form:

$$\frac{p}{n^a(p^0 - p)} = \frac{1}{n^a_m C} + \frac{(C-1)p}{n^a_m C p^0}$$

where n^a is the amount adsorbed at the relative pressure p/p^0 and $n^a{}_m$ is the monolayer capacity. C is related exponentially to the enthalpy (heat) of adsorption in the first adsorbed layer; even if C does not provide a quantitative measure, it may be used to characterise the shape of the isotherm: a high value ($C \approx 100$) is associate with a sharp knee in the isotherm while, if C is low ($C<20$) the Point B cannot be identified as a single point on the isotherm.

The BET equation requires a linear relation between $p/(n_a(p^0-p))$ and p/p^0. The range of linearity is restricted to a limited part of the isotherm-usually for p/p^0 in the range of 0.05-0.30 that is the range in which the monolayer is complete ($\theta = 1$).

The second stage is the calculation of the surface area or BET area (A_S (BET)) of the adsorbent from the monolayer capacity:

$$A_S(BET) = n_m^a N_A a_m \qquad \text{and} \qquad a_S(BET) = \frac{A_S(BET)}{m}.$$

a_S is the specific surface area and N_A is the Avogadro constant.

Nitrogen is generally considered the most suitable adsorptive for surface area determination but in principle it is possible to use others gases, the only requirement is to know the average area a_m (*molecular cross-sectional area*) occupied by the adsorbate molecule in the complete monolayer (for N_2 it is 0.162 nm^2 at 77 K; other values are reported in literature).[3]

The BET analysis does not take into account the possibility of micropore filling or penetration into cavities of molecular size. These effects could falsify the BET surface areas.

A.7 Assessment of microporosity (Langmuir)

The mechanism of physorption obviously depends on the pore diameter, so that in pore of molecular dimensions, the strength of the adsorbent-adsorbate interactions are increased. The pores are thus filled at low p/p^0. Because in this region individual adsorbate molecules fill the narrow pores, a *monolayer equivalent area* has been defined instead of the not correct BET area.

For the determination of the pore volume and the pore size, it is not so simple to choose an equation, because each one gives a reasonably good fit over a certain range of an isotherm but does not provide sufficient evidence for a particular mechanism of adsorption.

A general good method is the *t-method*[5] that compares the shape of an isotherm with that of a standard on a non-porous solid. The amount adsorbed is plotted against t, that is the multilayer thickness calculated from the standard isotherm obtained with the non-porous reference solid. Any deviation in the shape of the isotherm s detected as a departure of the "t-plot" from the linearity. Really, for the assessment of the microporosity, the thickness of the multilayer is irrelevant so that it is preferable to replace t by α_S, defined as (n^a/n^a_S) where n^a_S is the amount adsorbed by the reference solid at a fixed relative pressure p/p^0=s.

A.8 Assessment of mesoporosity

Porosity is a concept related to the *texture* of a material, defined by the detail geometry of the void and pore space; porosity refers to the pore space. An *open pore* is a cavity or channel communicating with the surface of a particle, in opposition to the *closed pore* while *void* is the space or interstice between particles. *Powder porosity* is, in that sense, the ratio of volume of voids plus that of open pores, to the total volume occupied by the powder.[1]

The *total pore volume*, V_P, is derived from the amount of vapour adsorbed at p/p^0 close to one, assuming that the pores are then filled with condensed adsorptive in the liquid state.

The *mean hydraulic radius*, r_h, of a group of mesopores is defined as

$$r_h = \left(\frac{V}{A_S} \right)_P$$

where $(V/A_S)_P$ is the ratio of the volume to the area of walls of the group.

If the pores have a well-defined shape, as in the case of non-intersecting cylindrical pores, there is a simple relationship between r_h and the mean pore radius r_p:

$r_p = 2r_h$.

while for parallel-sided slit-shaped pores, r_h is half the slit width.

The *pore size distribution* is the distribution of pore volume with respect to pore size.[1]

The *Kelvin equation,* valid only for pores greater than 2 nm, relates the principal radii, r_1 and r_2, of curvature of the liquid meniscus in the pore to the relative pressure, p/p^0, at which condensation occurs:

$$\frac{1}{r_1} + \frac{1}{r_2} = -\frac{RT}{\sigma^{1g} v^1} \ln\left(\frac{p}{p^0} \right),$$

where σ^{1g} is the surface tension of the liquid condensate and v^1 is its molar volume.

From this equation it is possible to obtain the *pore radius* or *pore width* with the following assumptions:

- the pores have a cylindrical or slit shape;
- that the curvature of the meniscus is directly related to the pore width.

For the first type of pores the meniscus is hemispherical and $r_1=r_2$, while for the second type of pores, the meniscus is hemicylindrical and so r_1=width of slit and $r_2=\infty$.
Thus, rearrangement of the Kelvin equation for cylindrical pores is:

$$r_k = \frac{2\sigma^{1g} v^1}{RT \ln \frac{p^0}{p}},$$

with r_k as Kelvin radius.
If the radius of the pore is r_p and a layer of thickness t has been already adsorbed on the pore walls:

$$r_p = r_k + t .$$

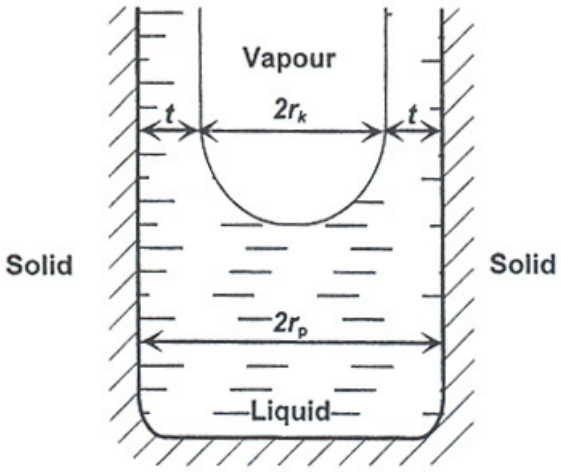

Figure A.7

Relation between the Kelvin radius and the pore radius in a cylindrical mesopore

For slit pores, the slit width, d_p, is:

$$d_p = r_k + 2t .$$

Values of t are obtained from adsorption measurements on a non-porous sample having a similar surface to that of the sample under investigation.

To calculate the mesopore size distribution from physisorption isotherms it is usually assumed that:

- pores are rigid and with regular shapes, as described above;

- micropores are absent;
- the size distribution does not extend continuously from the mesopore to the macropore range.

Thus, it is possible to compute the pore size distribution curve, usually expressed in the graphical form $\Delta V_P/\Delta r_p$ vs. r_p.

The method of Barett-Joyner-Halenda (BJH),[7] which was proposed in 1951 is certainly the most popular for mesopore size analysis. The BJH-approach provides an algorithm to calculate the pore size distribution (PSD) by assuming a cylindrical pore geometry from nitrogen desorption data (obtained at 77 K). The BJH-approach attracted much attention and was later modified by Dollimore and Heal, Cranston-Inkley[6,8] and others.
All methods related to the original BJH approach are based on the modified Kelvin equation and the accuracy of the calculated PSD depends on the applicability and the deficiencies of the Kelvin equation (pores have to be rigid and of well-defined shape, the filling of each pore does not depend on its location within the network,…). In narrow pores attractive fluid-wall interactions are dominant and the macroscopic, thermodynamic concept of a smooth liquid-vapor interface and bulk-like core fluid cannot realistically be applied. In addition, methods based on the modified Kelvin equation do not take into account the influence of the adsorption potential on the position of the pore condensation transition. It is further assumed that the pore fluid has essentially the same thermophysical properties as the correspondent bulk fluid. For instance, the surface tension of the pore liquid is thought to be equal to the properties of the corresponding bulk liquid, but the surface tension of the pore liquid depends on the radius of curvature. Significant deviations from the bulk surface tension are however expected to occur in narrow mesopores.[6,9] Another problem is that the thickness of the preadsorbed multilayer film is assessed by the statistical thickness of an adsorbed film on a nanoporous solid of a surface similar to that of the sample under consideration. However, in particular for narrow pores of widths < ca. 10 nm this mean thickness does not reflect the real thickness of the preadsorbed multilayer film, because curvature effects are not taken into account.

A more realistic method of determining the pore size distribution is based on the Density Functional Theory (DFT). After a pioneering work by Seaton et al.[10] in 1989, over the past few years, it has become a powerful tool for the interpretation of physisorption data, and in particular an alternative valuable procedure for evaluating the pore size distribution.[11] It is necessary to suppose that the pores are open and that the confined fluid is in thermodynamic equilibrium with the same fluid in the bulk state. Thus, the fluid in the pore is not of constant density, because of the adsorption forces in the vicinity of the pore walls; a density distribution can be defined in terms of a density profile, $\rho(r)$, expressed as a function of the distance r from the wall across the pore.

It can be obtained minimizing the free energy of the system (at constant μ, V and T), called grand Helmholtz free energy, or grand potential functional, $\Omega[\rho(r)]$, with a statistical mechanical approach. For one-component fluid, the grand potential functional becomes:

$$\Omega[\rho(r)] = F[\rho(r)] + \int dr\rho(r)[\phi(r) - \mu]$$

where $F[\rho(r)]$ is the intrinsic Helmholtz free energy functional, $\Phi(r)$ is the external potential and the integration is performed over the pore volume, V.

Once the density profile is defined for a given pressure, the amount adsorbed by a particular pore can be obtained from the area under the curve.

Considerable progress has already been made in the theoretical treatment of physisorption mechanisms, and DTF method is a first result.

A.9 References:

1) K.S.W. Sing, D.H. Everett, R.A. Haul, L. Moscou, R.A. Pierotti, J. Rouquerol, T. Siemieniewska; *Pure & Appl. Chem*. **1985**, *57*, 603-619

2) H.J. Butt, K. Graf, M. Kappl, *Physics and Chemistry of Interfaces*, Wiley-VCH, Weinheim, **2006**

3) F. Rouquerol, J. Rouquerol, K. Sing, *Adsorption by powders and porous solids*, Academic Press, London, **1999**

4) S. Brunauer, P.H. Emmett, E. Teller; *Adsorption of gases in multimolecular layers* **1938**, 309-319

5) J.H. De Boer, B.C. Lippens, B.G. Linsen, J.C.P. Broekhoff, A. van den Heuvel, T.J. Osinga; *J. Colloid Interface Sci.* **1966**, *21*, 405-414

6) S.J. Gregg, K.S.W. Sing, *Adsorption, Surface Area and Porosity, 2nd ed.,* Academic Press, London, **1982**

7) P. Barrett, L.G. Joyner, P.P. Halenda; *The Volume and Area Distributions in Porous Substances* **1951**, *73*, 373-380

8) S. Lowell, J.E. Shields, *Powder Surface Area and Porosity*, Chapman & Hall, London, **1991**

9) a) A. Galarneau, D. Desplantier, R. Dutartre, F. Di Renzo; *Microporous Mesoporous Mater.* **1999**, *27*, 297-308; b) H.Y. Zhu, L.A. Ni, G.Q. Lu, *Langmuir* **1999**, *15*, 3632-3641

10)N.A. Seaton, J.P.R.B. Walton, N. Quirke; *Carbon* **1989**, *27*, 853

11)a) P.B. Balbuena, C. Lastoskie, K.E. Gubbins, N.Quirke; *Studies in Surface Science and Catalysis* **1993**, *80*, 27-34; b) J.P. Olivier, W.B. Conklin, M.V. Szombathely; *Studies in Surface Science and Catalysis* **1994**, *87*, 81-89

Appendix B

Thermal analysis

Thermal analysis are those techniques in which a physical property of a substance and/or its reaction product(s) are valued as a function of temperature. In this work we have performed two types of thermal analysis: differential scanning calorimetry (DSC) and Thermogravimetric analysis (TGA).

B.1 Differential scanning calorimetry

DSC is generally used to point out thermal properties of a material such as phase transition of the first order (fusion, crystallization), phase transition of the second order (glass transition) and degradation. Moreover, chemical reactions that involve an heat change with environment could be detected by this analysis.[1]

In fact, DSC curves reflect changes in the energy of the system under analysis. DSC measures the heat necessary to maintain the same temperature in the sample versus an appropriate reference material in a furnace.[2] Enthalpy changes due to a change of state of the sample are determined. Typical DSC trace are shown in figure B.1:

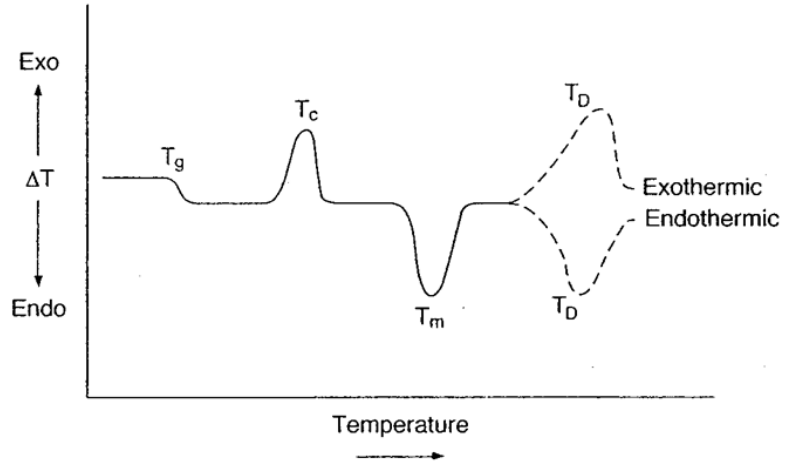

Figure B.1

Example of a typical DSC thermogram [2]

There are two types of differential scanning calorimeters: calorimeters at heat flux (ΔT) and calorimeters at power compensation (ΔP). In either the type of calorimeters, the measurement is compared to that for a reference material having a known specific heat.[3] The first type maintains constant the heating of the sample and the reference, measuring the difference of temperature, while the second model measures the difference of heat between the two necessary to maintain both at the same temperature.

For the following discussion the two models are considered the same, because they give the same results. For our experiments, we have used a calorimeter at power compensation.

B.2 Instrument description

The instrument core consists in a thermal-resistance plate, generally in constantane, with two gold thermocouples where are placed the sample, contained in an aluminum crucible, and the reference, an empty crucible. The instrument could be programmed to perform controlled heating and cooling with defined rate, heating the sample and the reference by an electrical heat flow. The heat flow into the sample holder can be approximated by:[4]

$$\frac{dQ}{dT} = K(T_b - T)$$

where K is the thermal conductivity of the thermal-resistance layer around the sample, assumed to be dependent on geometry but independent of the temperature; T is the sample temperature and T_b is the programmed block temperature:

$$T_b = T_0 + qt$$

where T_0 is the initial temperature and q is the programmed heating rate. A similar equation may be written for the reference material.

The basis for all calorimetric measurements is the determination of heat capacities. In the absence of any other transition, the DSC curve represent the change in the heat capacity of the sample over the experimental temperature range.[5] The heat adsorbed on heating a sample with constant heat capacity, C_p, between temperatures T_0 and T is:

$$Q = C_p(T-T_0)$$

and the basic equation for DSC, obtained confronting the three previous equations, is:[6]

$$\Delta T = \frac{q\, C_p}{K}$$

where ΔT is the difference in temperature between the reference material and the sample. The calibration factor K, thermal conductivity, should be independent of temperatures for both power compensation and heat flow DSC.
If the mass, m, of the sample is in grams, then

$$C_p = mc_p$$

where c_p is the specific heat

B.3 Enthalpy calculation

The area of a DSC peak could be used to estimate the enthalpy of transition, ΔH. Considering only the assumption of no difference in the heating rates for the sample and the reference and that the DSC curve then returns to the original baseline after the transition, then the enthalpy can be described in the following way:[4]

$$\Delta H = \int_{T_i}^{T_f} C_p dT = \int_{T_i}^{T_f} \left(\frac{K\, \Delta T}{q} \right) dT$$

where the T_i and T_f refer to the initial and final temperatures of the transition.
Calibration with respect to an enthalpy requires an area that corresponds to a well-defined enthalpy change and for this an heat of fusion is generally used, often of an indium piece.

B.4 Glass transitions

From a thermodynamic and mechanical point of view, the glass transition, T_g, is one of the most important parameters for characterizing a polymer system.[4,5] A polymer may be amorphous, crystalline or a combination of both (semicrystalline polymers). The glass transition is related to the chain motion in the amorphous region of the polymer.[2,4,7] Below the T_g, an amorphous polymer can be said to have the characteristic of a glass, while it becomes more rubbery above the T_g. On the molecular level, the glass transition corresponds to the onset of motion of short chain segments, which do not occur below the T_g. The glass transition temperature depends on the heating rate and the sample thermal history, jointed to other molecular parameters that affect chain mobility, as reported in table B.1 (see below).

From the point of view of DSC measurements, an increase in heat capacity occurs at T_g due to the onset of these additional molecular motions, which shows up as an endothermic response with a shift in the baseline.

Factors favouring a decrease in T_g	**Factors favouring an increase in T_g**
Main chain flexibility	Main chain rigidity
Flexible side chains	Bulky or rigid side chains
Increased tacticity	Increased cohesive energy density
Increased symmetry	Increased polarity
Addition of diluents or plasticizers	Increased molecular weight
Branching	Cross-linking

Table B.1

Structural factors affecting T_g

B.5 Melting, crystallization and heat reactions

The most common applications of DSC are melting processes, that contain information on both the quality (temperature) and the quantity (peak area) of crystallinity in solids.[4] Property changes at T_m are characteristic of a thermodynamic first-order transition and include a heat of fusion, and discontinuous changes in heat capacity, volume or density.

The melting point of a solid correspond s to a change from solid to liquid state and gives rise to an endothermic peak in DSC curve. The equilibrium melting point may be defined as:

$$T_m = \frac{\Delta H_m}{\Delta S_m}$$

where ΔH_m is the enthalpy of fusion and ΔS_m is the entropy of fusion. In addition to determining the melting point and heat of fusion from DSC, the width of the melting range is indicative of the range of crystal size and perfection. Because crystal perfection and crystal size are influenced by the rate of crystallization, T_m depends to some extent on the thermal history of the sample.[2,4,7]

Similar to the melting peak is the crystallization peak. This is an exothermic peak that is visible in cooling process or, sometimes, just before melting. Other peaks in DSC curves could be associated to thermal degradation of the sample.

Finally, DSC is also sensitive to those chemical reactions that are thermally activated and involve heat exchange with the environment. These reactions are visible with associated endo- or exothermic peaks in DSC curves.[8]

B.6 TGA analysis

Thermogravimetric analysis measure the sample mass variation in function of the temperature. With this technique it is possible to find degradation temperature of different substances or, in the case of adsorbent systems, temperature of adsorbate release.[9]

The sample is placed on a microbalance in a controlled atmosphere chamber. This chamber has a heating system that could be programmed to heat the sample with a pre-defined heating rate, to associate each temperature to the mass measured by the microbalance. Results are reported in curves that show the sample weight loss in function of the temperature.

TGA measurements could be performed in nitrogen atmosphere, air or other gas flux, depending on the type of thermal properties we want to investigate.

B.7 References:

1) S.R. Sandler, W. Karo, J. Bonesteel, E.M. Pearce, *Polymer Synthesis and Characterization*, Academic Press, New York, **1998**

2) E.M. Pearce, C.E. Wright, BB.K. Bordoloi, *Laboratory Experiments in Polymer Synthesis and Characterization*, The Pennsylvania state University, University Park, PA, **1982**

3) a) ASTM E 967-92, *Standard Practice for Temperature Calibration of Differential Scanning Calorimeters and Differential Thermal Analyzers,* **1992**; b) ASTM E 968-83, *Standard Practice for Heat Flow Calibration of Differential Scanning Calorimeters,* **1983**

4) M.J. Richardson, *Comprehensive Polymer Science: The synthesis, Characterization, Reactions and Applications of Polymers* (G. Allen and J.C. Bevington editors), Vol.1, Pergamon Press, New York, **1989**

5) a) B. Wunderlich, *Thermal Analysis*, Academic Press, New York, **1990**; b) A.J. Pasztor in *Handbook of Fundamental Techniques for Analytical Chemistry* (F. Settle editor), Prentice Hall PTR, New Jersey, **1997**

6) a) A.P. Gray in *Analytical Calorimetry* (R.S. Porter and J.F. Johnson editors), Plenum Press, New York, **1968**; b) R.A. Baxter in *Thermal analysis: instrumentation, Organic Materials and Polymers* (R.F. Schwenker and P.D. Garn editors), Vol. 1, Academic Press, New York, **1969**

7) E.A. Collins, J. Bares, F.W. Billmeyer, jr., *Experiments in Polymer Science*, Wiley, New York, **1973**

8) T. Hatakeyama, F.X. Quinn, *Thermal Analysis: Fundamental and Applications in Polymer Science*, Wiley, New York, **1994**

9) a) H.H. Willard, L.L. Merritt, Jr., A. Dean, *Instrumental Methods of Analysis 5th Ed.*, Van Nostrand, New York, **1974**; b) R.C. Mackenzie; *Talanta* **1969**, *16*, 1227-1230; c) R.C. Mackenzie; *J. Therm. Anal.* **1978**, *13*, 387-392

Appendix C

X-ray diffraction experiments

X-ray scattering techniques are a family of non-destructive analytical techniques which reveal information about the crystallographic structure, chemical composition, and physical properties of materials. These techniques are based on observing the scattered intensity of an X-ray beam hitting a sample as a function of incident and scattered angle, polarization, and wavelength or energy.[1]

C.1 Diffraction mechanism

In a crystal or in a periodic structure is often possible to trace ideal parallel planes that follow closely the system symmetry. These layers could be considered as real thin films and, irradiated with an opportune wavelength, could give rise to phenomena of interference.[2]

As illustrated in figure C.1 (see below), a radiation with wavelength λ, incident with an angle θ (between the plane and the ray) on a system with parallel planes at a distance d (blue line), gives rise to interference because the two reflected beams have two different optical paths. The difference ($\lambda_1+\lambda_2$) could be calculated by geometrical considerations:

$$\lambda_1+\lambda_2 = 2d \sin\theta$$

Considering that a positive interference happens when this distance is equal to a multiple of wavelength λ, we can express the fundamental law of the X-rays diffraction experiments:

$$2d \sin\theta = n\lambda$$

This law is named Bragg law and point out the conditions to have a diffraction signal.[3]

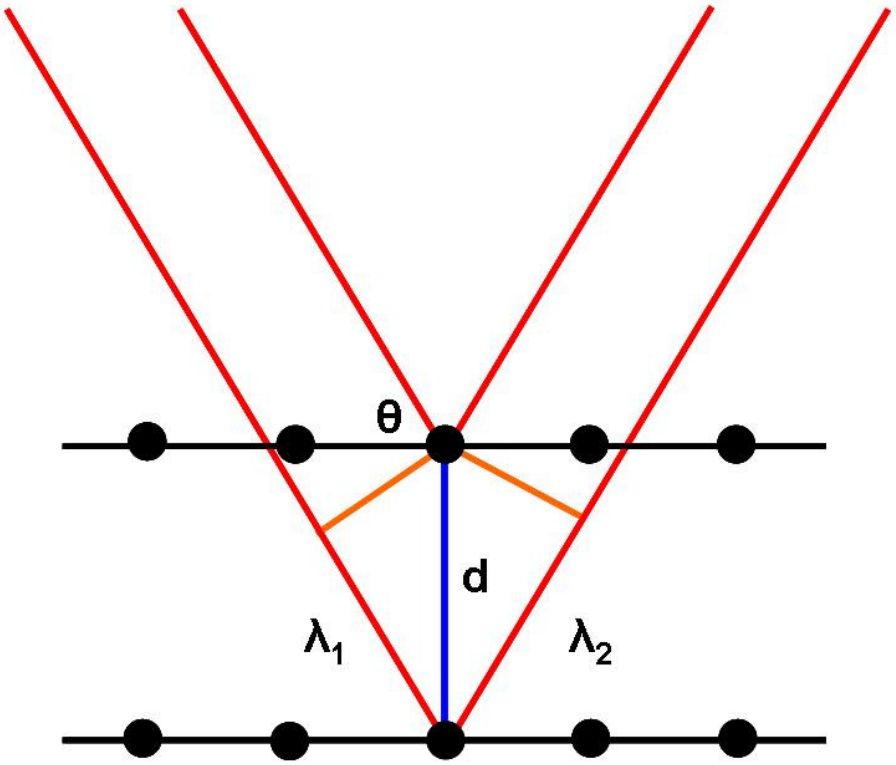

Figure C.1

Schematic representation of the radiation interference in a multilayer system

From a XRD pattern it is possible to calculate the distances in a system and, by these, to reconstruct the structure of the analyzed system.

C.2 Diffraction on single crystals or powders

X-rays diffraction experiments could be performed both on single crystals than on powders.[1,4] The main difference between the two is that diffraction measurements on single crystals are strictly dependent on crystal orientation. In fact, the radiation beam hits different crystal planes with different angles, but the incident angle for a single plane does not change until the crystal or the beam are moved. To perform a complete analysis is so necessary to move the crystal in all possible orientations.

With a powder sample, instead, this problem does not occurs, because single particles are already arranged in a stochastic manner and the X-ray beam hits at the same time all crystallographic planes with all possible incident angles.

C.3 The diffractometer

A diffractometer is principally composed by a X-ray source, a sample vessel and a detector. Generally the X-ray source is a metallic filament heated under vacuum to extract electrons by thermoelectric effect. Extracted electrons are accelerated by a electrical potential and impact on a thin copper plate. Copper atoms are excited by these electrons and emit a specific frequency that corresponds to Cu K radiation (1.5408 Å). The detector is normally a photomultiplier, when the sample vessel depends on the sample type.

Depending on the type of analysis and on the sample nature, these elements are disposed in different geometries, but generally one or more of them are mobile to collect X-ray scattering at different angles. In fact, a XRD pattern represents the intensity of scattered light at different 2θ angles of incidence and, by this, it is possible to relate the single peak (constructive interference) to the corresponding θ angle.

For XRD on powders, the most used geometry is the Bragg-Bentano θ-θ diffractometer, that maintains the sample in horizontal position, while the X-ray source and the detector are disposed at the angle θ respect to the sample, as illustrated in figure C.2. Despite the geometry, angles in diffraction pattern are the same reported in 2θ values because they are calculated from the distance between the incident beam.

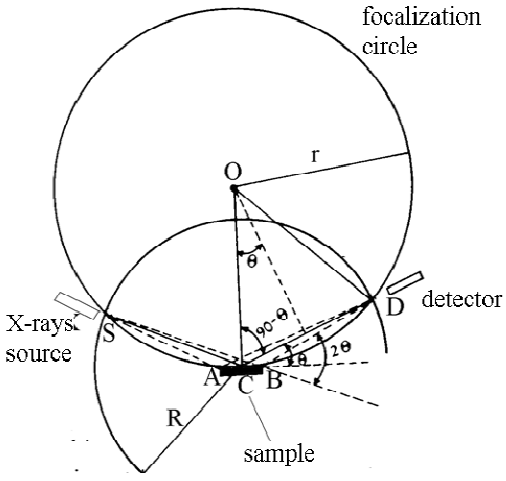

Figure C.2

Scheme of θ-θ Bragg-Bentano diffractometer

In a typical XRD experiments, starting and ending θ angles are set, as well as the angle motion and the waiting time for each step. In fact, diffraction patterns are collected in a defined number of steps, in which the detector counts the number of scattered rays and report it in the final pattern.

C.4 References:

1) C. Giacovazzo, *Fundaments of crystallography*, Oxford University Press, UK, **1992**

2) D. Halliday, R. Resnick, *Fundamental of physics, 2nd edition*, John Wiley & Sons, New York, **1981**

3) C. Kittel, *Introduction to solid state physics*, John Wiley & Sons, New York, **1996**

4) M.F.C. Ladd, R.A. Palmer, *Structure determination by X-ray crystallography*, Plenum, New York, **1985**

Appendix D

ATR and Raman spectroscopic analysis

Spectroscopic techniques are based on the interaction between an electromagnetic radiation and a material sample. During this interaction there is an exchange of energy between the two states, that could be rationalized in mathematical formulae using quantum physic principles. In fact, consequences of light-matter interaction are strictly dependent from the wavelength λ of the radiation and on the nature of the material under analysis, and generally involve rise of vibrational or rotational motions, excitation of atom electrons and emission of electrons or electromagnetic radiations.[1]
There are different spectroscopic techniques and we focus here the attention on two of them that are useful in chemistry and physic to investigate the chemical structure of materials: the Infrared and the Raman spectroscopy experiments.

D.1 Electromagnetic Spectrum

Electromagnetic radiation, and visible light that represents an important part of it, could be considered as an harmonic wave that propagates in a straight motion in the space at the light speed (c).[2] It is composed by electrical and magnetic fields, that are perpendicular and in phase between them. An electromagnetic radiation is characterized by a defined wavelength λ, that represents the distance between two consecutive maximum in the sinusoidal wave, and by a frequency ν, that represents the number of maximum that pass in a same place in the unit of time. These two parameter are related with the wave rate by:

$$c = \lambda \nu$$

The energy of the electromagnetic wave is:

$$E = h\nu$$

where h is the Plank's constant. In spectroscopic experiments, moreover, could be useful to put in direct relationship the energy and the wavelength of a radiation:

$$E = \frac{hc}{\lambda}$$

and to introduce a parameter, the wavenumber $\bar{\nu}$, that is expressed:

$$\bar{\nu} = \frac{1}{\lambda}$$

By consequence, the wave energy can be expressed:

$$E = hc\bar{\nu}$$

The electromagnetic spectrum could be devised in different regions on the base of the radiation wavelength, as illustrated in figure D.1 (see below)
Usually, each region is associated to a specific type of spectroscopic analysis:

- **Radio waves** are used in NMR experiments
- **Microwaves** are used for electron resonance or rotational spectra
- **Infra red** is used for vibrational spectroscopy
- **Visible and Ultra-Violet** are used to investigate electronic transitions
- **X-rays** are used for diffraction experiments

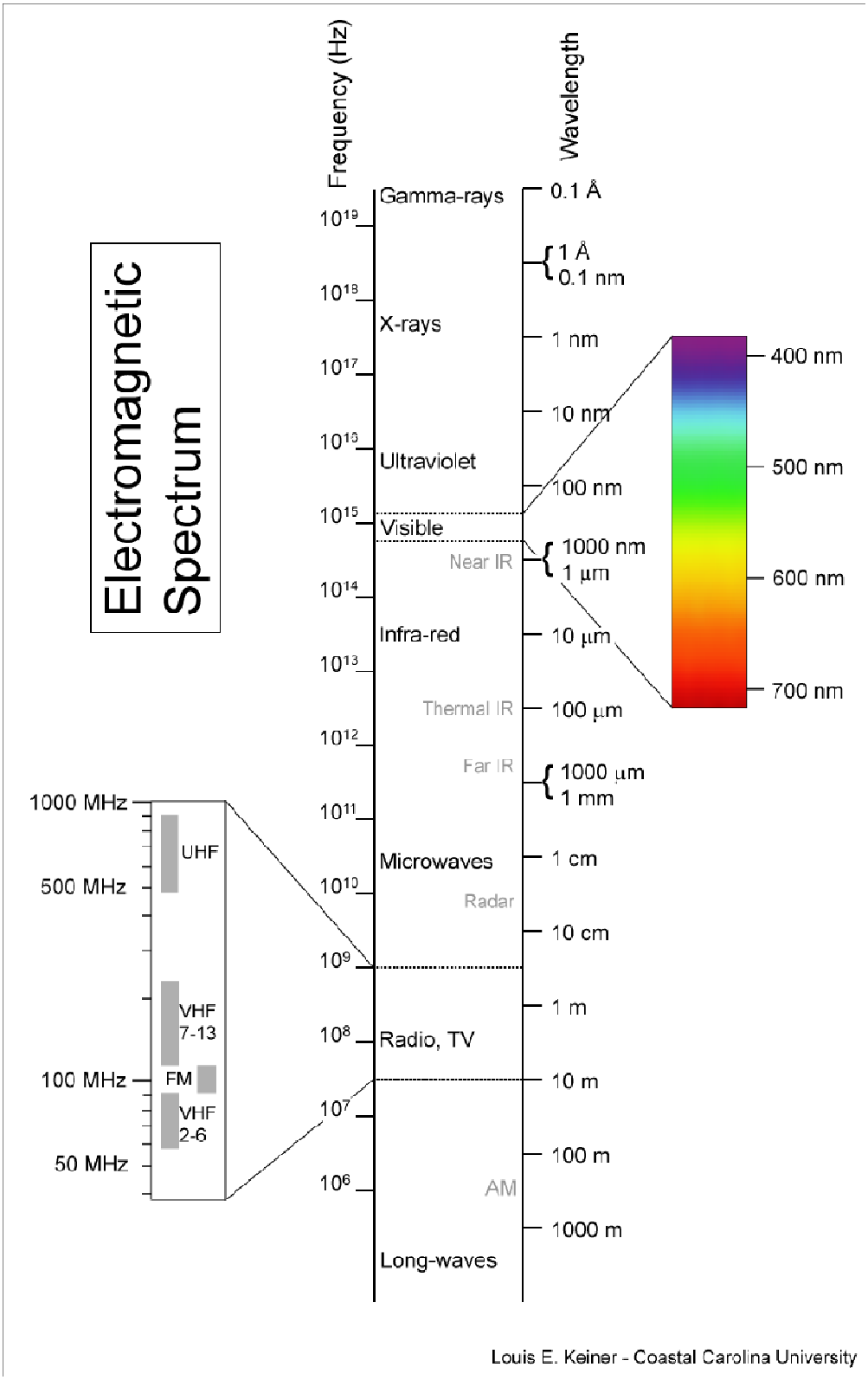

Figure D.1

Division of spectral ranges by wavelength and frequency of the radiation

D.2 Molecular rotations and vibrations

Rotational and vibrational motion of molecules could be easily described by quantum physic principles using some approximations. Here below we will only discuss about those formulae that are necessaries for IR and Raman spectroscopy, for a more detailed discussion we will remand to specific books of quantum mechanic.[3]

The energy of a body rotating around an axis is:

$$E = \frac{1}{2} I_a \omega_a^2$$

where ω_a is the angular rate ($rad*s^{-1}$) and I_a the inertia momentum referred to that specific axis. For a body free to rotate around three axis, the totals energy is:

$$E = \frac{1}{2} I_a \omega_a^2 + \frac{1}{2} I_b \omega_b^2 + \frac{1}{2} I_c \omega_c^2$$

Introducing the classical angular moment ($J = I\omega$), the total energy becomes:

$$E = \frac{J_a^2}{2I_a} + \frac{J_b^2}{2I_b} + \frac{J_c^2}{2I_c}$$

This is a general formula. In case of symmetric molecules it could be simplified because two or more I become equal. In the simplest case, a spherical rotor, the three are the same and the total energy is:

$$E = \frac{J_a^2 + J_b^2 + J_c^2}{2I} = \frac{J^2}{2I}$$

substituting the quantistic angular moment:

$$J^2 = J(J+1)\hbar^2$$

thus, the final energy is:

$$E = J(J+1)\frac{\hbar^2}{2I} \text{ with J=0,1,2,…}$$

During the discussion, we have assumed that molecular bonding are rigid to simplify the calculation on the inertia momentum, however distances between atoms change around a medium value that is the distance of minimum energy. Atomic bonding motion are classified as *vibrational* motions.

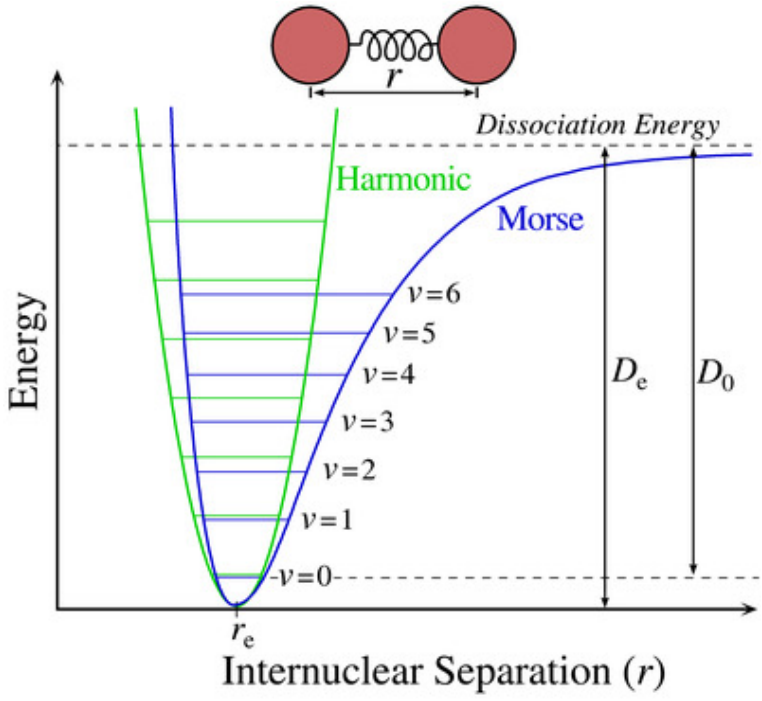

Figure D.2

Interatomic potential (Morse model) confronted with Harmonic potential

As illustrated in figure D.2, the interatomic potential near the equilibrium distance could be approximated to an harmonic potential, that could be expressed as:

$$V = \tfrac{1}{2}\, k(r-r_e)^2$$

Where r_e is the equilibrium distance an k the bond strength. Using this potential, it is possible to calculate energy levels, that result:

$$E_v = (v + \tfrac{1}{2})\hbar\omega, \text{ with } \omega = \sqrt{\frac{k}{\mu}} \text{ and } v=0,1,2,\ldots$$

where μ is the effective mass calculated as follow:

$$\frac{1}{\mu} = \frac{1}{m_1} + \frac{1}{m_2}$$

Interaction of matter with radiation could bring to an electron excitation, that has as consequence the passage of the electron to an higher rotational and/or vibrational energy level. For selection rules, this passage could be of only one level, so that ΔJ and Δν could be only ±1. IR and Raman spectroscopy are used to investigate overall vibrational motions, that could be related to the atom mass and bond strength giving the possibility to identify different chemical groups and to reconstruct material structure.[4]

Before to start to descript the two techniques, it could be useful to explain how much transitions a molecule could show. Rotational and vibrational modes are strictly related to the molecular degrees of freedom. A molecule with N atoms has 3 degrees of freedom for each atom, so 3N. Among them, 3 degrees are related to translational motions in the three spatial directions, while other 3 degrees are related to rotational modes. By this, a non-linear molecule has 3N-6 degrees of freedom, that correspond to 3N-6 vibrational modes. Linear molecules, instead, have only two rotational modes (that around molecular axis is not considered), so they have 3N-5 vibrational modes.

The most common vibrational modes include: molecular stretching (symmetric or asymmetric) in which bond length change, and molecular bending where there is a change in bond angles.

Depending on the molecular symmetry, these modes could be IR or Raman active.

D.3 IR spectroscopy

Infrared region is the portion of electromagnetic spectrum included between 10 and 14000 cm^{-1} and it is divided in three main zones: FAR-infrared, near microwave region and approximately 400–10 cm^{-1} (1000–30 μm), MID-infrared, approximately 4000–400 cm^{-1} (30–2.5 μm), and NEAR-infrared, approximately 14000–4000 cm^{-1} (2.5–0.8 μm).[2] For IR spectroscopy analysis mid-infrared wavelength are generally used.[1]

In this portion of electromagnetic spectrum, in fact, resound a great number on vibrational modes of most common groups of organic chemistry, such as hydrocarbons, double or triple bonds and hydrogen atoms bonded to oxygen or nitrogen, as reported in figure D.3.

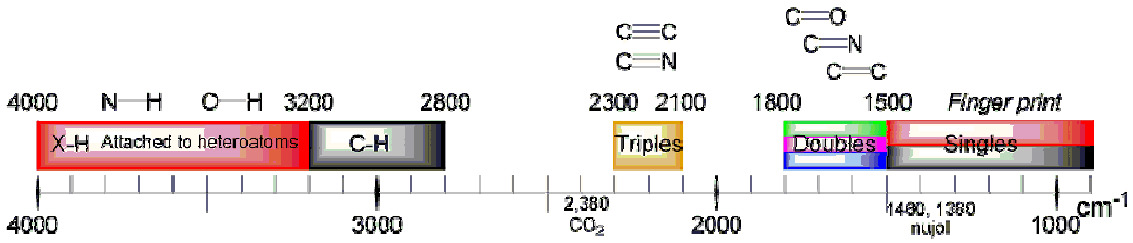

Figure D.3

Infrared resounding intervals of common bonds in organic molecules

To be IR active, a vibrational mode must change the dipolar moment of the molecule. It is not necessary that the molecule has already a natural dipole, it could be generated during the motion and disappear during relaxation. Symmetrical stretching of homonuclear molecules cannot be detected by IR spectroscopy.

During an IR experiment, the sample is irradiated by a monochromatic radiation that changes the wavelength during the experiment.[5,6] A detector placed back the sample analyzes the not-absorbed frequencies and, at the end of the experiment, reports the sample absorbance in function of the wavenumber. Absorbance (A) is calculated comparing the intensity of the starting beam (I_0) versus the intensity collected from the sample (I):[4]

$$A = -Log\frac{I}{I_0}$$

Absorbance also depends from the molar concentration of the analyzed specie [J], from the molar absorbent coefficient ε and from the sample length l:

$$A = \varepsilon[J]l$$

To measure the intensity ratio with precision, the starting beam is split in two and the two beams are reflected on the sample and on a reference (generally an empty cell to direct eliminate the cell absorption) and so re-directed in the detector for a comparison.
Monochromatic radiation is obtained using a monochromator, but this causes also a loss of beam intensity.
Otherwise, a spectrophotometer at Fourier transform (FTIR) could be used.[7] This instrument uses an interferometer that generates an interferogram using a beam splitter and a mobile mirror to change the optical path of the split beams and to generate interference phenomena. The collected interferogram is then compared with that obtained once placed the sample between the interferometer and the detector. Using the Fourier transform, we obtain the IR spectrum. With this method it is possible to collect the spectrum in relative short time, on a wider spectral range and with a greater precision on the frequency value.

D.4 ATR infrared spectroscopy

One of the great disadvantage of IR spectroscopy is the sample preparation. In fact, the material must be enough thin, to consent the passage of the infrared beam trough itself, dispersed in a second medium, in the case of powders, or enough concentrated in the case of solutions.[8]
Attenuated total reflectance (ATR) is a particular technique, associated to infrared spectroscopy, which enables samples to be examined directly in the solid or liquid state without further preparation. ATR exploits a property of total internal reflection called the evanescent wave. A beam of infrared light passes through the ATR crystal in such a way that it reflects at least once on the internal surface in contact with the sample. This reflection forms the evanescent wave which extends into the sample, typically by a few micrometres. The beam is then collected by a detector as it exits the crystal.
This evanescent effect works best if the crystal is made of an optical material with a higher refractive index than the sample under study, to obtain a correct total reflection. In the case of a liquid sample, pouring a shallow amount over the surface of the crystal is sufficient. In the case of a solid sample, it is pressed into direct contact with the crystal. Because the evanescent wave into the solid sample is improved with a more

intimate contact, solid samples are usually firmly clamped against the ATR crystal, so that trapped air is not the medium through which the evanescent wave travels, as that would distort the results. Typical materials for ATR crystals include germanium, KRS-5 and zinc selenide, while silicon is ideal for use in the Far-infrared region of the electromagnetic spectrum. The excellent mechanical properties of diamond make it an ideal material for ATR, particularly when studying very hard solids.
Concerning obtained spectra and data process, ATR is the same as IR spectroscopy.

D.5 Raman spectroscopy

Raman spectroscopy relies on inelastic scattering, or Raman scattering, of monochromatic light, usually from a laser in the visible, near infrared, or near ultraviolet range.[8] The laser light interacts with phonons or other excitations in the system, resulting in the energy of the laser photons being shifted up or down. The shift in energy gives information about the phonon modes in the system. It is a technique complementary to IR spectroscopy, because vibrational modes that are IR inactive are Raman active and vice versa.[6,10]
The Raman effect occurs when radiation alight upon a molecule and interacts with the electron cloud and the bonds of that molecule. For the spontaneous Raman effect, a photon excites the molecule from the ground state to a virtual energy state. When the molecule emits a photon and returns to the ground state, it returns to a different rotational or vibrational state as illustrated in figure D.4 (see below). The difference in energy between the original state and this new state leads to a shift in the emitted photon frequency away from the excitation wavelength.
If the final state of the molecule is more energetic than the initial state, then the emitted photon will be shifted to a lower frequency in order to remain balanced for the total energy of the system. This shift in frequency is designated as a anti-Stokes shift. If the final state is less energetic than the initial state, then the emitted photon will be shifted to a higher frequency, and this is designated as an Stokes shift. Raman scattering is an example of inelastic scattering because of the energy transfer between the photons and the molecules during their interaction.

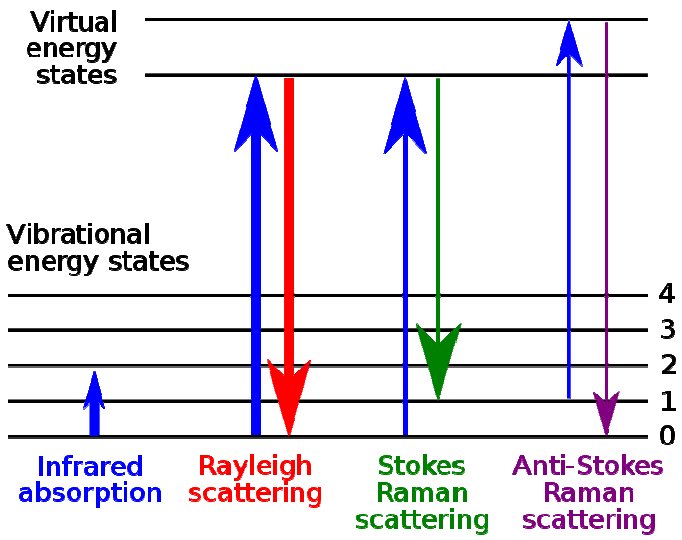

Figure D.4

Schematic representation of electronic transitions for IR and Raman spectroscopy

In figure are also reported Infrared adsorption and Rayleight scattering. This happens when there is not a coupling between the incident photon and a material phonon, so the emitted photon do not change energy.

A change in the molecular polarization potential — or amount of deformation of the electron cloud — with respect to the vibrational coordinate is required for a molecule to exhibit a Raman effect. The amount of the polarizability change will determine the Raman scattering intensity. The pattern of shifted frequencies is determined by the rotational and vibrational states of the sample.

Typically, a sample is irradiated with a laser beam. Light from the illuminated spot is collected with a lens and sent through a monochromator. Wavelengths close to the laser line, due to elastic Rayleigh scattering, are filtered out while the rest of the collected light is dispersed onto a detector.

Raman spectroscopy offers several advantages for microscopic analysis. Since it is a scattering technique, specimens do not need to be fixed or sectioned. Raman spectra can be collected from a very small volume (< 1 µm in diameter); these spectra allow the identification of species present in that volume. Water does not generally interfere with Raman spectral analysis. Thus, Raman spectroscopy is suitable for the microscopic examination of minerals, materials such as polymers and ceramics, cells and proteins. A

Raman microscope begins with a standard optical microscope, and adds an excitation laser, a monochromator, and a sensitive detector (such as a charge-coupled device (CCD), or photomultiplier tube (PMT)). FT-Raman has also been used with microscopes.

D.6 References:

1) J.M. Hollas, *Modern spectroscopy*, Wiley, New York, **1991**

2) D. Halliday, R. Resnick, *Fundamental of physics, 2nd edition*, John Wiley & Sons, New York, **1981**

3) R. Eisberg, R. Resnick, *Quantum physics of atoms, molecules, solids, nuclei and Particles 2nd edition*, John Wiley & Sons, New York, **1985**

4) P.W. Atkins, *Physical Chemistry 5th edition*, Oxford University Press, UK, **1994**

5) H. Günzler, H.U. Gremlich, *IR spectroscopy, an introduction*, Wiley-VHC, Germany, **2002**

6) J.W. Robinson, *Handbook of spectroscopy, Vol. II*, CRC press, US, **1974**

7) W.D. Perkins; *J. Chem. Educ.* **1987**, *64*, A269-A271

8) a) N.J. Harrick, *Internal reflection spectroscopy*, John Wiley & Sons, New York, **1967**; b) J.A. Pawlack, G. Fricke, H.A. Szymanski; *Progress in infrared spectroscopy* **1967**, *3*, 39-54

9) D.J. Gardinier, *Pratical Raman Spectroscopy*, Springer-Verlag, **1989**

10) P.W. Atkins, R.S. Friedman, *Molecular quantum mechanics 3rd edition*, Oxford University Press, UK, **1997**

Appendix E

High resolution NMR techniques for solids

Nuclear magnetic resonance is a sophisticated tool for the investigation of organic and inorganic solids on atomic and molecular level.

Nanostructured adducts and nanoporous materials contain groups of atoms or molecules arranged in nanophases showing intermediate degrees of order and a variety of motional states. In addition, polymorphic behavior is frequently observed. In this context magnetic resonance is able to measure some parameters, which can be exploited for an exhaustive description of many different types of materials.

In recent years, the field of solid-state NMR has enjoyed rapid technological and methodological developments. Much of the success of the solid-state NMR spectroscopy is due to the evolution of a wide variety of techniques for studying internuclear distances, anisotropy, torsion angles, atomic orientations, phase structure, molecular dynamics, and exchange processes.

NMR is a method of choice when mixtures of compounds and static or dynamic disorder are present. The signal multiplicity and internal ratios can identify the structures of pure crystalline phases. Furthermore, high speed magic angle spinning and multidimensional NMR, that can provide high resolution both on carbon and hydrogen domain without isotopic enrichment, are sensitive to phase structure and to local interaction between nuclei. New approaches for obtaining high resolution two-dimensional (2D) ^{1}H-^{13}C correlation experiments have recently developed. The dipolar coupling between two nuclei has an inverse cubed dependence on the internuclear separation, and, thus, solid-state NMR experiments which provide access to this interaction can be used to determine specific distance constraints.

On the other hand, by an analysis of one-dimensional experiments, fast dynamic processes (10^{-4} to 10^{-7} s) can be quantitatively measured, some relaxation times are sensitive to the kHz regime, while two dimensional exchange experiments allow the investigation of slower motions (up to seconds).

In this chapter, our aim is to describe the most common spin-interactions in the solid-state and, secondly, to discuss the methods that have been developed to overcome the negative effect of some of these interactions and thus to produce high resolution spectra in solids.[1]

E.1 Spin interactions in solids

A general Hamiltonian for the interactions experienced by a nucleus of spin *I* in the solid-state may thus be written as in equation:

$$H = H_Z + H_{RF} + H_D + H_{CS} + H_Q + H_J + H_{SR} \qquad [E.1]$$

where:

H_Z is the Zeeman interaction which account for the coupling of nuclear spins with the external magnetic field $\mathbf{B_0}$.

H_{RF} represents the coupling of nuclear spins with the applied *rf* field $\mathbf{B_1}$.

H_D is the dipole-dipole interaction of nuclear spins with each other via their magnetic dipole moments.

H_{CS} describes the chemical shift associated with the electronic screening of nuclei, which is generally anisotropic.

H_Q accounts the coupling between nuclear spins with quadrupole moments (I>½) and electric field gradients.

H_J describes the indirect electron-coupled nuclear spin interaction.

H_{SR} is the coupling between nuclear spins and the magnetic moment associated with molecular angular momentum, the spin-rotation interaction.

The component Hamiltonians fall into two general categories. H_Z and H_{RF}, for a given nucleus, depend only on the external parameters such as the strength of $\mathbf{B_0}$ and $\mathbf{B_1}$ and are thus referred to as *external Hamiltonians:* H_Z establishes the resonance condition whereas H_{RF} describes the coupling of the *rf* field to the spins.

The remaining terms are in a second category of *internal Hamiltonians* since they depend on internal interactions and contain the molecular information of interest.

For spin ½ nuclei, the major differences between liquids and solids involve magnetic dipolar interactions (which average to zero in liquids) and the anisotropy in chemical shielding (which averages to a single value in liquids). For nuclei with I>½, the interaction between the nuclear electric quadrupole moment and the gradient in the electric field caused by surrounding electrons and ions is an important factor in solids. Usually it dominates chemical shift and magnetic dipolar interactions, and in some instances it competes with the Zeeman interaction between the nuclear magnetic moment and the applied magnetic field. Except for some quadrupolar effects, all the interaction mentioned are small compared with Zeeman interaction between the nuclear spins ant the applied magnetic field.

In the next section the origin of the heteronuclear and homonuclear dipolar couplings, and the chemical shift anisotropy (CSA) are examined.

E.2 Heteronuclear dipolar coupling

The heteronuclear dipolar coupling arises from an interaction between the nuclear magnetic moments of two different nuclear spins (by convention, nuclear spins are indicated as *I* for "abundant" spins, for example, that of the protons, and *S* for "rare" spins such as that of ^{13}C or ^{15}N).

The degree to which spin *I* affects the magnetic field felt by spin *S* is characterized by the strength of the heteronuclear dipolar coupling, which is represented by the Hamiltonian in Equation E.2:

$$H_{IS} = -d\left(3cos^2\theta - 1\right) I_z S_z \qquad [E.2]$$

The parameter *d* is the dipolar coupling constant (Eq. E.3):

$$d = \left(\frac{\mu_0}{4\pi}\right)\frac{\hbar\gamma_1\gamma_S}{r_{IS}^3} \qquad [E.3]$$

where r_{IS} = internuclear distance; μ_0 = permeability of free space; γ_1 and γ_S = gyromagnetic ratios of the *I* and *S* spins; I_Z and S_Z = z components of the nuclear spin angular momentum operators *I* and *S*. The angle θ describes the orientation of the internuclear vector with respect to the orientation of the external magnetic field (Figure E.1).

Because the magnitude of the coupling between two nuclear spins depends on the internuclear distance, the dipolar coupling is *through-space* interaction and also occurs between nuclei in different molecules.

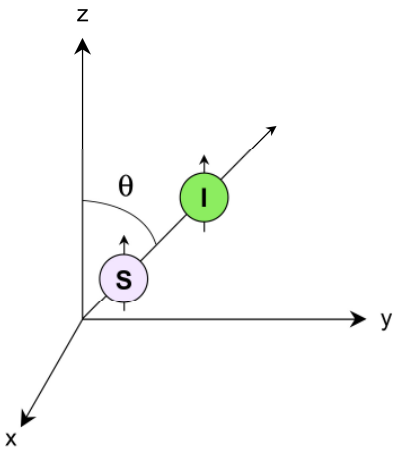

Figure E.1

θ is the angle between ^{1}H-^{13}C bond vector and the direction of the external magnetic field $\mathbf{B_0}$

The dipolar coupling is dependent on the orientation, which is evident from the $\left(3cos^2\theta - 1\right)$ term in the dipolar Hamiltonian. This means that for two nuclei of spins *I* and *S*, which are separated by a fixed distance, the magnitude of the dipolar interaction will be greater for particular orientations of the *I* - *S* internuclear vector.

The reorientation time of a molecule in solution in much faster than the time the dipolar coupling would need to evolve, averaging to zero the $\left(3cos^2\theta - 1\right)$ term of the heteronuclear dipolar coupling Hamiltonian.

In a polycrystalline powder sample, in which the crystallites are oriented in all the possible directions, the presence of a heteronuclear dipolar coupling produces a pattern which is the envelope of spectra from all possible values of θ, each weighted according the probability of its occurrence (Figure E.2).

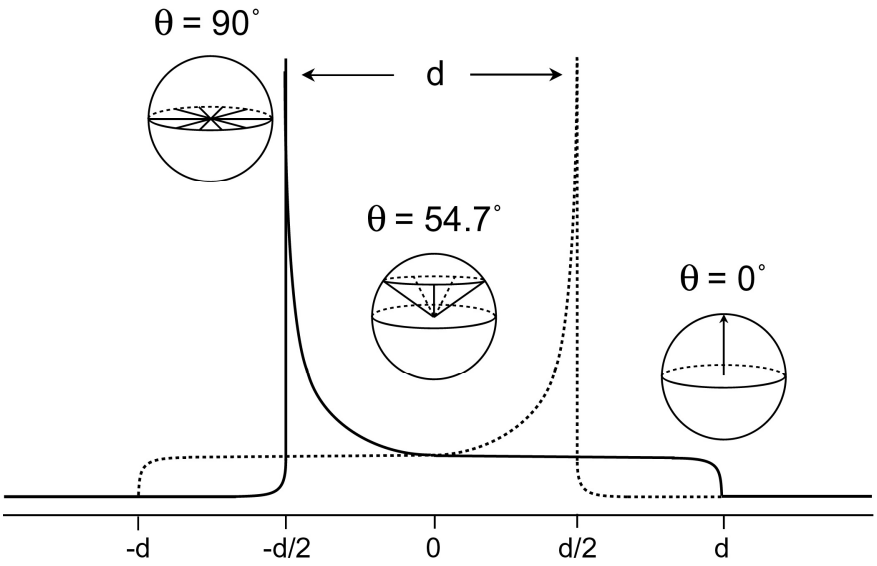

Figure E.2

Dipolar Pake pattern ("Pake doublet") for two coupled spins in a powder sample; the two signals correspond to a positive (parallel spins) and a negative (antiparallel spins) value of the $I_z S_z$ component The points with maximum intensity correspond to θ = 90°; a perpendicular orientation to $\mathbf{B_0}$ of is adopted by a majority of the crystals. The smallest number of crystals has the internuclear vector parallel to $\mathbf{B_0}$. At the magic angle of θ = 54.74°, the dipolar coupling is zero. The spacing between the points of maximum intensity is equal to the dipolar coupling constant d

The two complementary patterns, named the "Pake doublet", arise from energy differences determined by H_{IS}, depending on the parallel or antiparallel alignment of the *I* spins with the respect to *S* spins.

The singular peak of the Pake pattern corresponds to crystallites for which the *I* - *S* internuclear vector lies perpendicular to the magnetic field. The low edge of the pattern is associated to the relatively few crystallites whose *I* - *S* internuclear vectors are parallel to the external field. There is only one orientation of *I* - *S* vector at which the resonance frequency of the crystallites is independent by the heteronuclear dipolar coupling: this is the case at the "magic angle" $\theta = 54.74°$ ($(3cos^2\theta - 1 = 0)$).

E.3 Homonuclear dipolar coupling

The homonuclear dipolar coupling is a result of an interaction between the magnetic fields produced by like neighboring nuclear spins, such as two ^{13}C nuclei. Whereas two unlike nuclear spins (heteronuclei) have very different resonance frequencies (for example when ^{1}H resonate at 300.13 MHz, ^{13}C spins resonate at 75.5 MHz), two like spins are able to undergo an energy conserving "flip-flop" transition in which one spin flips up while the other spin flips down. To account for the "flip-flop" interaction, an additional term, normally ineffective in the heteronuclear case, is added to give the homonuclear dipolar Hamiltonian.

This term provides for an energy-conserving exchange of spin angular momentum between any two coupled spins whose resonance frequencies overlap. When two like spins have very different chemical shifts so that there is no overlap between their resonance frequencies, there can be no energy-conserving transition; in the latter case, the homonuclear dipolar Hamiltonian reverts to the form of the heteronuclear dipolar Hamiltonian shown in Equation E.2.

E.4 High resolution techniques for solids

E.4.1 Magic Angle Spinning (MAS)

The fast isotropic tumbling of molecules in the liquid state leads to the averaging to zero of the line broadening due to the dipolar coupling as well as the other anisotropic interactions. There is an experimental technique, which, under many circumstances, has a similar effect for solid samples: *Magic Angle Spinning* (MAS).

Anisotropic interactions such as the dipolar coupling between pair of nuclei, the CSA, and the first order quadrupolar interaction all have an orientation dependence that can be represented by a second rank tensor. For such interactions, a physical rotation of the macroscopic sample around an axis inclined at an angle of 54.74°, the so-called magic angle, to the external magnetic field suffices (Figure E.3). This method focuses on the geometric part of the Hamiltonians, namely the term $\left(3\cos^2\theta - 1\right)$ (Eq. E.2). This term vanishes if $\cos^2\theta = 1/3$, which implies that $\theta = 54.74°$.

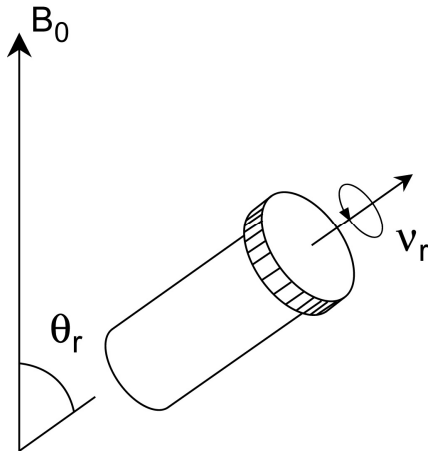

Figure E.3

Mechanical spinning with air-driven rotor around an axis inclined at θ = 54.74° to the external field

The sample rotation around a single axis leads to the components perpendicular to the rotation axis being zero on average, and only the component parallel to the rotation axis remains nonzero on average. Thus, in a powdered sample, for any orientation of, e.g., the internuclear vector for a pair of dipolar-coupled spins, rotation around an axis yields to an "average orientation" parallel to the axis of rotation. Under MAS, this parallel component has an anisotropic frequency equal to zero for all cases, and the anisotropic broadening is averaged to zero for all the crystalline orientations. In this technique the spinning speed plays an important role: increasing the MAS frequency the lines of the spectra become narrower. The difference between the effects of MAS on CSA and homonuclear decoupling is explained in a paper of Waugh.[2]

E.4.2 Heteronuclear dipolar decoupling

Heteronuclear interactions, such as couplings between observed nuclei and abundant protons, are suppressed with different spin-decoupling techniques.

A typical coupling constant for a ^{1}H-^{13}C pair (at a distance of 1Å) is approximately 30 kHz. However, close inspection of the Hamiltonian in Equation E.3 suggests two possible means of eliminating the interaction to give narrower lines. One approach is to take advantage of the fact that the dipolar coupling is zero when the internuclear vector is oriented at the magic angle with the respect to the magnetic field.

The second method that can be used to eliminate the effect of the ^{1}H nuclei on the ^{13}C spectrum is to manipulate the proton spins in such a way that their effect on the ^{13}C nucleus, when averaged over time, is equal to zero.

A proton whose spin is parallel to the external field ("spin-up") produces a shift in the resonance frequency of a ^{13}C nucleus that is opposite to the shift produced by a proton whose spin is antiparallel to the external field ("spin down"). By constantly applying radio-frequency (RF) pulses that rotate the proton nuclear spins between their "spin-up" and "spin-down" states, the average orientation of the ^{1}H magnetic moments tend to zero, and the dipolar coupling is essentially averaged away. This continuous-wave (CW) spin decoupling is widely used to eliminate heteronuclear couplings in solid state NMR. Recently, in order to improve upon CW decoupling in ordinary diamagnetic solids, the two pulse phase-modulation (TPPM) decoupling[3] approach has been introduced.

E.4.3 Homonuclear dipolar decoupling

For low-γ nuclei such as ^{13}C and ^{15}N, the homonuclear dipolar coupling can be often removed by MAS, as even for directly bonded ^{13}C nuclei the dipolar coupling constant *d* does not exceed 5kHz.

The homonuclear dipolar interaction has perhaps the largest impact on ^{1}H solid-state NMR spectroscopy, as the strength of the homonuclear coupling between two proton spins can routinely approach 100 kHz because their large gyromagnetic ratio. The problem of strong ^{1}H-^{1}H dipolar coupling is enhanced by the high abundance of protons in most organic systems, which results in a network of strongly coupled spins that are very difficult to decouple from each other.

Fast magic angle (up to 35-50kHz) is not the only means by which the line narrowing can be achieved in ^{1}H solid-state NMR. One of the alternative approaches for obtaining a good proton homonuclear decoupling with fast MAS applies the Lee-Goldburg (LG) irradiation. A description of this decoupling sequence will be illustrated in the section E.6.1 dedicated to 2D Hetcor Experiment.

E.4.4 Cross Polarization

Cross-polarization (CP) from abundant spins *I* to dilute spins *S* is a double-resonance technique which overcomes two common problems in the NMR of solids. The first derives from the fact that solid state NMR of dilute nuclei, such as ^{13}C, ^{29}Si and ^{15}N (isotopic abundance of 1.1%, 4.7% and 0.03% respectively), suffers from low sensitivity, particularly when these nuclei have a low gyromagnetic ratio. The second problem concerns the fact that the spin lattice relaxation times of dilute spin ½ nuclei are usually long (tens of seconds for ^{13}C in organic powders and minutes for ^{29}Si in framework silicates). This because strong homonuclear dipolar interactions, which can promote relaxation transitions, are largely absent, and only the much weaker heteronuclear dipolar interactions remain. The long spin-lattice relaxation time means that long delays must be left between consecutive scans. When several thousand scans are required to lower the noise to a desirable level, the spectra take a very long time to acquire.

Cross-polarization technique exploits the fact that in the solid state the dilute and abundant nuclei are in close proximity and are thus coupled via magnetic dipolar interaction.

For homonuclear spins the magnetization can be exchanged through mutual energy-conserving spin flips. For heteronuclear pairs such as ^{1}H and ^{13}C the exchange of magnetization can be driven externally by the application of RF fields.

A particularly effective approach for establishing a dipolar contact between two different spin systems, *I* and *S*, is the method of Hartmann-Hahn.[4]

By applying two simultaneous continuous RF fields, one tuned to the *I* spins the other to the *S* spins, both the *I* and the *S* spins can be rotated independently around a particular axis at rates determined by the amplitudes of the two applied fields. When the rotation frequencies of *I* and *S* are equal:

$$\gamma_I B_{1I} = \gamma_S B_{1S} \qquad [E.4]$$

an energy-conserving dipolar contact between the two spin systems is created. It is through this dipolar contact that the polarization is transferred between the *I* and *S* spins.

The process of CP exploit the tendency of the magnetization to flow from highly polarized nuclei to nuclei with lower polarizations when the two are brought into contact, similar to the heat flow from a hot object to a cold object when the two are in thermal contact.

The Hartmann-Hahn match, $\gamma_I B_{1I} = \gamma_S B_{1S}$, brings the subsystems *I* and *S* to thermal contact, which enable the flow of energy and the concomitant polarization transfer to occur. During cross-polarization the hot dilute subsystem *S* is cooled via thermal contact with the cool reservoir of the abundant spins *I*. At the same time, the subsystems *I* and *S* are also in contact with the lattice through the relaxation processes in the rotating frame, governed by the relaxation time constants $T_{1\rho}(I)$ and $T_{1\rho}(S)$, respectively. The overall process proceeds over a contact time *t*. (Figure E.4).

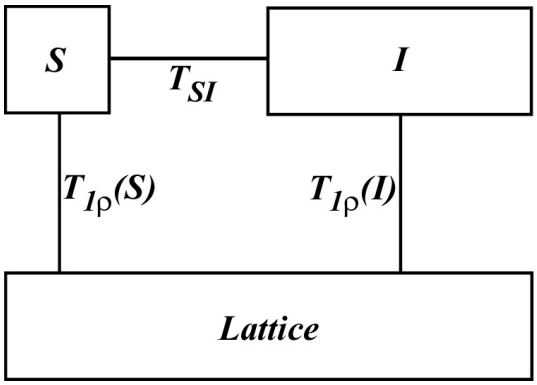

Figure E.4

Block diagram showing the lattice, the I and S reservoirs, and the interaction between them

E.5 ^{29}Si NMR

The ^{29}Si solid state NMR spectroscopy is a very useful technique to study the condensation of siloxane units and thus the structure of silica, silicate and organo-silica compounds. They are classified according to the number of oxygen atoms that are grouped around the silicon core. The silicon atom can form one to four siloxane bridges whereby mono-, di-, tri- and tetrasubstitution is named with the letters M, D, T, and Q respectively. Each letter has also a number at apex, indicating how many of the oxygen atoms, linked to the silicon, are hydroxyl groups.

Because of the different chemical environment, each type of silicon shows a typical peak in a specific range of ppm (Figure E.5). Furthermore, applying MAS or CPMAS techniques it is possible to quantify them or highlight the signals of those silicon atoms closer to the surface.

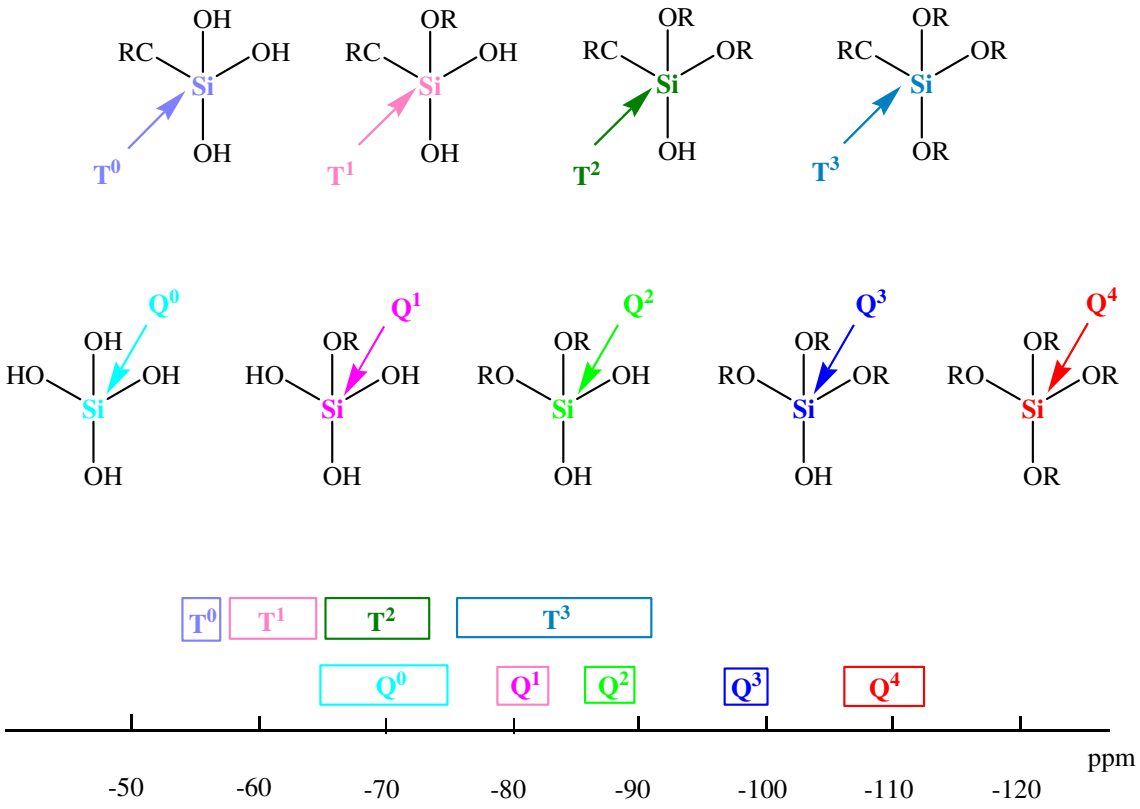

Figure E.5

T^n and Q^n atoms with the different range of chemical shift

E.6 2D NMR spectroscopy

Although many different two-dimensional (2D) NMR techniques have been proposed in literature, most of these experiments can be considered as variations on a rather small number of basic approaches.[5]

For a typical 2D experiment four time intervals can be distinguished, as shown in figure E.6: a preparation period (τ_p), an evolution period (t_1), a mixing period (τ_m), and a detection period (t_2).

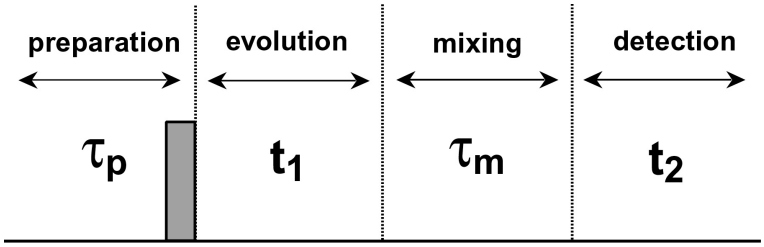

Figure E.6

Schematic representation of a basic two-dimensional NMR experiment in terms of four periods: preparation, τp; evolution, t_1; mixing, τ_m; detection, t_2. For a given experiment, τp e τ_m are usually fixed periods, while t_1 and t_2 are variable time periods

First, the magnetization is prepared in a state appropriate to whatever properties are to be detected in the indirect dimension. This step causes the magnetization **M** to be rotated in the plane xy, often by a simple 90° pulse but occasionally by a more complex pulse sequence. Next, the magnetization is allowed to evolve freely during the time t_1 under a specific NMR Hamiltonian. The period τ_m gives nuclear magnetizations in the xy plane an opportunity to interact or to "mix" their wave functions. As with the initial preparation period, the nature of the mixing period depends largely on the spectrum desired. In heteronuclear experiments, it is often necessary to transfer the magnetization from one set of spins to another. For instance, in an experiment correlating ^{1}H and ^{13}C chemical shifts, the mixing period might involve CP from ^{1}H to the ^{13}C spins. Finally, the resulting magnetization is detected in the direct dimension t_2, as usual in a one-dimension experiment.

This procedure is then repeated a large number of times, with different durations of the evolution period t_1, keeping all the other settings constant. For each value of t_1, the signal that is acquired during t_2 is digitized and stored in computer memory. Upon completion of the entire 2D experiment, a data matrix representing the two-dimensional time domain signals (t_1, t_2) is available. By performing a Fourier transform in both dimensions t_1 and t_2 (obtaining F_1 and F_2 frequencies dimensions), a 2D spectrum containing a single pick is produced which correlates the interactions detected in the indirect dimension t_1 with the interactions detected in the direct dimension t_2.

A nuclear spin whose precession frequency is the same during the evolution and acquisition periods yields a single resonance on the diagonal of the (F1, F2) plot; several *noninteracting* nuclei in the sample provide separate resonances along the

diagonal. In general, 2D experiments are designed to provide useful information on the interaction of nuclear spins during the mixing time (τ_m). When such interaction occurs, the magnetization may be transferred from one nucleus to another, thus introducing additional modulation frequencies in the interferograms and generating off-diagonals peaks in the 2D spectrum (Figure E.7).

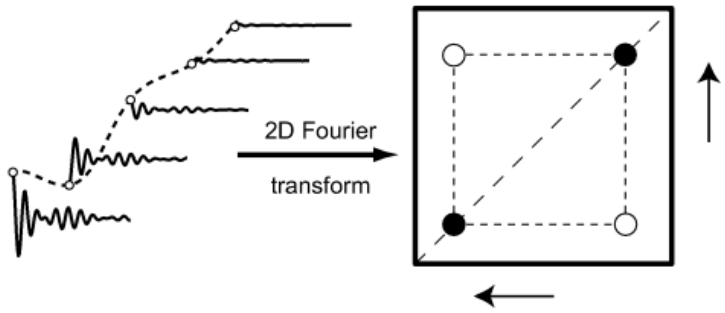

Figure E.7

Schematic illustration of a 2D spectrum represented as a contour plot. The off-diagonal peaks indicate an interaction of nuclear spins during τ_m

E.6.1 Heteronuclear correlation spectroscopy

Phase-Modulated Lee-Goldburg (PMLG) heteronuclear ^{1}H – ^{13}C correlation (HETCOR) experiment coupled with fast magic angle spinning (MAS) allows the registration of 2D spectra with high resolution both in the proton and carbon dimension.[6-8] Fast MAS (15 kHz spinning speed) averages the chemical shift anisotropy (CSA) of ^{13}C nuclei and practically reduces to zero the spinning side bands, dramatically decreasing the complexity of the carbon spectrum, especially in systems containing carbons with large CSA as aromatic carbons. Narrow proton resonances, with line widths in the order of 1 - 2 ppm, are obtained with homonuclear decoupling during t_1; this resolution permits a sufficiently accurate determination of the various proton species present in the system.

The LG scheme is particularly efficient for the homonuclear decoupling and is well suited with high spinning speed because the full cycle time is usually less then 20 μs, significantly shorter than the rotor period at a spinning speed of 15 kHz. The key point of the Lee and Goldburg approach was the use of an *rf* field off-resonance according to $\Delta LG/\omega_1 = \sqrt{2}$, where ΔLG is the offset and ω_1 is the *rf* strength, this *rf* field produces an

effective field in the rotating frame inclined at the magic angle θ_m to the static field H_0. The fast precession of the spins around the magic-angle axis causes the zero-order average dipolar Hamiltonian to vanish. A few strategies have been proposed for higher decoupling efficiency. The LG irradiation can be frequency - switched (FSLG)[8] after successive 2π rotation of the proton magnetization around the tilted axis, in this case also all the odd-order terms in average dipolar Hamiltonian vanish on account of the introduced symmetry. An ingenious alternative to FSLG was proposed by Vega and co-workers,[6] in the so called phase-modulated Lee-Goldburg experiment (PMLG) only the phase of a series of adjacent pulses is changed without frequency switching. The pulse sequence used in this work exploits the PMLG approach and is depicted in Figure B.8.

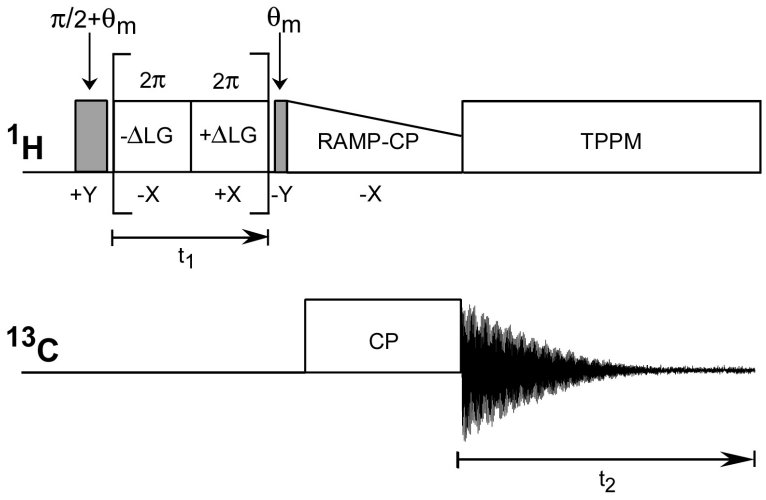

Figure E.8

Pulse sequence used for 2D PMLG-HECTOR NMR experiments. A $(\pi/2+\theta_m)_y$ preparation pulse puts the ^{1}H polarization perpendicular to z axis of the effective field in the tilted rotating frame, during t_1 a PMLG irradiation sequence is applied. At the end of t_1 a θ_m pulse brings back the magnetization into the xy plane. In order to have an efficient transfer of magnetization to the carbon nuclei under fast MAS during the contact time a RAMP-CP is applied, this procedure restores a broader matching profile between proton and carbon nuclei. During acquisition TPPM heteronuclear decoupling is applied

A $(\pi/2+\theta_m)_y$ preparation pulse puts the ^{1}H polarization perpendicular to z axis of the effective field in the tilted rotating frame during the LG irradiation, and during t_1 a PMLG sequence is applied. This consists in the application of a train of pulses with phase described by $\phi(t) = \omega_{PMLG}t$ satisfying $|\omega_{PMLG}| = \omega_1/\sqrt{2}$. An LG irradiation unit corresponds to 2π cycle in the effective field with $\tau_{LG}=\sqrt{(2/3)}(2\pi/\omega_1)$, thus the angle

through which the *rf* precesses is 207.8°. The sign of ω_{PMLG} is alternated in subsequent LG units, ensuring the removal of odd-order terms in average dipolar Hamiltonian. The LG unit consists of a number of pulses m with well-defined phases, $\alpha_{i,}$ for i^{th} pulse length. The number m defines the duration of the pulses, in fact the pulse width is t_{LG}/m. The increment in the phase angle of each pulse amounts to $\Delta\alpha$=207.8°/m. LG irradiation also has an effect on the chemical shift, in fact in two successive PMLG period the chemical shift dispersion is scaled by the factor $\cos\theta_m = 1/\sqrt{3}$. At the end of t_1 a θ_m pulse returns the magnetization to the xy plane.

In order to have an efficient transfer of magnetization to the carbon nuclei under fast MAS a Ramped-Amplitude Cross-Polarization (RAMP-CP)[9] is applied, this procedure restores a broader matching profile between proton and carbon nuclei. The ramp is obtained changing the strength of the proton rf from 80 kHz at the beginning of the contact time to a value of 60 kHz at the end of the cross polarization period in 100 steps.

E.7 References:

1) a) F. A. Bovey, *Nuclear Magnetic Resonance Spectroscopy*, Academic Press In.: New York, **1991**. b) C. A. Fyfe, *Solid State NMR for Chemists*, C. F. C. Press: Guelph, **1984**. c) E. O. Stejskal, J. D. Memory, *High Resolution NMR in the Solid State*, Oxford University Press, New York, **1994**. d) A. Abragam, *The Principles of Nuclear Magnetism*, Clarendon Press: Oxford University Press, London, **1961**.

2) M. M. Maricq, J. S. Waugh; *J. Chem Phys.* **1979**, *70*, 3300-3316.

3) A. E. Bennet, C. M. Rienstra, M. Auger, K. V. Lakshmi, R. G. Griffin; *J. Chem. Phys.* **1995**, *103*, 6951-6958.

4) S. R. Hartmann, E. L. Hahn; *Phys. Rew*. **1962**, *128*, 2042-2053.

5) a) F. A. Bovey, P. A. Mirau, *NMR of Polymers*, Academic Press, San Diego, **1996**. b) K. Schmidt-Rohr, W. Spiess, *Multidimensional Solid-State NMR and Polymers*, Academic Press Inc, San Diego, **1994**.

6) E. Vinogradov, P.K. Madhu, S. Vega; *Chem. Phys. Lett.* **1999**, *314*, 443-450.

7) M. Lee, W. I. Goldburg; *Phys. Rev.* **1965**, *140*, 1261-1271.

8) B.J. Van Rossum, H. Förster, H. J. M. de Groot; *J. Magn. Reson.* **1997**, *124*, 516-519.

9) G. Metz, X. Wu, O. S. Smith; *J. Magn. Reson. A* **1994**, *110*, 219-227.

Appendix F

SEM and TEM microscopic techniques

Electron microscopes use a beam of electrons to investigate a sample and create highly-magnified images. The use of electrons instead of light gives these instruments much greater resolving power and possibility to obtain much higher magnification respect to common optical microscopes. In fact, image resolution is limited by the wavelength of radiation used. Because accelerated electrons have smaller wavelength (de Broglie wavelength) than electromagnetic radiation, electron microscopes can obtain magnifications of up to 1 million times, while the best light microscopes are limited to magnifications of 1000 times.[1,2]

The electron microscope uses electrostatic and electromagnetic lenses to control and focus the electron beam on a specific plane relative to the sample. This manner is similar to how a light microscope uses glass lenses to focus light on or through a sample to form an image. The electron beam is normally generated by heating a tungsten filament cathode placed in an electron gun that accelerates extracted electrons with a strong potential, typically between 40 to 400 keV. To avoid beam extinction, caused by electron collision with gas molecules, electron microscopes generally work in high-vacuum conditions (up to 8×10^{-3} Pascal).

There are different types of electron microscopes. Here below we describe the two we have used in this work: the Transmission Electron Microscope (TEM) and the Scanning Electron Microscope (SEM)

F.1 Transmission Electron Microscope (TEM)

In transmission electron microscope the electron beam is transmitted through the sample that is in part transparent to electrons and in part scatters them out of the beam.[3] When the electron beam, emerges from the sample, it carries information about the sample structure. The spatial variation in this information (the "image") is viewed by projecting the magnified electron image onto a fluorescent viewing screen coated with a phosphor or scintillator material such as zinc sulfide. The image can be photographically recorded by exposing a photographic film or plate directly to the electron beam, or a high-resolution phosphor may be coupled by means of a lens optical system or a fiber optic light-guide to the sensor of a CCD (charge-coupled device) camera. The image detected by the CCD may be displayed on a monitor or computer.

Resolution of the TEM is limited primarily by spherical aberration, but a new generation of aberration correctors have been able to partially overcome spherical aberration to increase resolution. Hardware correction of spherical aberration for the High Resolution TEM (HRTEM) has allowed the production of images with resolution below 0.5 Ångström (50 picometres) at magnifications above 50 million times.[4] The ability to determine the positions of atoms within materials has made the HRTEM an important tool for nanotechnologies research and development.[5]

TEM sample must to be enough thin to consent the electron passage trough themselves. The maximum thickness depends from the acceleration voltage, but generally must be around 100nm. To obtain a sample enough thin from a bulk material, common procedure involves the cut of the sample with a microtome followed by a ion-beam excavation. The electron beam is then focused on the border of obtained hole, where the material thickness becomes smaller. Powder samples, instead, are deposited on a standard TEM metal grid, generally by wet deposition with a drop of water.

F.2 Scanning Electron Microscope (SEM)

Unlike the TEM, where electrons pass through the sample, the electron beam of the Scanning Electron Microscope (SEM)[6] perform a surface investigation. The SEM produces images by probing the sample with a focused electron beam that is scanned across a rectangular area of the sample (raster scanning). Hitting the sample, electrons could be directly backscattered, re-emitted as secondary electrons or induce an electromagnetic radiation emission, which frequencies fall generally in the X-ray region of the electromagnetic spectrum. SEM image is obtained investigating the energy loss of secondary electrons. These electrons interact with a small sample volume, which extends from less than 100 nm to around 5 μm into the surface (depending on electron acceleration) and, once scattered, are collected by electron amplifiers. The study of the electron energy loss in function of the beam position brings to the SEM image.

Generally, the image resolution of an SEM is about an order of magnitude poorer than that of a TEM. However, because the SEM image relies on surface processes rather than transmission, it is able to image bulk samples up to many centimeters in size and (depending on instrument design and settings) has a great depth of field, and so can produce images that are good representations of the three-dimensional shape of the sample.

Some sample instruments, moreover, have specific detectors for radiation emitted by the sample. These are due to high energy electron transition and are strictly linked to the chemical nature of sample atoms. The study of these frequencies allows to a chemical investigation of sample nature. This method is called microanalysis.

The sample in investigation is placed on a metal support (stab) and fixed with an adhesive graphitic disc or a conductive metal paste. SEM samples must be conductive to consent electron interactions. To analyze non-conductive samples it is necessary to make a conductive layer on their surface. To do this, common techniques are sputtering or evaporation of metals (generally gold or platinum).

F.3 *References:*

1) D. Halliday, R. Resnick, *Fundamental of physics, 2nd edition*, John Wiley & Sons, New York, **1981**

2) R. Eisberg, R. Resnick, *Quantum physics of atoms, molecules, solids, nuclei and Particles 2nd edition*, John Wiley & Sons, New York, **1985**

3) D.K. Racher, *Transmission Electron Microscopy, Methods of Applications*, Thomas, Springfield, Illinois, US, **1983**

4) R. Erni, M.D. Rossell, C. Kisielowski, U. Dahmen; P*hys. Rev. Lett.* **2009**, *102*, 096101-1,4

5) M.A. O'Keefe, L.F. Allard; *National Nanotechnology Initiative workshop on Instrumentation and Metrology for Nanotechnology*, Gaithersburg, MD, **2004**

6) J.W.S. Hearle, J.T. Sparrow, P.M. Cross, *Use of the Scanning Electron Microscope*, Pergamon, Oxford, UK, **1972**

Appendix G

Experimental conditions for characterizations

G.1 Gas adsorption

Nitrogen adsorption-desorption isotherms were measured at liquid nitrogen temperature using a Micromeritics analyzer. The samples were outgassed overnight. Surface area was calculated using the Brunauer, Emmet, and Teller (BET) model. For mesoporous samples, the pore-size distributions were evaluated following the method developed by Barret, Joyner and Halenda (BJH model) for cylindrical pores with Kruk-Jaroniec-Sayari correction and, as comparison, by Density Functional Theory (DFT) analysis. The mesoporosity of the polymer objects was determined by nitrogen adsorption at 77 K and the pore distribution is calculated by BJH cylindrical model on the adsorption branch. The DFT analysis with slit-pore model was used to confirm the results.

The adsorption of benzene and the other gases were performed using a gas adsorption manometry apparatus, equipped for low temperature (175 K) measurements. The gas pressure was determined by an active strain gauge (Edwards ASG) with a sensitivity of 0.1 torr.

The samples were outgassed overnight at 100°C, below 10^{-3} torr. Adsorption equilibrium was normally reached in less than 30 minutes. The measurements were carried out at room temperature and in the pressure range where the vapor phases behave as an ideal gas.

G.2 X-Ray Diffraction

All powder X-ray diffraction patterns were recorded using a Bruker D8 Advance diffractometer ($Cu_{K\alpha}$ radiation) in the 2θ range 1.5° to 70°, with $\Delta(2\theta)$=0.02° and 2-4sec per step as counting time.

Synchrotron X-ray powder diffraction experiments were performed at the BeamLine D8, Grenoble, France. The radiation wavelength λ was 0.78 Å. 2θ range was from 2° to 35°, at 1 atm and 200 K. In the case of the sample containing carbon dioxide molecules, the benzene-silica system was allowed to reach the equilibrium in about two hours.

G.3 Differential Scanning Calorimetry

Differential scanning calorimetry (DSC) traces were performed on Mettler Toledo Star^e Thermal Analysis System equipped with N_2 low temperature apparatus. The experiments were run under nitrogen atmosphere in an open Al-crucible. The samples were first heated from room temperature to 200°C at 10°C/min, cooled down to room temperature, and then heated again from room temperature to 400°C at 10°C/min. The sample weights for the DSC measurements were about 5 mg and were measured to an accuracy of 0.05 mg.

G.4 Thermogravimetric Analysis

The Thermogravimetric Analysis (TGA) measurements were made using a Perkin-Elmer TGA-7 instrument. About 15 mg of sample was heated from 35°C to 750°C at a heating rate of 10°C/min under nitrogen atmosphere.

G.5 Scanning Electron Microscopy (SEM)

The images were obtained by a TESCAN-VEGA TS 5136 XM-SEM instrument operating at 30 kV for silica and the nanocomposite and, for the polymer samples, at 20 kV equipped with a EDAX-GENESIS 4000 microanalysis accessory. The samples were coated with a thin layer of gold before imaging.

G.6 Transmission Electron Microscopy (TEM)

The TEM images were obtained using a JEOL JEM-3010 with V=300 kV. Laser Light Diffraction analysis were performed using Tri-laser Microtrac S3500 apparatus.

G.7 ATR spectroscopy

ATR experiments were performed on a Nexus 470 FT-IR instrument, using a system Thermo Nicolet Continuμm by Thermo spectra tech., with a resolution of 150 x 150 μm. For samples treated under 300°C a diamond ATR crystal was used, while for samples treated at 500 and 1100°C the ATR crystal was in germanium.

G.8 Micro Raman spectroscopy

Micro Raman spectra were collected using a He-Ne laser (632.8 nm wavelength) on a Labra Jobin-Yvon spectrometer at room temperature.

G.9 Liquid-State NMR

Solution ^{1}H NMR experiments were recorded on a Varian Mercury-Series AS-400 spectrometer operating at 400 MHz and spinning speed of 20 Hz. The recycle delay was 5s. The spectra were obtain in $CDCl_3$ with 2% of solution concentration and TMS as reference.

G.10 Solid-State NMR

The solid–state NMR spectra were run at 75.5 MHz for ^{13}C and at 59.6 MHz for ^{29}Si, on a Bruker Avance 300 instrument operating at a static field of 7.04 T equipped with 4 mm double resonance MAS probe. The samples were spun at a spinning speed of 15 kHz, and Ramped-Amplitude Cross-Polarization (RAMP-CP) transfer of magnetization was applied. The 90° pulse for proton was 2.9 μs (86 kHz). ^{13}C Single Pulse Excitation (SPE) experiments were run using a recycle delay of 10 s and 100 s and Cross Polarization (CP) MAS experiments were performed using a recycle delay of 10 s and a contact time of 2.5 ms.

Phase-Modulated Lee-Goldburg (PMLG) heteronuclear ^{1}H-^{29}Si and ^{1}H-^{13}C correlation (HETCOR) experiment coupled with fast magic angle spinning (MAS) allows the

registration of 2D spectra with high resolution both in the proton and silicon dimension. Narrow proton resonances, with line widths in the order of 1-2 ppm, are obtained with homonuclear decoupling during t_1; this resolution permits a sufficiently accurate determination of the proton species present in the system. Phase-Modulated Lee-Goldburg (PMLG) ^{1}H-^{29}Si and ^{1}H-^{13}C HETCOR spectra were run with LG period of 18.9 μs. The efficient transfer of magnetization to the carbon nuclei was performed applying RAMP-CP sequence. Quadrature detection in t_1 was achieved by time proportional phase increments method. Carbon signals were acquired during t_2 under proton decoupling applying two pulse phase modulation scheme (TPPM). Before each heteronuclear experiment samples are outgassed overnight and inserted in the ZrO_2 rotors in a dry box under nitrogen atmosphere.

Acknowledgements

(Shuffle)

At the end of darkness, let the sun rise again…
(William S. Carter)

… and at the end of this thesis, let me say thank you very much to all people who helped me, who make my life interesting and who trusted me. Someone once said me: "Life is like a card play: that it is important are the cards in your hand", so let me see what kind of "cards" I've had in my hand in these three years…

The Chariot

Thanks to professor Sozzani for this great opportunity and the time he gave me. Great thanks also to other people of research group for all nice moments we have had together: Angiolina, Silvia, Lisa, Alice, Benny, Tano, Andrea B., Roberta, Eleonora, Martino, Marco, Francesca, Thara, Sergio, Andrea D., Marzia, and Stefano.

A very special thank you is for Patrizia, who has ever looked on my work with patience and sympathy and, overall in this last period, has been near to me with all her friendship and kindness. Thank you boss!

The World

Thanks to professor Froeba for his hospitality in the University of Hamburg and for the enthusiasm he ever showed about my work. With him, I would say thank you very much also to his groups and in particular to Jurgen for all the laughs, the discussion about science, films and books, and for all nice Saturday evenings drinking beer.

We must still play a chess match, remember it!

Judgement

To write this thesis has been a hard and long work, but it has brought great satisfactions. I would say thank you to professor Sokolov for the enthusiastic comment, to professor Miglio for his patience with me (despite some little mutual incomprehension) and to professor Bernasconi for his ever interesting and stimulating questions during the year by year PhD seminars.

The Lovers

To my sweet Laura, the first of the most beautiful things in my life, thank you for all your love, for all your smiles, for all things you've given me and to have been ever at my side in these four months despite the little time I've could give you.

The Fool

A little bit of madness is necessary in the life. Mine are all my friends: Bosses, Gatis, Friends of ancient date, Fair trade collaborators, Theatre people, Oratorio guys, Defcon people, Animation team and Assault squad; to all of them thank you for all moments of liberating foolishness. Finally, the fool of fools: my Basque brother Buel-la; thank you, brother, for everything!

Strength

My strength is my family: very special people who have ever been in my life with all their love and their kind presence also if often I've been far away. Thanks to all, with a particular attention to my mother, who sometimes, I think, asks herself: "What the hell I've done wrong to have a son so crazy?" and, despite this, she is ever with me with her smile, her love and her wonderful cakes!

Death

Death is not the end, I don't believe this. But the death of loved people is the same a great and deep pain for the heart. To my father and my uncles, who now look at me from the heaven: if I've reached this point is overall because you've ever trusted me and given me all your support. To you I say my greater thank you, with the hope, one day, to could meet again and show you that the seeds you've given me have become a forest.

For all those people and others I've surely forgot, thank you again for everything.

At the end of darkness, let the sun rise again. And let his light fills your heart like love, to become yourself a sun for all people around you.

Bario